ABSTRACT

Title of thesis: EXPERIMENTAL INVESTIGATION OF A QUAD-ROTOR BIPLANE MICRO AIR VEHICLE

Christopher Michael Bogdanowicz
Master of Science, 2015

Thesis directed by: Dr. Inderjit Chopra
Department of Aerospace Engineering

Micro air vehicles are expected to perform demanding missions requiring efficient operation in both hover and forward flight. This thesis discusses the development of a hybrid air vehicle which seamlessly combines both flight capabilities: hover and high-speed forward flight. It is the quad-rotor biplane, which weighs 240 grams and consists of four propellers with wings arranged in a biplane configuration. The performance of the vehicle system was investigated in conditions representative of flight through a series of wind tunnel experiments. These studies provided an understanding of propeller-wing interaction effects and system trim analysis. This showed that the maximum speed of 11 m/s and a cruise speed of 4 m/s were achievable and that the cruise power is approximately one-third of the hover power. Free flight testing of the vehicle successfully highlighted its ability to achieve equilibrium transition flight. Key design parameters were experimentally

investigated to understand their effect on overall performance. It was found that a trade-off between efficiency and compactness affects the final choice of the design. Design improvements have allowed for decreases in vehicle weight and ground footprint, while increasing structural soundness. Numerous vehicle designs, models, and flight tests have proven system scalability as well as versatility, including an upscaled model to be utilized in an extensive commercial package delivery system. Overall, the quad-rotor biplane is proven to be an efficient and effective multi-role vehicle.

EXPERIMENTAL INVESTIGATION OF A QUAD-ROTOR BIPLANE MICRO AIR VEHICLE

by

Christopher Michael Bogdanowicz

Thesis submitted to the Faculty of the Graduate School of the
University of Maryland, College Park in partial fulfillment
of the requirements for the degree of
Master of Science
2015

Advisory Committee:
Professor Inderjit Chopra, Chair/Advisor
Professor James Baeder
Professor Allen Winkelmann

Acknowledgments

Foremost, I would like to express my sincere gratitude to my mother, father, and sister for their love and support throughout my graduate career. I would like to thank my advisor Dr. Inder Chopra for the continuous support of my studies and research, for his motivation and immense knowledge. I want to thank Dr. Vikram Hrishikeshavan, whose knowledge, support, and guidance made this research possible. His help has been invaluable throughout my time as a research assistant and during the writing of this thesis. I would like to thank the rest of my thesis committee, Dr. James Baeder and Dr. Allen Winkelmann, for taking the time to hear about my work and ask the tough questions. I thank my fellow lab-mates in the Alfred Gessow Rotorcraft Center including Derrick Yeo and Brandyn Phillips for all of their help in the designing, building, and testing of the vehicle. I would also like to thank Omri Rand, Avi Weinreb, and the Israeli Defense Ministry for helping to make this research possible. Last but not least, I would like to thank my friends for keeping me sane throughout the process.

Contents

List of Tables

List of Figures

List of Abbreviations

Symbol	Units	Description
α	^{o}	Aerodynamic angle of attack
AR	–	Aspect ratio
β	^{o}	Shaft tilt
D	in	Rotor diameter
c	ft	Wing chord
C_d	–	Drag coefficient
C_l	–	Lift coefficient
C_P	–	Coefficient of power
C_T	–	Coefficient of thrust
$C_{l_{\max}}$	–	Maximum lift coefficient
η	–	Propeller efficiency
J	–	Advance ratio
n	Hz	Rotor rotations per second
P	W	Propeller power
R	ft	Rotor radius
ρ	slugs/ft^3	Air density
Re	–	Reynolds number
S	ft^2	Wing planform area
T	N	Propeller thrust
V	m/s	Wind speed
W	lbs	Weight

Chapter 1

Introduction

1.1 Motivation

In recent years, the potential uses for unmanned aerial vehicles (UAVs) has increased drastically. These applications include but are not limited to surveillance, bio-chemical sensing, search and rescue, "over the hill" or "around the corner" reconnaissance, as well as medical supply and consumer package delivery. Simple diagrams depicting several of these missions are shown below in Fig. 1.1 [1]. Yet another example of such a mission profile can be seen in Fig. 1.2, provided by DARPA [2]. This figure depicts a UAV taking off and landing vertically, maneuvering in edgewise flight to deliver payloads, and flying in a high-speed cruise configuration, all of which are highly desirable capabilities of modern UAVs. It is worth noting that, as of late, the military has made these vehicles an indispensable tool for war-fighters. Many UAVs, such as the Reaper, are quite large and offer a substantial coverage of battlefields and contested areas. Smaller vehicles, like the Shadow, are carried and flown by soldiers on the ground and require minimal interaction with ground stations. However, rapid progress in micromechanics and microelectronics, along with this major increase in unmanned vehicle capability, performance, and utility, has brought about special interest in the development of even smaller vehicles called micro aerial vehicles (MAVs).

From a military standpoint, it was envisioned that these MAVs would be easily portable aircraft for the purpose of increasing the soldier's situational awareness. These vehicles are typically used in an attempt to minimize soldier exposure to

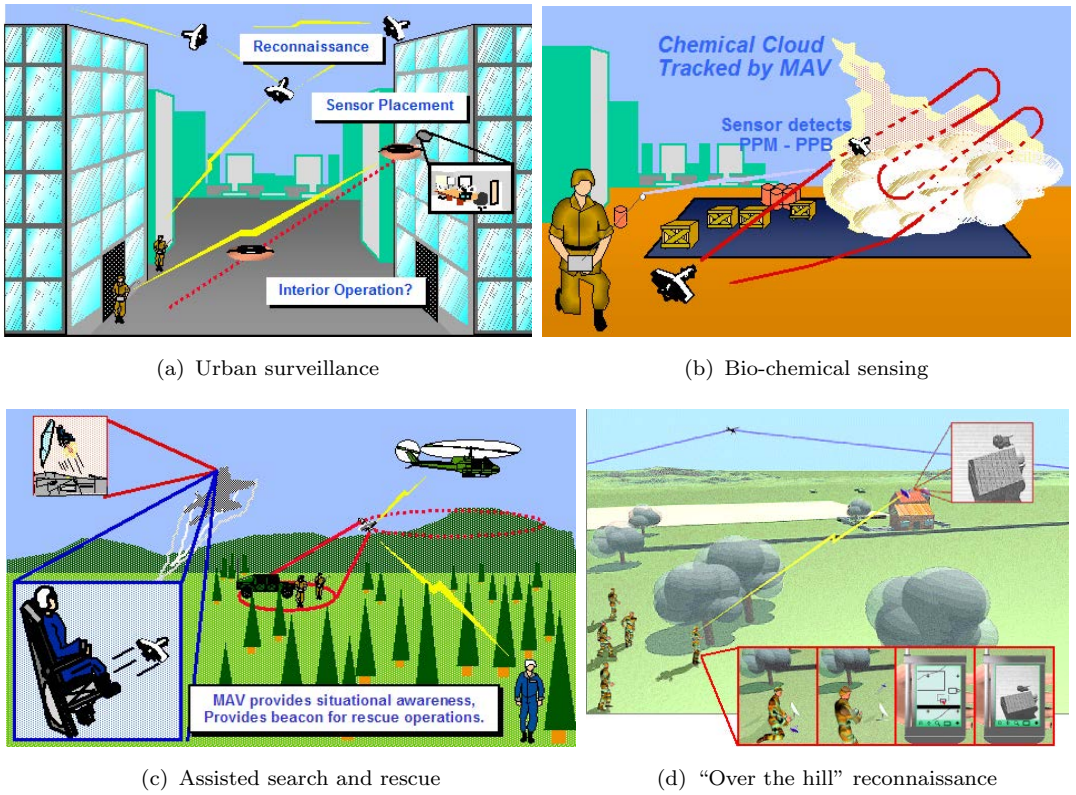

(a) Urban surveillance

(b) Bio-chemical sensing

(c) Assisted search and rescue

(d) "Over the hill" reconnaissance

FIGURE 1.1: Typical UAV missions, [1]

dangerous situations. MAVs can have many specialized applications that range from surveillance, reconnaissance, search and rescue, and even terrain and environment mapping, to name a few. However, these vehicles are also valuable from a commercial standpoint in that they offer high maneuverability, as well as small payload delivery capabilities, among other merits. Due to their small size, MAVs can fly into areas including inside buildings or caves that are inaccessible by traditional aircraft. These vehicles have a small ground footprint and require little to no infrastructure, as they can be piloted by a single person or even flown autonomously.

FIGURE 1.2: Typical multirole MAV mission, [2]

1.1.1 Technical Challenges

Although MAVs offer numerous inherent utilities and exciting new capabilities, they also offer numerous challenges in design, stemming from their small scale. From aerodynamic performance to the number of moving parts, each MAV configuration faces design challenges. MAVs operate in low Reynolds number flow regimes which result in a drop in aerodynamic performance. Vehicle configuration can have a large impact on this, as well. Today, most existing MAVs can be broadly classified into the fixed-wing, rotary-wing, and flapping-wing categories. Each configuration brings its own merits and weaknesses and these are detailed in the following subsections

1.1.1.1 Aerodynamic Performance

A major challenge when designing small scale vehicles is efficient aerodynamic flight. As vehicle size decreases, so too does the vehicle Reynolds number. This

quantity, used as a non-dimensional description of the flow regime, can be represented as

$$Re = \frac{\rho V l}{\mu} \tag{1.1}$$

where ρ is air density, V is air speed, l is the characteristic length, and μ is the fluid viscosity. Figure 1.3 shows a comparison between the Reynolds numbers of typical MAVs and other forms of modern aircraft [3]. It can be seen that the Reynolds numbers of MAVs are low as compared to well-understood vehicles, like the F/A-18. Micro aerial vehicles operate in a very sensitive Reynolds number regime, which can affect aerodynamic performance. In this regime, many complex flow phenomena take place within the boundary layer. Flow separation, transition, and reattachment can all occur within a short distance along the chordline of a rotor or wing. These disturbances can dramatically affect the performance of the lifting surface.

Lately, some studies have been conducted on aerodynamic surfaces operating at Reynolds numbers below 70,000, in an attempt to gain dependable performance data for lifting surfaces operating in these air flows [4]. The studies of Laitone provided lift and drag measurements for a NACA0012 airfoil, as well as flat and cambered plate airfoils. The study found that traditional airfoil shapes, such as the NACA0012, have poor performance compared to cambered plate profiles with sharp leading edges. This can be seen in Fig. 1.4. Laminar flow was found to be the cause of low maximum lift coefficients, nonlinear lift and moment curves, and lower lift to drag ratios with low Reynolds number lifting surfaces. It was found, that the flat plate airfoil had a 10% higher lift-to-drag ratio as compared to the NACA0012. Based on the studies conducted by Laitone, it is clear that

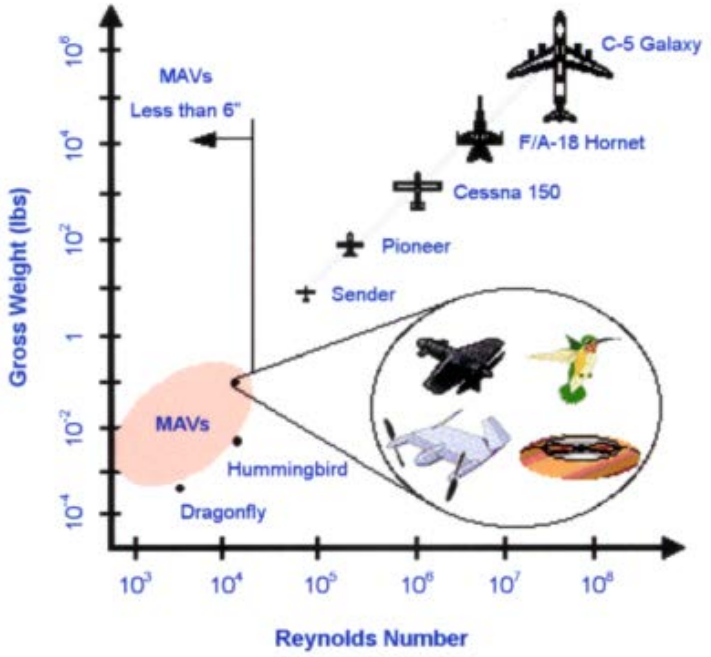

FIGURE 1.3: Reynolds number comparison between different sized aircraft, [3]

aerodynamic performance is hindered for traditional airfoils when operating in low Reynolds number regimes.

Hence, designing vehicles that can efficiently fly in this flight regime represents an entirely new challenge to aerospace design engineers. It is of utmost importance to reach an in-depth understanding of the aerodynamics of this flight regime in order to design an MAV that can still be flown efficiently in this low Reynolds number regime, and these are main goals of this investigation.

1.1.2 Vehicle Configurations

The type of vehicle used in the micro aerial design can have a large impact on the vehicle's capabilities. This section examines several vehicle conventions as well as

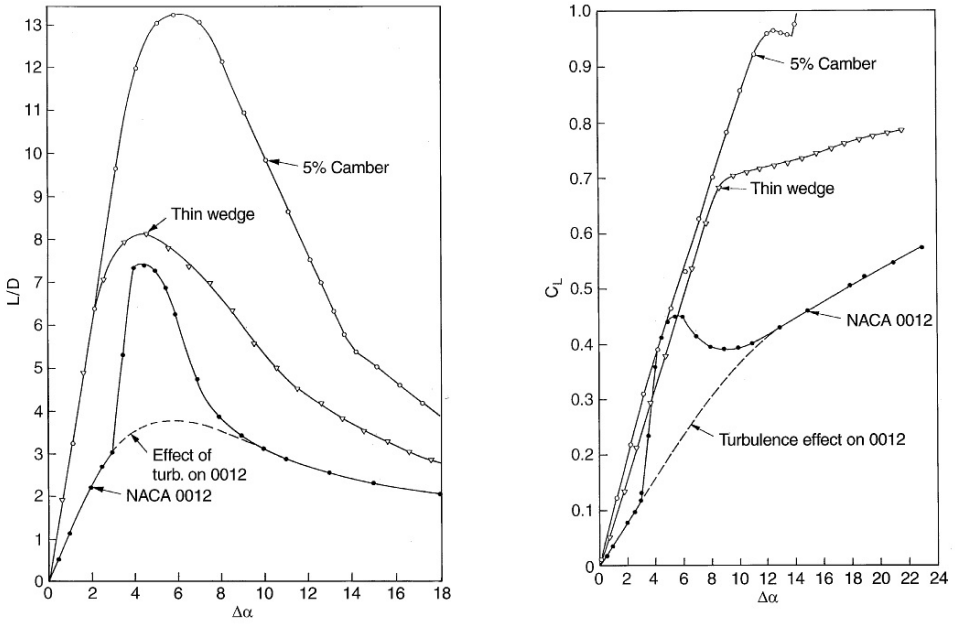

FIGURE 1.4: Degraded aerodynamic performance at low Reynolds number, [4]

their strengths and weaknesses.

1.1.2.1 Fixed-Wing

Fixed-wing MAVs can efficiently perform high cruise-speed missions. These vehicles typically require a takeoff and landing zone and can achieve higher cruise efficiencies than other aerial vehicle configurations. One such vehicle is shown in Fig. 1.5. The vehicle pictured is the Black Widow MAV. It has a span of only 6" and is capable of reaching speeds of 30 mph with an endurance of 30 minutes [5]. These characteristics are impressive for a vehicle weighing less than 100 grams. However, fixed-wing aircraft, like the Black Widow, typically cannot perform hover and offer little to no edgewise maneuverability. Small fixed-wing vehicles suffer from poor gust tolerance, as well.

FIGURE 1.5: Fixed-wing MAV, Black Widow, [5]

1.1.2.2 Rotary-Wing

Rotary-wing vehicles have been designed and explored for many years and, at this point, are a well-understood concept [6–10]. These can vary from conventional single-main-rotor (SMR) concepts as shown in Fig. 1.6 to multi-rotor concepts as depicted in Fig. 1.7. Rotary-wing MAVs are well-suited for low speed loiter and hover tasks with great lateral maneuverability. Additionally, SMR helicopters and multi-rotor concepts are typically very efficient in hover and can achieve high payload fractions, among other utilities. However, unfortunately these vehicles suffer from poor forward flight performance and offer limited speed and range capabilities as compared to other configurations. A lack of cruise efficiency truly limits the usefulness of these MAV configurations.

1.1.2.3 Flapping-Wing

Recently, many flapping-wing technologies have been explored, including the ornithopter seen in Fig. 1.8 [11]. These vehicles typically mimic the wing motions

FIGURE 1.6: Rotary-wing MAV

(a) Quadrotor UAV

(b) Coaxial helicopter UAV

FIGURE 1.7: Typical rotary-wing vehicle configurations

utilized by birds and flying insects to achieve flight. These MAVs represent a novel approach to flight and can typically offer hovering as well as forward flight capabilities. One of the anticipated advantages with such a design is its superior gust tolerance. The functionality of these concepts has been shown via technology demonstrations at the University of Maryland and Texas A&M University, among other research institutions (Fig. 1.9) [12–14].

A drawback of these vehicles is that the wing movements utilized by most insects and birds are very complex and involve twists and other motions that are not yet fully understood by experts. Additionally, efficient mechanical systems to drive and withstand the large inertial loads produced by the wings have not yet been developed. These vehicles require far more developmental effort before they become readily available for implementation.

FIGURE 1.8: Ornithopter flapping-wing UAV, [11]

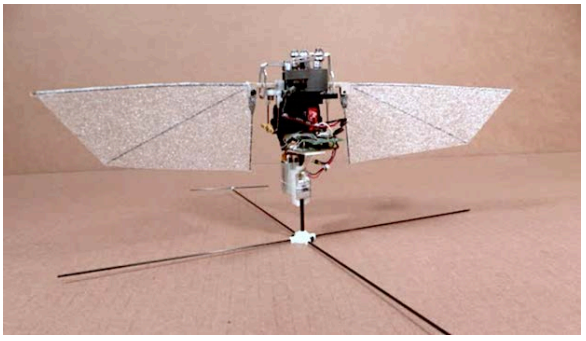

FIGURE 1.9: UMD flapper technology demonstrator, [14]

1.1.3 Hybrid Air Vehicles

For numerous missions, such as the profile illustrated in Fig. 1.2, aerial systems are required to have the ability to hover and maneuver in edgewise flight, as well as travel a significant distance between two locations quickly. Therefore, it is of interest to combine the strengths of both the fixed and rotary-wing vehicle classes into a single hybrid air vehicle. Various hybrid UAV configurations have been explored in the past, such as fixed-wing with hover capabilities, tilt-wing, cyclorotor, tilt-rotor, fan-in-wing, and tail sitters, among others [15–23]. Each of these vehicle configurations will be discussed in detail in the following subsections.

1.1.3.1 Fixed-Wing Hybrid Vehicles

Fixed-wing MAVs are an attractive platform for outdoor surveillance missions, as they generally offer better payload and endurance capabilities than comparably sized rotorcraft or flapping-wing vehicles. They are also generally easier to control than helicopters in outdoor environments. Recent studies have been conducted on the utility of fixed-wing aircraft attempting to sustain hover [24–26]. The capability of achieving hover by utilizing propeller driven fixed-wing aircraft is verified in these studies. The aircraft achieve transition via the installed control surfaces. This allows them to reach the hover configuration. However, this vehicle configuration has some inherent issues. As with typical fixed-wing aircraft, these vehicles require takeoff and landing zones. This makes them less versatile than a vehicle which has VTOL capabilities. High wing loading, associated with MAV dimension constraints, requires high cruise speeds for fixed-wing MAVs. Achieving hover using a single propeller implies that this design requires an extremely low structural weight or a high installed power-weight fraction. This can lead to reduced payload carrying capabilities. Therefore, it is difficult to achieve preferable performances at low-speed flight using fixed-wing configurations. Also, there are associated altitude changes during stages of transition, which can lead to crashes.

1.1.3.2 Cyclorotor Vehicles

Many breakthroughs in cyclorotor research have occurred in recent years [27–30]. Recently, the feasability of this concept was demonstrated at the University of Maryland by the development of a hybrid twin-rotor cyclocopter [29] and quad-rotor cyclocopter [30], capable of free hover. The twin-rotor cyclocopter can be seen in Fig. 1.11.

FIGURE 1.10: Fixed-wing MAV capable of hover, [24]

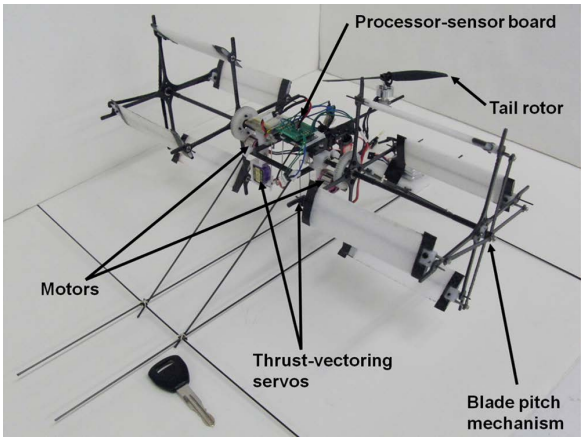

FIGURE 1.11: Cyclorotor MAV, [28]

The cyclorotor vehicle is unique in its ability to vector its thrust components. This utility can be seen in Fig. 1.12. By changing the pitch of the airfoil as it passes through its rotation, the collective lift over the sections can be vectored in any direction in 360°. However, the cyclocopter utilizes a very high number of moving parts and complicated control schemes, which diminish the returns of using such a configuration.

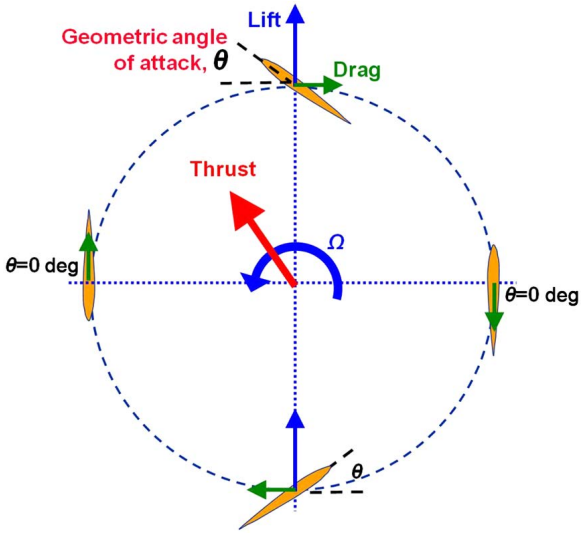

FIGURE 1.12: Cyclorotor thrust vectoring, [28]

1.1.3.3 Tilt-Rotor Vehicles

Numerous studies have been conducted on the tilt-rotor vehicle and its application to small scale vehicle flight [31]. Tilt-rotors are popular due to their ability to easily take off and land vertically, as well as reach high cruising velocities. They also allow for transitions between flight modes without disturbing fuselage attitude. However, at these small scales, where vehicles are unmanned and fuselage and payload tilting is less of an issue, this utility represents less of an advantage. The tilting mechanisms installed on most tilt-rotor vehicles represent a large gross takeoff weight percentage of the vehicle. This leads to a larger, heavier vehicle overall. Moreover, since only rotors are tilted, the efficiency of the slipstream effect decreases. This occurs because the wings are not linked to the rotor tilting mechanism and the wing planform presents a large drag area to the rotor downwash.

FIGURE 1.13: Tilt-rotor configuration MAV

1.1.3.4 Tilt-Wing Vehicles

Tilt-wing MAVs have also experienced increased exploration in recent years. Figure 1.14 shows a tilt-wing concept vehicle [32] explored in *Autonomous Flying Robots: Unmanned Aerial Vehicles and Micro Aerial Vehicles*. This is a popular configuration because, like the tilt-rotor vehicle, it allows for transitions between VTOL and forward flight modes without fuselage pitching. Tilt-wings present an advantage over tilt-rotors in that their wings are aligned with propeller slipstream, increasing vehicle efficiency.

FIGURE 1.14: Tilt-wing configuration MAV, [32]

Still, unfortunately studies have shown that there is little interest in developing a tilt-wing concept for MAVs, except for very high tilt angles where the reduction in equivalent aspect ratio is beneficial to the lift force [33]. Flight testing with this design has also shown that the inertia of the wing-tilting mechanism and the fuselage are comparable. This leads to less than desirable wing-tilting performance during transition to forward flight.

1.1.3.5 Fan-in-Wing Vehicles

As technology has advanced, a more novel approach to unmanned vertical flight has been studied: the fan-in-wing design [34]. A vehicle of this design can be seen in Fig. 1.15. With this approach, multiple rotors are housed within the wings, allowing for vertical lift. Typically, propulsive mechanisms provide the necessary vehicle thrust. However, while these vehicles represent an exciting concept, they suffer from high mechanical complexity and bring an undesirable level of technological risk owing to their relatively low developmental lifespan. Additionally, the fans in the wings are not operable in forward flight which can lead to increased 'dead-weight' in that mode. These vehicles typically lack efficiency in both hover and forward flight as compared to comparable conventional aircraft, as well.

FIGURE 1.15: Fan-in-wing configuration MAV

1.1.3.6 Tail Sitter Vehicles

Another popular hybrid vehicle is the tail sitter configuration. This vehicle concept is pictured in Fig. 1.16, which highlights the simplicity of the design. The tail-sitter configuration is similar to most fixed-wing aircraft and is usually simple in construction. This inherent benefit in design leads to a lower overall vehicle weight and less difficult maintenance and repair. Tail sitters also do not require takeoff and landing strips.

FIGURE 1.16: Tail sitter configuration MAV, [35]

Google explored this concept when it designed, built, and tested "Project Wing" for small payload deliveries [22]. This vehicle can be seen in Fig. 1.17. For tail-sitter vehicles, the entire body tilts as the vehicle transitions from vertical takeoff and hover to forward flight. This however, involves the operation of single or multiple propellers in conjunction with aerodynamic surfaces that are activated in the downwash of the vehicle's propellers. This action, depicted in Fig. 1.18, generates the required pitching moments for maneuvering between the various flight modes. As a result, high disk loadings and downwash velocities are required

for adequate control forces. This leads to high power requirements, which are typically not desirable for lightweight MAV designs. Additionally, efficiency in hover mode would deteriorate significantly at these high disk loadings.

FIGURE 1.17: Google's "Project Wing" tail sitter vehicle [22]

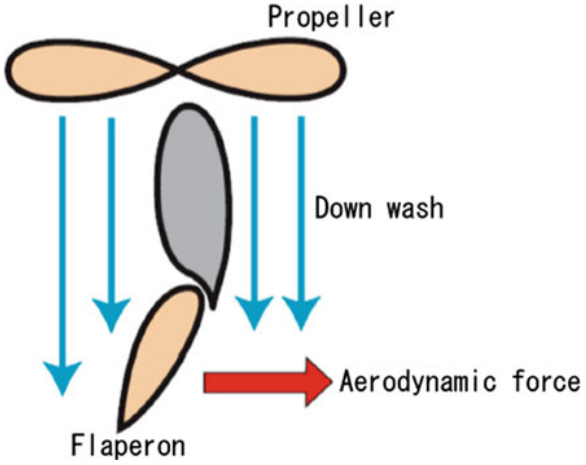

FIGURE 1.18: Propeller downwash used for control forces, [32]

1.2 Objective

To solve the issues outlined above, a novel vehicle concept has been designed and is proposed as an alternate hybrid MAV design concept. This is the quad-rotor

biplane tail sitter. The configuration is a unique and ingenious design and can be seen in Fig. 6.24 in Chapter 6. The advantages of this particular configuration are:

1. The maneuverability of a quad-rotor is utilized in hover
2. Pitching moments to enter and exit the transition flight mode are generated entirely by the relatively large control authority offered by differential rotor thrust and the substantial 'moment-arm' between the rotors
3. Increased compactness with biplane configuration
4. Simple construction and maintenance
5. No additional aerodynamic control surfaces are required

The utilities of this system are greatly improved if the transition maneuver from hover to forward flight can be achieved in a gradual manner without any loss of altitude (Fig. 2.3). This is referred to as equilibrium transition which, by definition, implies that the forces and moments are balanced at every stage of flight. This type of transition is far safer than the "stall-tumble" method typically utilized by most modern tail-sitters. Studies have been conducted in the past to explore the transition of tail-sitters from hover to forward flight [25, 36–40]. However, systematic studies on the performance of micro-scale wing-propeller systems in non-axial flow at low Reynolds number have been limited. In this thesis, these issues are addressed, in order to improve the understanding and implementation of design and control laws for these class of vehicles. Additionally, the work explores numerous important design parameters pertinent to the proposed vehicle design that are used for comprehensive design analysis. The goal of this body of work

is to present a basis for designing, constructing, and testing lightweight, efficient, and versatile MAVs to be used for any modern day flight task.

1.3 Thesis Outline

The outline of the thesis is as follows. A brief description of the vehicle design and system is initially provided in Chapter 2. A few important design parameters, such as choice of propeller, airfoil profile, wing aspect ratio, biplane wing spacing, and propeller-wing offset, among others, are systematically investigated in Chapter 3. In Chapter 4, the performance results of the propeller-wing system in axial and non-axial flow from a series of wind tunnel tests are discussed. Following this, the conditions to achieve equilibrium transition are extracted. A brief description of free flight testing of the quad biplane vehicle to achieve transition flight is presented in Chapter 5. Deficiencies in initial vehicle design and control are highlighted and resolved in Chapter 6, including a necessary roll control study which includes the exploration of three alternate roll control methods. These include pivoting wing tips, shaft tilting, and variable collective pitch. Vehicle versatility and scalability are detailed in Chapter 7 as well, via a package delivery case study. The case study is subsequently validated through a scaling study conducted in the same chapter. Throughout the entire thesis, multiple variants of the original quad-rotor biplanes will be shown in various stages of construction and flight testing, highlighting the overall versatility and longevity of the design.

Chapter 2

Vehicle Proposal

The conceptual design of the quad-rotor biplane is shown in Fig. 2.1. An initial proof-of-concept vehicle was constructed using this proposed design. It consists of two pairs of counter rotating propellers arranged in a quad-rotor configuration. Two wings are affixed to each pair of rotors through a set of rigid motor attachments. The battery and on-board microcontroller are incorporated in the center of the vehicle in a streamlined hub. For propulsion, a series of 2000 kV Hextronix Brushless outrunner motors are used with Turnigy 6-A electronic speed controllers. These specific brushless outrunner motors are utilized, as in this case, they do not require the inclusion of a gearbox. Figure 2.2 shows the complete construction of the proof-of-concept vehicle. The wings are constructed from low density polyurethane foam using a high lift, low Reynolds number airfoil. The wing chord is aligned along the propeller axis. The wing span and aspect ratio are 22" and 5.5 respectively and are spaced about 10" apart. The propellers were chosen to be two-bladed 6" 6x5 GWS SlowFlyer propellers due to their relatively satisfactory hover (power loading = 12 gram/W, figure of merit = 0.59) and forward flight performance (maximum efficiency in axial flow = 0.67). More information regarding the choice of propeller and wing airfoil will be outlined in Chapter 3. The gross weight of the vehicle is approximately 240 grams and a component weight breakdown can be seen in Table 2.1.

The various operating modes of the quad-rotor biplane concept are shown in Fig. 2.3. Vertical take-off and landing operations are performed through conventional quad-rotor mode. The vehicle sits on the trailing edge of its wings when on

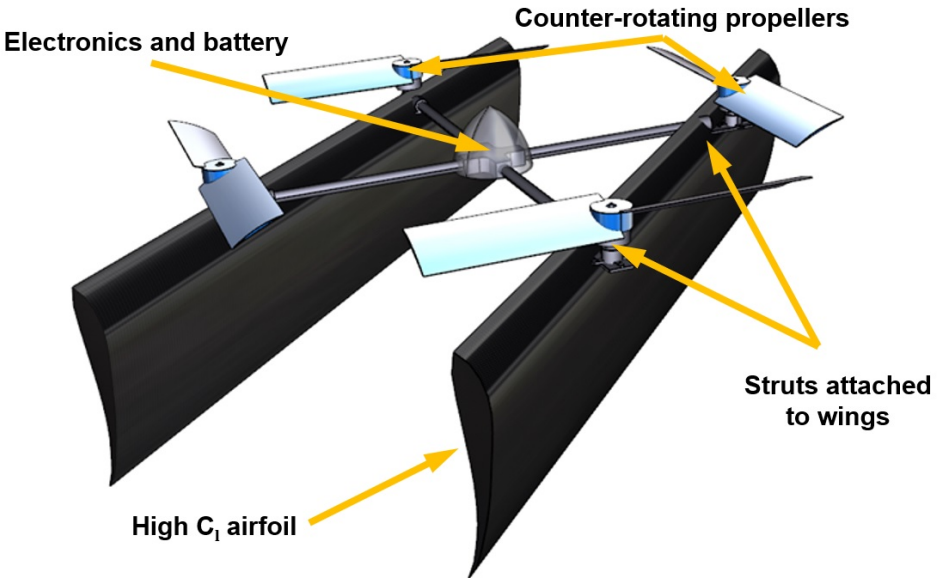

FIGURE 2.1: Conceptual design of quadrotor biplane

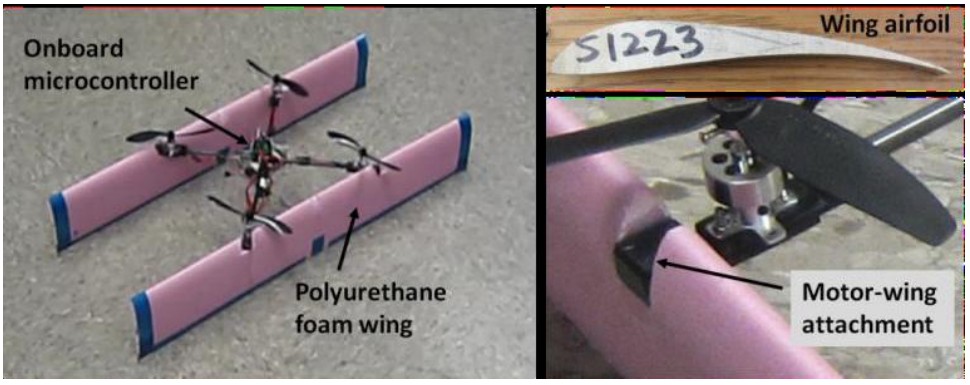

FIGURE 2.2: Constructed vehicle

the ground. Transition is attained through a pitching moment provided through RPM variation of the propellers. Varying RPM of propeller pairs allows for differential thrust which, when coupled with the installed moment arm, generates a sizable pitching moment. As the vehicle enters forward flight mode, at sufficiently high cruise speeds, the loads are then transferred to the wings. The wings are sized to carry the weight of the vehicle at high speeds (above 3 m/s), offloading

TABLE 2.1: Vehicle weight breakdown

Component	Weight (g)
Rotors (4)	8
Motors (w/ speed controllers and wiring) (4)	75
Sensor-processor (w/ aux. battery)	8
Structre and motor mounts	10
Flight battery	70
Total	236

the propellers lift requirements during cruise. It is seen that one of the main utilities of this configuration is that conventional quad-rotor control methodology is retained in both hover and forward flight modes. During these modes, no redundant actuators are required. More information regarding how control is achieved at these different modes, is detailed in Chapter 5.

FIGURE 2.3: Equilibrium transition from hover to forward flight

The pitch, roll, and yaw axes are defined based on the inertial frame in hover mode, instead of than the vehicle body frame. These axes are invariant to transition and body pitch angle, α. Therefore, it can be seen that as the vehicle transitions from hover to forward flight, the roll and yaw axes change with respect to the body frame of reference. This is illustrated in Fig. 2.4. Banking and turning can be achieved in any mode through the available control moments, which will be explored in greater detail in a later section (Chapter 5). Using this, it is also

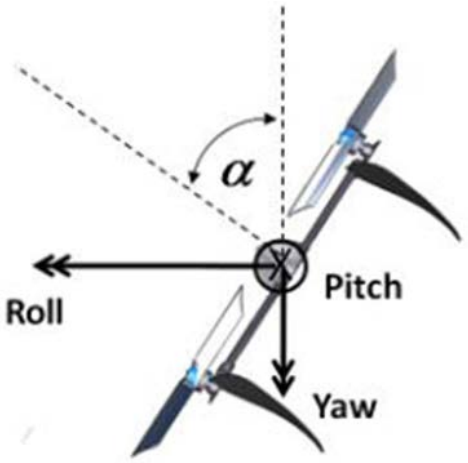

FIGURE 2.4: Vehicle with non-zero pitch angle

envisaged that associated gyroscopic forces and propeller slipstream effects during these maneuvers can be handled appropriately.

Chapter 3

Design Studies

The objective of this section is to investigate the performance effects of certain design parameters typical of the quad-rotor biplane configuration through a series of wind tunnel tests. These parametric studies included studying the choice of the vehicle's propeller, wing airfoil, wing aspect ratio, wing spacing, as well as propeller-chord alignment (refer to Fig. 2.1). The effects of closing the wing sections via a boxed-wing configuration is also explored. Some of these design criteria were found to present a trade-off between vehicle compactness and desirable performance. As a result, design principles were established in order to build a lightweight and efficient quad-rotor biplane to be used in future studies.

3.1 Choice of Propeller

Since the vehicle is designed to operate in hover and forward flight, a choice of propeller with preferable axial flight characteristics as well as high hover efficiency is important. Based on previous rotary wing MAV designs and tests [6, 23], hover disk loading below 70 N/m^2 is appropriate for satisfactory performance. Therefore a small, representative set of propellers were chosen for comparison. These included:

1. 5x3 GWS 3-blade
2. 6x3 GWS 3-blade
3. 6x5 GWS 2-blade

4. 7x3.5 GWS 2-blade

These propellers were tested on a micro-scale rotor stand in both static and axial flow conditions. This test setup was installed in front of a 22" x 22" open jet wind tunnel as detailed in Fig. 3.1. The stand consists of a shaft attached to a torque sensor. This torque sensor is then connected to a thrust load sensor through a low friction bearing mechanism. A Hall Effect sensor provided the rotational rate of the propeller. For each propeller, the wind speed was varied from static (0 m/s) to up to approximately 10 m/s. For each wind speed, an RPM sweep was conducted (3000-7000) and the thrust produced and mechanical power consumed were measured. From the thrust and power curves, the efficiency of each propeller was extracted and compared as a function of advance ratio. The mean errors in thrust, power, RPM and wind speed measurements were determined to be about 0.01 N, 0.1 W, 50 RPM, and 0.1 m/s respectively.

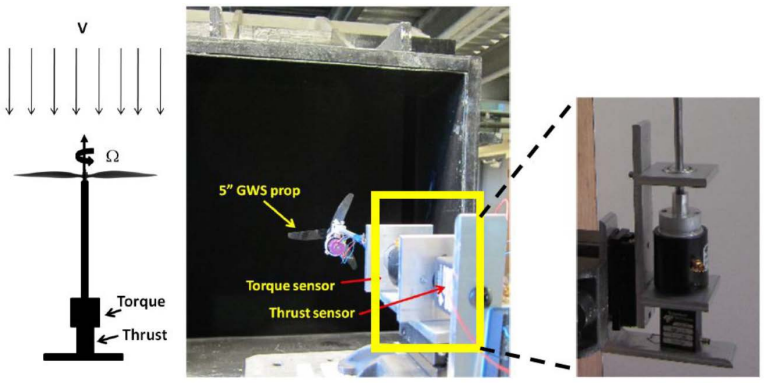

FIGURE 3.1: Setup to measure propeller performance in axial flight

Hover performances of the propellers are compared in Fig. 3.2(a). It can be seen that the performance of all the propellers are satisfactory with a power loading of about 11-12 grams/W. However, since the vehicle is designed to operate mostly in cruise, it is important to compare the forward flight performance of the vehicle.

From a measurement of the thrust and power at a given wind speed and propeller RPM, efficiency curves for the propeller can be extracted using the following non-dimensional forms, consistent with propeller terminology:

$$\text{Thrust coefficient} : C_T = \frac{T}{\rho n^2 D^4} \tag{3.1}$$

$$\text{Power coefficient} : C_P = \frac{P}{\rho n^3 D^5} \tag{3.2}$$

$$\text{Advance ratio} : J = \frac{V}{nD} \tag{3.3}$$

$$\text{Propeller efficiency} : \eta = J\frac{C_T}{C_P} \tag{3.4}$$

In these equations, T is the propeller thrust, P is the mechanical power required, n is the propeller rotation frequency in Hz, D is the propeller diameter, V is the axial flow velocity, and ρ is the density of air. The variations in propeller efficiency, η, with advance ratio, J, for RPMs between 3000 and 7000 are compared in Fig. 3.2(b). From this plot, it can be seen that the 7x3.5 propeller has undesirable performance, both in hover and forward flight. This is most likely a result of the lower twist and root collective pitch. The three-bladed rotors offered a highest efficiency of 0.45 and this occurred at low advance ratios of about 0.4. However, the highly twisted 6x5 propeller provided the best overall efficiency of 0.67, occurring at high advance ratios. Due to its superior axial flow performance and a satisfactory hover power loading, the 6x5 propeller was chosen to be installed on the vehicle.

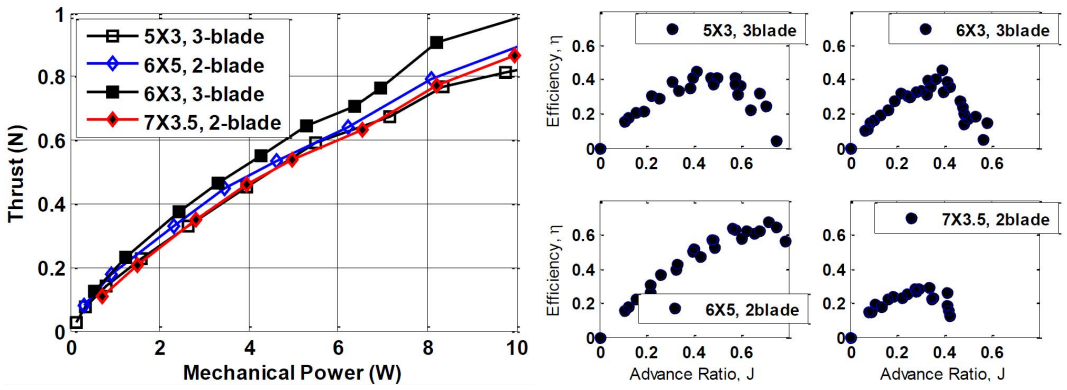

(a) Hover performance comparison

(b) Axial flow efficiency comparison

FIGURE 3.2: Propeller performance comparisons

3.2 Parametric Studies

In this section, several design criteria that influence system performance are systematically investigated. These parameters include:

1. Airfoil profile
2. Wing aspect ratio
3. Wing spacing in biplane configuration
4. Offset of propeller shaft axis relative to wing chord

Each parametric study can then be expanded for a more comprehensive vehicle design investigation.

3.2.1 Airfoil Selection

For the given design, the vehicle would be operating in a low Reynolds number regime with large variations in angles of incidence in its flight profile. In order

to keep the vehicle compact, low aspect ratio wings would also most likely be incorporated. Therefore, it is very important to choose an efficient airfoil profile with desirable flight characteristics, such as high maximum lift coefficient and gentle stall. A few candidate low Reynolds number airfoils that produced high C_L and C_L /C_D values (at Re $\cong$ 50,000) were selected from a previous study conducted on low Reynolds number airfoils [41]. These are shown in Fig. 3.3 and they include:

- Selig S1223: This is a high lift low Reynolds number airfoil (Fig. 3.3(a)) with a maximum thickness of 12.1% and a camber of 8.1% ($C_{m_0} = 0.24$).
- Gottingen GOE225: The Gottingen 225 airfoil is shown in (Fig. 3.3(b)) with a maximum thickness of 12.8% and camber of 7.6% ($C_{m_0} = 0.2$). As can be seen, this is similar to the S1223 airfoil.
- Wortmann FX63-100: As can be seen from (Fig. 3.3(c)), the maximum thickness-to-chord is lower (about 9.9%) and the camber is 4.3% ($C_{m_0} = 0.07$).

In order to measure the performance of the airfoils listed above, an experimental test stand was developed as shown in Fig. 3.4(a). The stand consists of a variable angle base plate that allows for a range of 180° with 3° increments. The rotating and non-rotating plates are locked at desired angle settings using a lock pin. Wings with the desired airfoil profiles were cut out of extruded polypropylene and a 1/4" aluminum rod was installed at quarter chord along the length of the wing to allow for attachment to the test stand. Due to the low density of the wing material, there was a tendency for the wing to exhibit large vibratory motion during tests. Therefore, the dimensions of the rod were carefully chosen to prevent

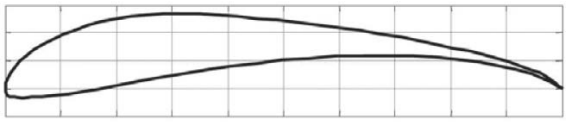

(a) Selig S1223

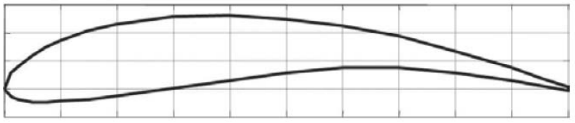

(b) Gottingen GOE 225

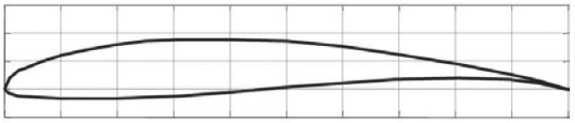

(c) Wortmann FX 63-100

FIGURE 3.3: List of tested high performance airfoils

undesirable vibrations. A small coupling piece was used to interface the 6 degree of freedom load sensor (the Nano17 F/T sensor) and the rotating base-plate with the aluminum rod. The test stand was then mounted in front of the open jet wind tunnel as shown in Fig. 3.4(b). The wings had an aspect ratio of approximately 3.8, as each had a span of 17" and a chord measuring 4.5". Care was also taken to place the wing within the 18° wind tunnel contraction zone to avoid undesirable flow effects in contraction areas. The wind speed was varied from 0 to 10 m/s with an angle sweep from 30° to 45° in steps of 3°. The lift and drag measurements for each airfoil section, wind speed, and angle of attack were averaged from three measurements to minimize error and account for drift. The measurement errors for wind speed and forces were about 0.1 m/s and 0.02 N respectively. For comparison, the lift and drag measurements were resolved to their respective non-dimensional coefficients. It should be noted that these coefficients are calculated for the wing and do not represent the 2-D values. A comparison between different aspect ratios

is performed in Section 3.2.2 to evaluate 3-D effects.

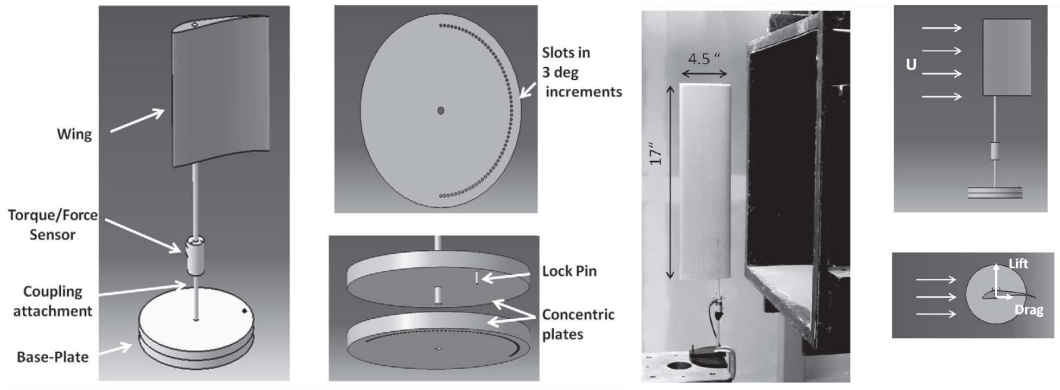

(a) Experimental test setup to measure performance (b) Airfoil test stand

FIGURE 3.4: Airfoil test apparatus

The lift and drag coefficient variation is compared for the three airfoils at a representative Reynolds number of 45,000 which occurs at a wind speed of 6.2 m/s. This comparison is shown in Figs. 3.5(a) and 3.5(b). As can be seen from Fig. 3.5(a), the 8.1% cambered S1223 airfoil consistently produced higher lift at all angles of attack. Also, it is shown that the drag for the FX 63 airfoil was the least, as in Fig. 3.5(b). Based on the drag polar plot shown in Fig. 3.5(c), it can be seen that the FX 63 had the best overall performance with a maximum C_L/C_D approximately equal to 5.5. For comparison, the other airfoils achieved a lower maximum C_L/C_D of about 4. Additionally, the variation of C_L/C_D versus C_L was close to uniform over a wider range of C_L values. The relative performances of these airfoils were found to be quite similar at other Reynolds numbers (20,000 to 60,000) as well. This is important since the vehicle wing Reynolds number varies with equilibrium angle of attack and flight speed. It should also be noted that during actual vehicle operation, much of the span of the wing operates within the propeller downwash. Therefore, it is important to choose an efficient airfoil with low

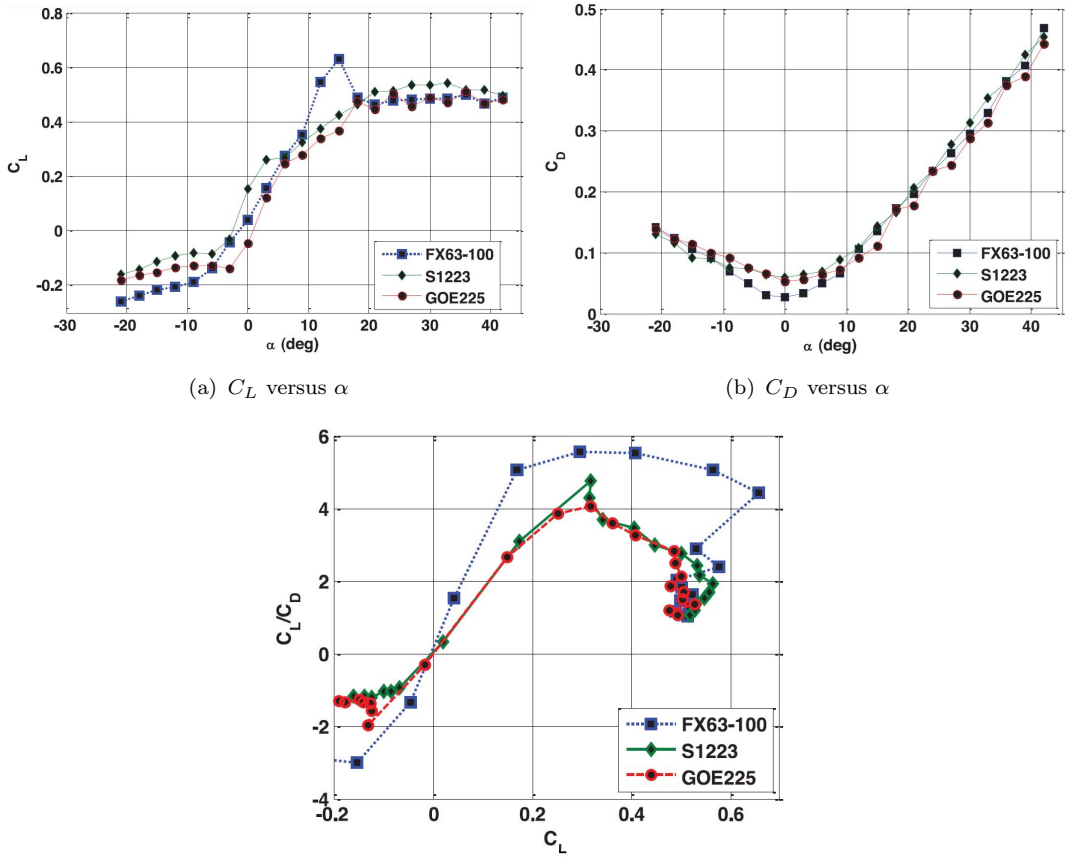

(a) C_L versus α

(b) C_D versus α

(c) C_L versus C_D

FIGURE 3.5: Comparison in airfoil performance at Re = 45,000 (V = 6.2 m/s)

drag characteristics and sufficient lift capability. Based on the above discussion, the FX 63 airfoil was chosen for vehicle implementation and further investigation.

3.2.2 Effect of Aspect Ratio

When designing an MAV, one of the chief concerns is the trade-off between efficiency and compactness. This issue is important in wing design, as illustrated in Fig. 3.6. Incorporating a low aspect ratio wing has the advantage of compactness, but suffers from a decreased performance as compared to a wing with a higher aspect ratio. On large scale fixed-wing aircraft, this degraded performance

is attributed to increases in induced drag. For small-scale vehicles, while the trade-off in compactness is clear, the differences in performance at these low Reynolds number regimes is less obvious. Therefore, the aerodynamic performance of three representative wings with aspect ratios 3.8, 2.4, and 1 (Fig. 3.7) were measured and compared. It is noted that this is different from the aspect ratio of 5.5 selected for the original prototype vehicle. However, it is within range of the aspect ratio for the one-quarter propeller-wing system, which was studied in the wind tunnel. The wing area was maintained at approximately 0.05 m^2 for each case. An alternative method for studying the effects of varying aspect ratio is to keep the wing span constant and alter only the chord length. However, since the wing area is not invariant and is sized specifically for the vehicle, the gross effects on equilibrium speed and shaft angle would be significantly affected. To avoid these problems, the wing area was held constant throughout. The experimental setups shown in Figs. 3.4(a)and 3.4(b) and test matrices outlined in Section 3.2.1 were utilized for the aspect ratio tests, as well.

FIGURE 3.6: Wing aspect ratio trade-off: efficiency and compactness

Figure 3.8 shows the variation of C_L with respect to aerodynamic angle of attack, α, for two different wind speeds and wings with aspect ratios 1 and 2.4. The C_L versus α variation for the 3.8 aspect ratio wing was shown previously in Fig. 3.5(a). It can be seen that the C_L versus α slope increases with aspect ratio as expected. It must be mentioned that, because the Reynolds number is based on wing chord, the lower aspect ratio wing operates at higher Re for the same wind speed. This

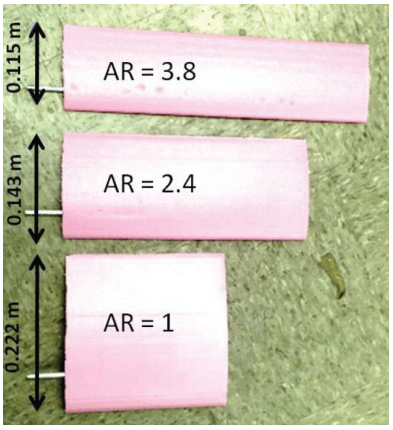

FIGURE 3.7: Wings tested with different aspect ratios

might explain the higher values of C_L at lower aspect ratios for a specified wind speed. Thus, it is not trivial to gauge the effect of Reynolds number through aspect ratio alone. The drag polars are compared in Fig. 3.9(a) at similar Re. It can be clearly seen that the performance improves as aspect ratio increases. However, the performance increase between AR=2.4 and AR=3.8 wings appears to be less significant, representing a point of diminishing returns. From a vehicle operation perspective, it is more meaningful to compare performance at the same wind speed (instead of Re). As can be seen from Fig. 3.9(b), the differences in performance between the larger aspect ratio wings is negligible. Therefore, it can be argued that from a standpoint of both compactness and efficiency, a wing with aspect ratio of 2.4 should be incorporated into the quad-rotor biplane. A future direction intended to be pursued as a result of this study is to examine the effect of propeller slipstream on wing performance. This would provide a more realistic comparison between high and low aspect ratio wings as applicable for the proposed vehicle design.

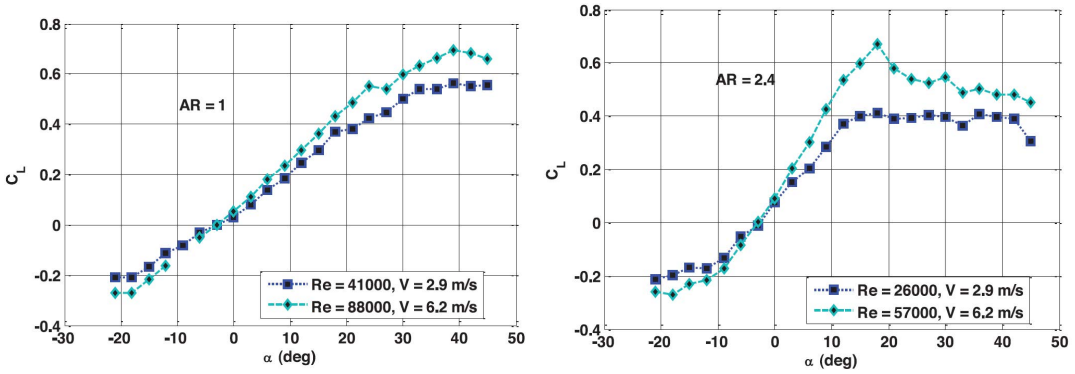

(a) Aspect ratio = 1 (b) Aspect ratio = 2.4

FIGURE 3.8: C_L versus α comparison at different wind speeds

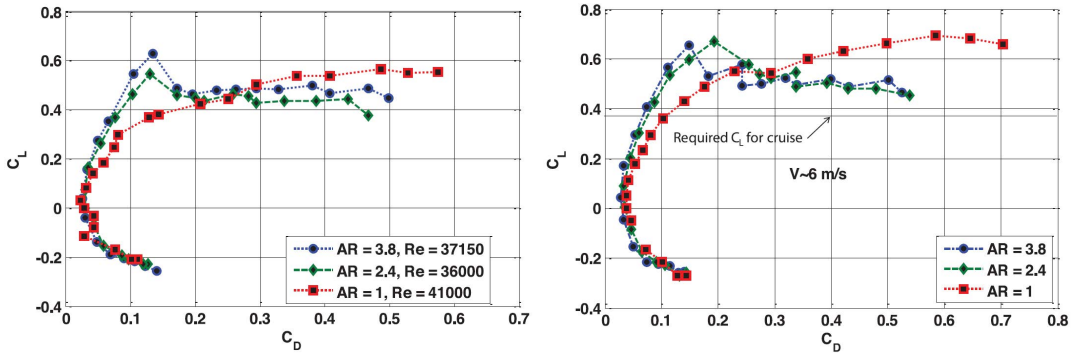

(a) Similar Re (b) Similar wind speed

FIGURE 3.9: Drag polar comparison showing diminishing returns as aspect ratio increases

3.2.3 Wing Spacing

Since the vehicle operates in a biplane configuration, it is also important to quantify the effect of the vehicle wing spacing on overall performance. To do this, two FX 63 wings with an aspect ratio of 2.4 (wing chord = 5.5") were attached to coupling struts and the Nano17 F/T sensor. The system was then mounted in front of the open jet wind tunnel as shown in Fig. 3.10. The wing spacing, r, was varied from 7" to 11" in steps of 1". As is done on the quad-rotor biplane,

both of the wing chords were installed parallel to each other. The angle of incidence and wind speed variation were the same as the experiments detailed in Section 3.2.1 and 3.2.2. The net lift and drag of the system were measured as shown in Figs. 3.11(a), 3.11(b), and 3.11(c). The drag forces from the exposed linkages were carefully removed from the total force through a separate series of tare tests. It must be noted that since both the wings were pivoted about a central point, a change in angle of incidence would result in a negative stagger, meaning that the top wing is oriented behind the bottom wing. This was intended to simulate actual vehicle operating conditions during the different stages of flight.

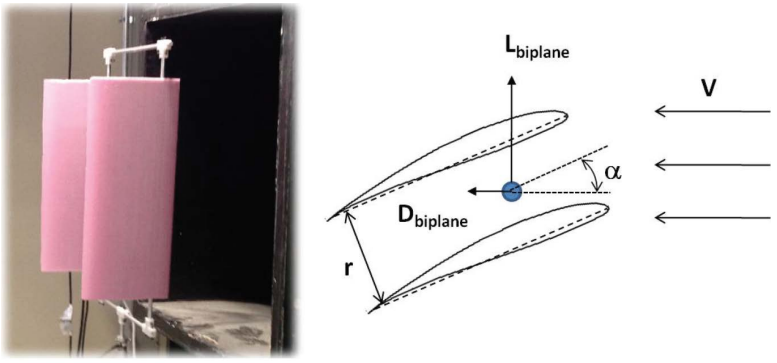

FIGURE 3.10: Wings mounted in biplane configuration to study effect of wing spacing on force production

Lift and drag coefficients were extracted from the measured forces using the total biplane wing area ($A_{\text{biplane}} = 2A_{\text{wing}}$) as shown in Eq. 3.5.

$$C_{L_{\text{biplane}}} = \frac{2L_{\text{Biplane}}}{\rho A_{\text{biplane}} V^2}, C_{D_{\text{biplane}}} = \frac{2D_{\text{biplane}}}{\rho A_{\text{biplane}} V^2} \tag{3.5}$$

Figures 3.11(a) and 3.11(b) show the net lift and drag coefficient variation with angle of incidence for the biplane configuration for these wing spacings. It can be clearly seen from Fig. 3.11(a) that the effect of decreased wing spacing is a reduction in lift. For example, at an angle of incidence of 10°, the lift produced

with 7" spacing is about 15% lower than that for the 11" spacing. However the differences in drag are negligible. The differences in performance are also evident in the drag polar plot featured in Fig. 3.11(c). From a comparison between Figs. 3.9(b) and 3.11(c), it is also interesting to observe that the net lift coefficient for the biplane configuration with 11" spacing is only about 10% lower than that produced by a single wing. Based on the above observations, a wing spacing of at least 1.5c is desirable, where c is the wing chord length. However, if a low aspect ratio wing, meaning a wing with a longer chord length, is required, these wing spacing constraints may not be met. Therefore, a trade-off in efficiency is to be expected.

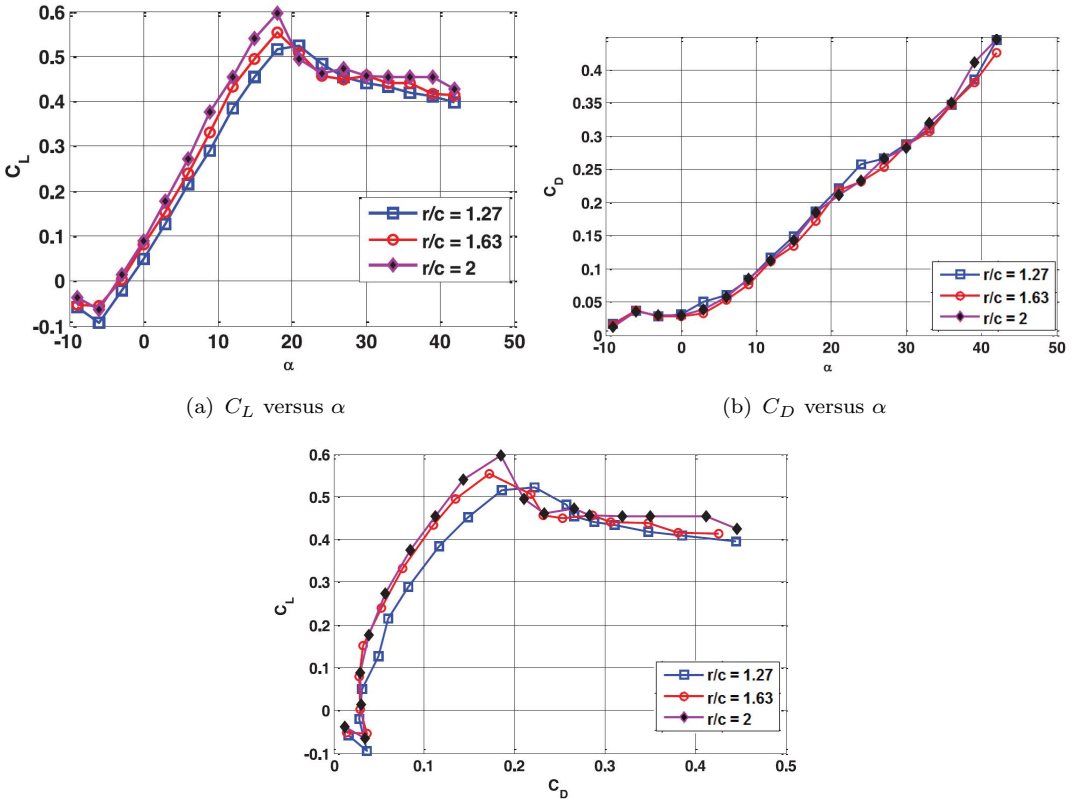

(a) C_L versus α

(b) C_D versus α

(c) C_L versus C_D

FIGURE 3.11: Effect of wing spacing on performance at Re = 45,000 (V = 6.2 m/s)

3.2.4 Propeller Shaft Offset

It is shown in Chapter 4 that the interaction effects between the propeller and wing are significant. In the design space considered in this chapter, the effect of offset between propeller shaft and wing chord on the forces generated is studied. One of the motivations of this study is to improve compactness which is possible by reducing wing span. The constraint for the span is then set by the dimensions of the propeller. Therefore, during this set of tests, the entire wing span was contained within the downwash of the propeller. The resulting wing-propeller system included a 6" diameter propeller and an FX 63 wing with dimensions of 6" span and 4.5" chord. This system was subsequently tested in front of the wind tunnel and all results pertain to this specific propeller-wing combination. The offset is defined as the perpendicular distance between the propeller shaft and wing chord as shown in Fig. 3.12. The setup was tested for the following shaft axis placements:

1. 1" below wing chord
2. Along wing chord
3. 1" above wing chord

The propeller RPM and shaft angle were varied from 2000 RPM to 5000 RPM and from 0^o to 45^o respectively. The forces measured by the load sensor were resolved to forces perpendicular and parallel to the mean free stream velocity. These forces are referred to as lift and thrust respectively. For the purpose of clarity, sample results are shown in dimensional form for a single wind speed and three shaft angles.

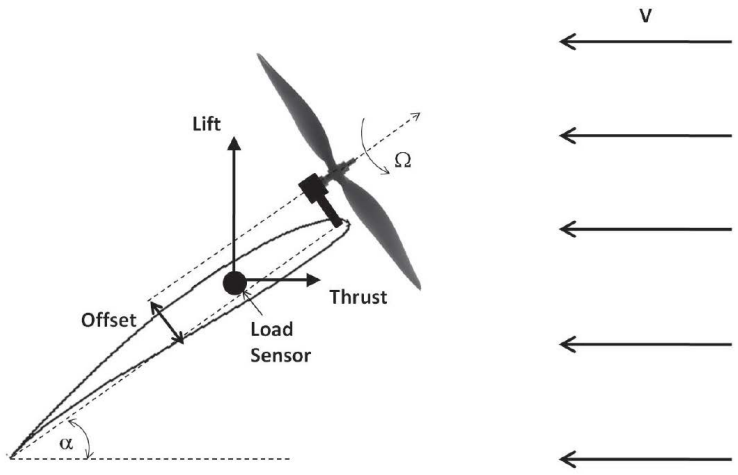

FIGURE 3.12: Offset between propeller shaft axis and wing chord and forces produced

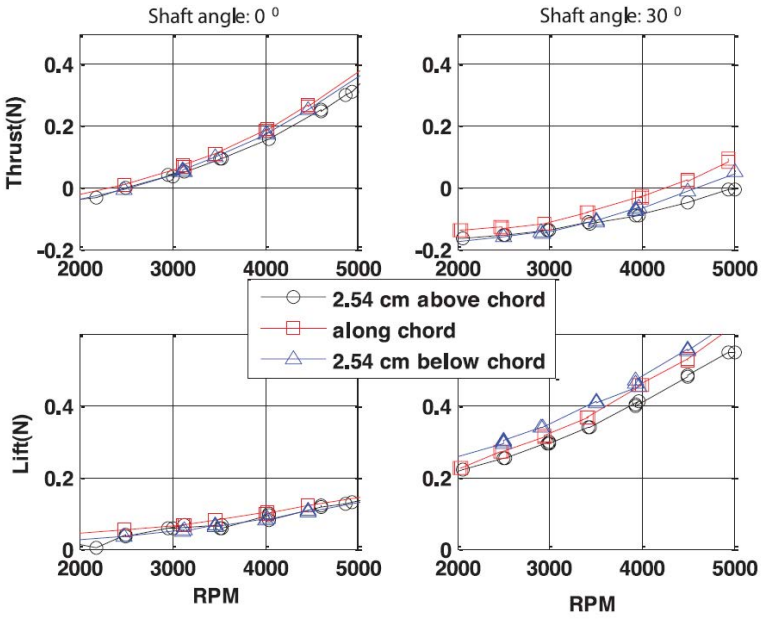

FIGURE 3.13: Effect of propeller offset on forces at 6.2 m/s wind speed

Figure 3.13 illustrates the effect of propeller-chord offset on thrust and lift for three different shaft angles at a fixed wind speed of 6 m/s. It is shown that for all three offset values, the net thrust is reduced and the net lift is increased as the shaft angle is increased. It is important to note that for almost all test cases, when

the propeller is positioned above the wing chord, the net thrust and lift are lower. This is a condition which should be avoided during vehicle construction when possible. At a shaft angle of 30° and propeller RPM of 4000, when the propeller is placed 1" above wing chord, the lift produced is about 10% lower than that for the other positions. However, the difference between 0 and -1" offset appears to be less significant. It can be noted that measurement error in forces was merely about 0.03 N. Overall, the placement of the propeller axis along the wing chord line was deemed a suitable design criterion.

3.3 Box Wing

In an effort to improve vehicle performance, design alterations were conducted on the quad-rotor biplane. Performance improvements were sought via the inclusion of aerodynamic surfaces. To prevent undesirable flight tendencies, such as side-slip, and provide adequate performance in different flight regimes, typically aerodynamic control surfaces are utilized on aerial vehicles. However, one of the main benefits of the quad-rotor biplane configuration is its lack of these control surfaces and hence a much lower number of moving parts. Since the vehicle does not use these measures to aid in its control and performance, the potential merits of a simple, passive method were investigated; a boxed, or closed, wing. Boxed wings, such as the Prandtl wing, have many benefits including reduced induced drag over the wing, reduced turbulence, and increased fuel economy [42]. This wing design method was studied in order to visualize the effect on vehicle induced drag.The wing system can be seen below in Fig. 3.14. The wing tips are closed by a thin 1/16" sheet of polyurethane foam and each weighs approximately 5 grams.

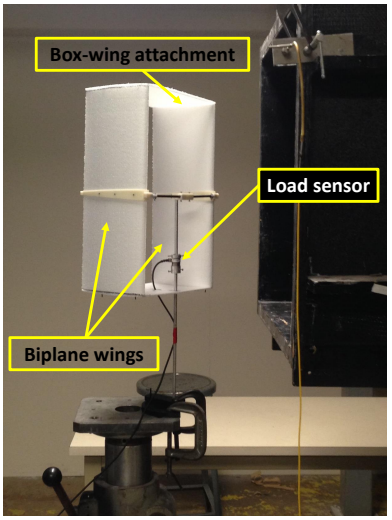

FIGURE 3.14: Boxed wing system and test setup

The wing section was constructed and placed in an open jet wind tunnel where it was subsequently tested for lift and drag. Again, Fig. 3.14 shows the test setup. The wing system, consisting of two wings with AR = 2.4, was mounted onto a 6-axis force and moment transducer and subjected to a range of wind speeds between 2 to 10 m/s and pitch angles ranging from -9^{o} to 45^{o} degrees, both with and without the foam tip connectors. Figure 3.15 show the performance for the system in both configurations. From these plots, it can be seen that the simple box configuration actually leads to a slight increase in overall drag. The potential reductions in induced drag on a low aspect ratio wing were more than offset by the increased profile drag of the boxed portion of the wing. As a result, this wing style was not implemented on the quad-rotor biplane.

3.4 Measurement Transducers

In order to help validate the proposed vehicle design, the data provided must be determined to be highly accurate. When the studies shown in this chapter as well

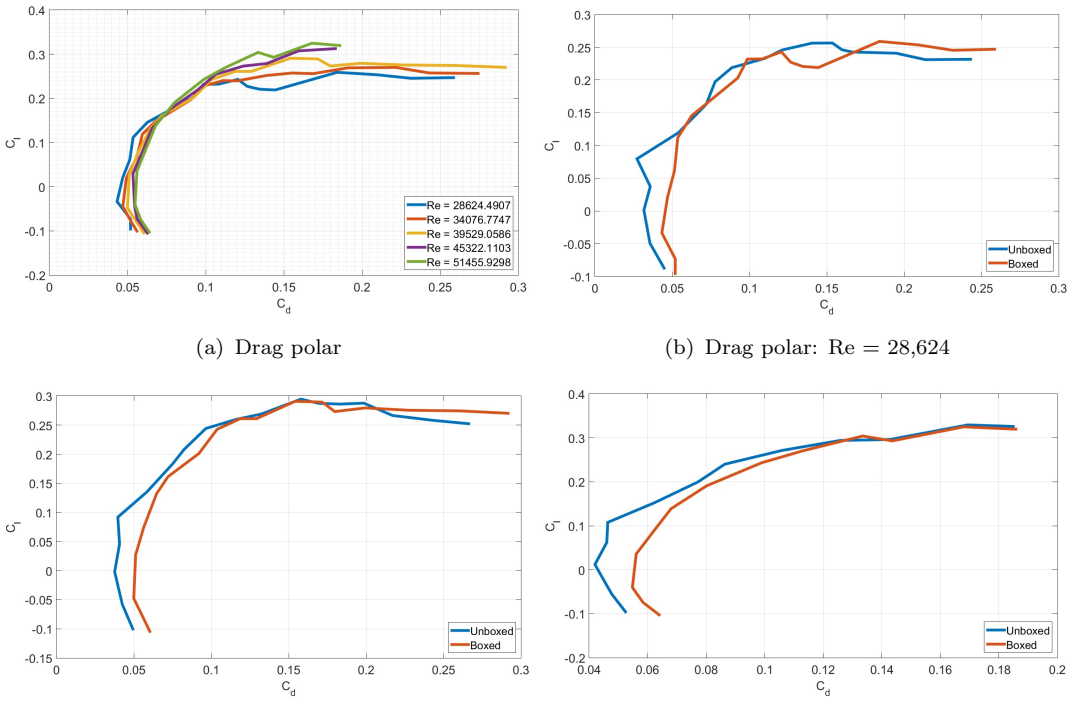

(a) Drag polar

(b) Drag polar: Re = 28,624

(c) Drag polar: Re = 39,529

(d) Drag polar: Re = 51,456

FIGURE 3.15: Performance plots for biplane system with and without box

as Chapter 4 and 6 were conducted, the measuring devices had uncertainties which can be seen below in Table 3.1. This table details the performance specifications for the measurement transducers utilized in all aerodynamic testing conducted in this thesis. These include the Nano17 6 degree of freedom sensor as well as the tacometer and wind tunnel controller. Pertinent specifications include information supplied and accuracies.

TABLE 3.1: List of measuerment accuracies

Parameter	Device	Uncertainty [English]	Tolerance [SI]
RPM	Tacometer	±10 [RPM]	±10 [RPM]
Forces	Nano17 F/T sensor	±0.01 [lb]	±0.05 [N]
Shaft angle, α	Digital level	±1[^{o}]	±1[^{o}]
Wind speed	Wind tunnel gauge	±0.25 [ft/s]	±0.076 [m/s]
Torque	Nano17 F/T sensor	±0.0004 [lb-ft]	±5.000 [g-cm]

3.5 Conclusions

This chapter discusses the alteration of the quad-rotor MAV's design and the subsequent effects on performance. This investigation was conducted through a systematic series of bench-top wind tunnel experiments. Parameters investigated included choice of propeller, airfoil profile, wing aspect ratio, biplane wing spacing, offset between propeller shaft and wing chord, as well as closing the vehicle's wings. A comparison between three relatively efficient high lift low Reynolds number airfoil showed that the 4.5% camber FX 63 airfoil had the best efficiency at low angles of attack. It was found that the difference in performance between wings with aspect ratios of 3.8 and 2.4 was found to be negligible. A biplane wing spacing of at least 1.5 times the wing chord length may be required to have the least interference effect on performance. However, if a low aspect ratio wing is required, such wing spacing constraints may not be met and a trade-off in efficiency is to be expected. It was seen that placement of the propeller axis along the wing chord provided the best performance. Finally, a box wing system was tested with representative vehicle dimensions to study aerodynamic effects at this micro-scale. It was shown that the closed wing configuration did not provide beneficial performance characteristics. The above design space can be further expanded and made comprehensive for future design optimization studies for the quad-rotor biplane.

Chapter 4

Aerodynamic Studies

In Chapter 3, the choice of propeller was established and its individual performance in hover as well as in axial forward flight was studied. Wing performance is also studied on its own as detailed in Chapter 3. An important aspect of this vehicle is it ability to perform hover, transition, and forward flight tasks. It is therefore important that the aerodynamic performance of the propeller-wing system at all angles of transition is investigated: from hover at 90° to horizontal flight at 0°. This involves operation of the propeller with components of upstream momentum in directions which are both parallel and perpendicular to the propeller plane. In other words, the propeller is operating in non-axial flow. From this, the parameters required to achieve trimmed flight at various flight speeds can be extracted and studied.

FIGURE 4.1: "One-quarter" system utilized in aerodynamic studies, shown in stages

The objective of this section is to study the performance of the propeller-wing system as a part of the quad-rotor biplane and to investigate the interaction effects between the two force contributors; the propeller and the wing. A "one-quarter" system (seen in Fig. 4.1) based on the quad biplane design, comprised of a propeller

and a proportionally sized wing, was investigated through a series of wind tunnel tests. First, the isolated propeller is studied at various angles of transition and non-axial wind. The wing is subsequently added to the propeller system to study the resulting interaction effects. Finally, important operating variables including propeller RPM and transition angle are extracted for given flight speeds that result in the trim case, meaning steady, level flight. Additionally the power requirements are extracted that can be used to improve flight speed and maximize efficiency in future designs.

4.1 Wing Performance

For the quad-rotor biplane to achieve flight in the horizontal cruise configuration, each wing on the vehicle would have to produce at least 1.2 N of lift while the propeller is thrusting in the horizontal direction. In order to ensure sufficient lift production, a representative wing was mounted on the Nano17 F/T sensor in front of the open jet wind tunnel and tested in flow. The testing was conducted prior to the design studies outlined in Chapter 3 and, as such, the wing was made using the S1223 airfoil geometry originally utilized on the vehicle. The wind speed was varied from 0 to 10 m/s and the wing was tested at angles of attack varying from 0° to 45°. Figure 4.2(a) shows the variation of wing lift with angle of attack. It is seen that the minimum speed that can be achieved by the vehicle while still producing the required amount of lift is approximately 6 m/s. Figure 4.2(b) shows the drag curves for the vehicle wing at different angles of attack. From this plot, it is found that a satisfactory lift to drag ratio of about 10 is achieved at an angle of attack between 3° and 6°. It is evident that the chosen wing properties produce

sufficient lift and also have acceptable performance characteristics based on these observations.

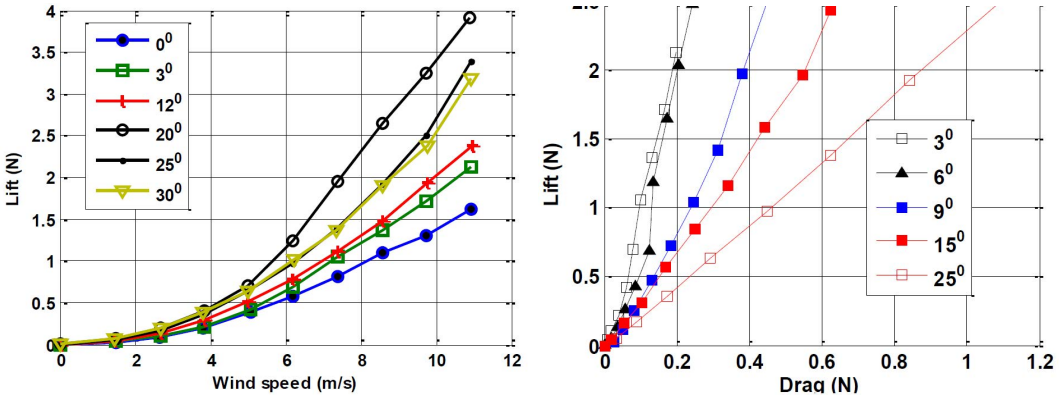

(a) Lift versus angle of attack for different wind speeds (b) Drag versus angle of attack for different wind speeds

FIGURE 4.2: Wing performance plots for S1223 airfoil of aspect ratio 2.8

4.2 Isolated Propeller in Non-Axial Flow

Since the vehicle is designed to operate in hover as well as in forward flight mode, it is necessary to study the aerodynamic performance of the propeller at various angles of transition between these two distinct modes. Experimental and numerical studies have been conducted in the past to study equilibrium transition mode of tail sitters [36–40]. However, to the author's knowledge, there have been limited studies on propeller performance in non-axial flow conditions especially at the low Reynolds numbers observed on the rotors of the quad biplane (Re $\cong$ 50,000). Therefore, a systematic series of experiments was performed to observe important performance characteristics at various forward flight speeds and angles of transition. These include vertical and horizontal components of the propeller thrust as well as the power required to drive the propeller in these conditions. Based on

these measurements, any key differences that may arise when a wing is added to the propeller system can be identified.

In the wind-off case, the propeller produces a force F_z along its rotation axis. Hence the vertical and horizontal forces, otherwise noted as lift and drag, can be rewritten as functions of shaft angle, α and axial thrust, F_z. These relationships are shown below.

$$L = F_z \sin(\alpha) \tag{4.1}$$

$$T = F_z \cos(\alpha) \tag{4.2}$$

However, in the presence of forward wind, there is a change in magnitude and direction of the upstream air flow momentum. As a result, there are forces produced in directions both parallel and perpendicular to the propeller's axis of rotation. F_z still represents axial thrust parallel to the rotor, however, there is a new force, F_y, which is perpendicular to the rotor shaft axis. Figure 4.3 shows a schematic of the forces generated by a propeller in the static case as well as non-axial flow. The net vertical and horizontal forces are then resolved as shown:

$$L = F_z sin(\alpha) + F_y cos(\alpha) \tag{4.3}$$

$$T = F_z cos(\alpha) - F_y sin(\alpha) \tag{4.4}$$

In order to study the variation of these forces with shaft angle and wind speed, a suitable test matrix was designed and experiments were performed. Based on

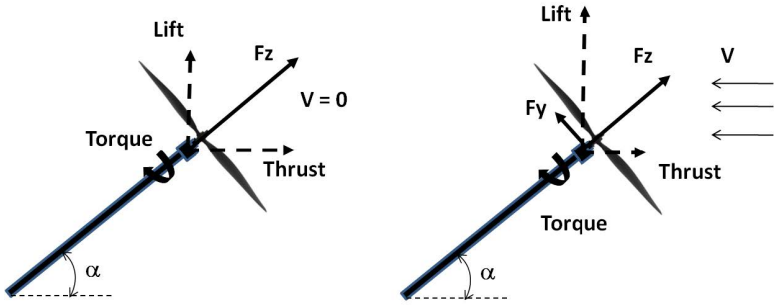

FIGURE 4.3: Propeller forces in non-axial flow

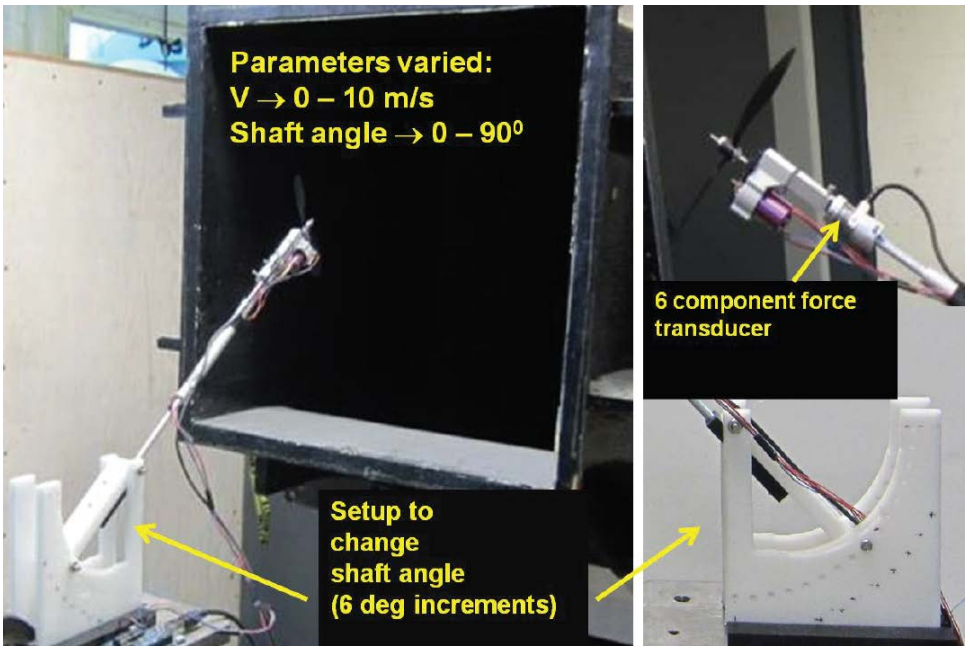

FIGURE 4.4: Setup to measure propeller performance

considerations from the static and axial flow propeller performance tests detailed in Chapter 3, the 6x5, two-bladed propeller was mounted on a stand in front of the open jet wind tunnel as shown in Fig. 4.4. The Nano17 F/T sensor was attached to one end of the propeller shaft and motor. The other end of the shaft was mounted to a setup that allows for changes in shaft angle with respect to the wind. Caution was taken to ensure throughout all tests that the mean position of the propeller was about 3" in front and at the center of the wind tunnel exit plane regardless

of shaft angle. The procedure for the non-axial flow propeller tests was as follows:

1. Select shaft angle
2. Operate wind tunnel to desired velocity
3. Remove tare values and zero out the force measurements
4. Drive the propeller at desired RPMs and take measurements of power required and forces produced

Steps 1 through 4 were repeated for shaft angles ranging from 0° to 90° in steps of 6°. The wind velocity was varied from 0 to 10 m/s. In each test case, measurements were repeated three times for error estimation and repeatability checks. As mentioned earlier, hover mode corresponds to a shaft angle of 90°.

For clarity, the results will look at propeller performance at a small group of representative shaft angles and wind speeds. First, the effect of wind speed on performance will be studied at the specified shaft angles. Then, the effect of shaft angle on performance will be discussed at the representative wind speeds. All results are presented in dimensional form to avoid confusion with definitions of non-dimensional parameters in non-axial flow.

4.2.1 Effect of Wind Speed

Figure 4.5 shows the variation of vertical and horizontal forces at different wind speeds for three different shaft angles. These forces will be referred to as lift and thrust respectively. Both lift and thrust exhibit a quadratic variation with RPM for all cases of shaft angle and wind speed. At high shaft angles, such as 84°, the generated propeller force is delegated mainly to lift. The horizontal

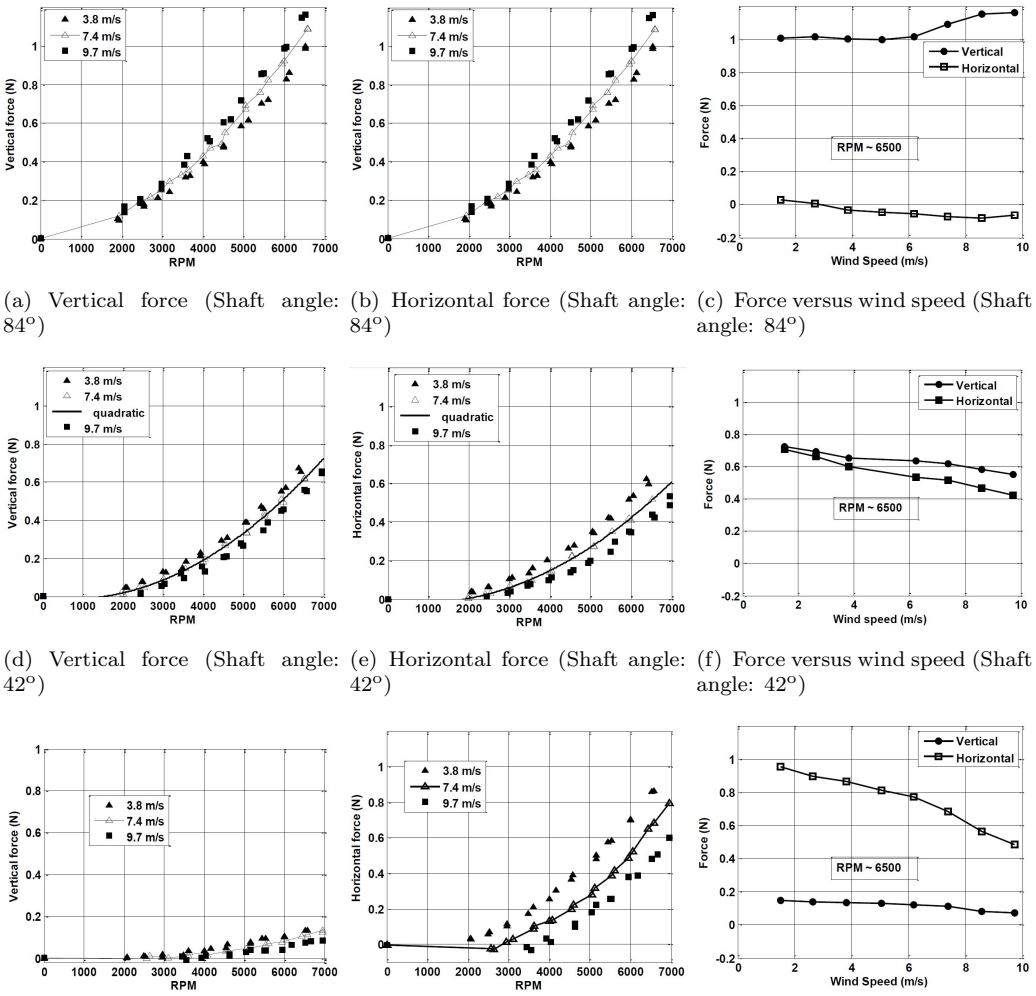

(a) Vertical force (Shaft angle: 84°) (b) Horizontal force (Shaft angle: 84°) (c) Force versus wind speed (Shaft angle: 84°)

(d) Vertical force (Shaft angle: 42°) (e) Horizontal force (Shaft angle: 42°) (f) Force versus wind speed (Shaft angle: 42°)

(g) Vertical force (Shaft angle: 6°) (h) Horizontal force (Shaft angle: 6°) (i) Force versus wind speed (Shaft angle: 6°)

FIGURE 4.5: Variation of forces with RPM and wind speed for isolated propeller at various shaft angles

force, which can be seen is a small fraction of the total force, is negative due to the effect of drag over the rotating propeller. The magnitudes of both lift and thrust increase marginally with wind speed as can be seen from Fig. 4.5(c). At a shaft angle of 42°, it might be expected that the horizontal force contribution be greater than the vertical force. However, from inspection of Fig. 4.3, there is a force produced perpendicular to the propeller shaft which tends to increase lift and decrease thrust.This explains the lower magnitude thrust value. Now, as

shown in Fig. 4.5(f), the magnitude of both these forces steadily decreases with wind speed which is expected. This decrease is a result of increases in inflow with wind speed. At low shaft angles, as in Figs. 4.5(g), 4.5(h), and 4.5(i), the majority of the thrust is in the horizontal direction. As a result of the previous reasoning, both the lift and thrust steadily decrease with wind speed. However, the thrust drops at a faster rate due to a higher component of the upstream flow being able to travel through the propeller disk.

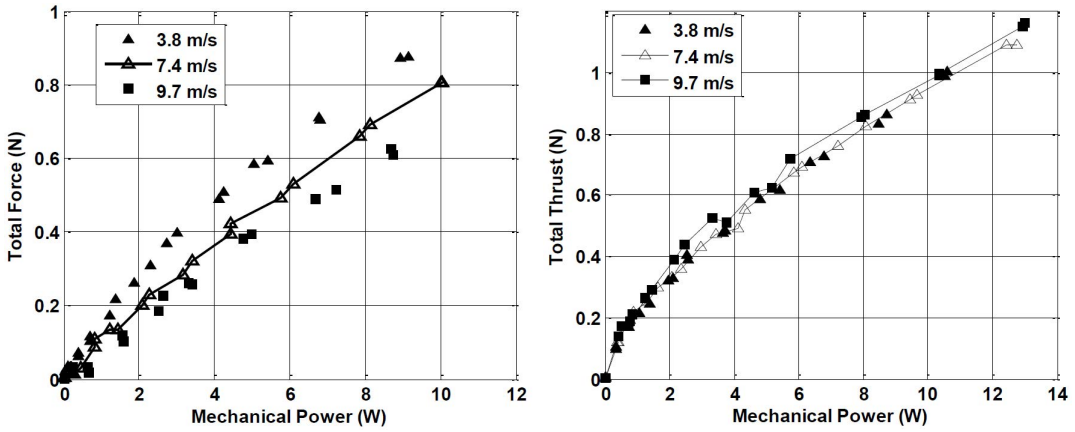

(a) Shaft angle: 6°

(b) Shaft angle: 84°

FIGURE 4.6: Variation of total force produced with mechanical power for isolated propeller

In regards to efficiency, it is beneficial to study the variation of the total force generated with the power required by the system. Figure 4.6 details this variation at two different shaft angles, 6° and 84°. It can be seen that at high shaft angles, the power requirements for a given total force do not change significantly with wind speed. However, as the shaft angle is reduced and the component of the upstream velocity through the propeller disk increases, there is a decrease in total force produced. Therefore, the power required to generate a specified force increases significantly as the shaft angle drops. This trend can be seen in Fig. 4.6(a).

4.2.2 Effect of Shaft Angle

As mentioned above, these results can also be expressed with respect to changes in shaft angles at fixed wind speeds. Figure 4.7 shows the variation of lift and thrust with RPM at various shaft angles and wind speed of about 7 m/s. It can be seen that there is a steady decrease in vertical force as the propeller is oriented from hover at 90° to forward flight mode at 0°. In hover, there is a drag generated in edgewise flow. As the shaft angle is decreased, there is a reduction in the component of the upstream momentum that is perpendicular to the propeller shaft. As a result, the horizontal force increases. It is worth noting that at shallow angles, such as 30°, there is a marginal increase in horizontal force while there is a two-fold decrease in vertical force. This can be partly explained by geometric effects. It can also be explained by the fact that the component of the upstream momentum parallel to the propeller rotation axis increases as the shaft angle drops. This increase in the momentum results in an overall decrease in magnitude of total force. It should be noted that the trends mentioned so far are maintained for all wind speeds measured in the experiment. Figure 4.8 shows the power requirements for producing desired vertical forces at various shaft angles at 7.4 m/s of upstream velocity. It can be seen that there is a severe penalty in power required for a given vertical force as the shaft angle is reduced. For example, in hover mode, 4.2 W is required to produce 0.6 N of vertical force whereas up to 8.4 W is required at an angle of 42°. This highlights the fact that in order to move fast in an efficient manner, lift augmentation is required at shallow shaft angles. This augmentation would allow for the propeller to be used primarily for propulsion purposes.

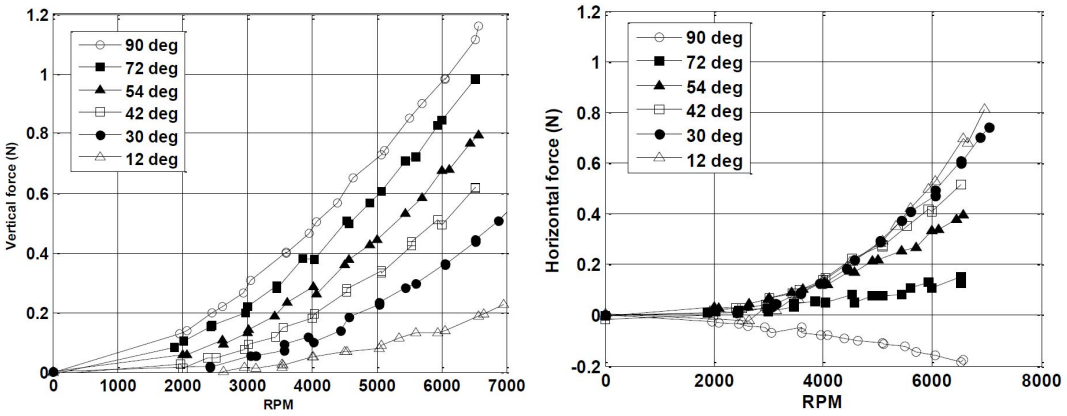

(a) Vertical force (b) Horizontal force

FIGURE 4.7: Force versus RPM for isolated propeller at various shaft angles and 7.4 m/s wind

4.3 Performance of Wing-Propeller System

The importance of including lift augmentation devices was evident in the previous section from an observation of propeller performance data at various stages of transition from 90° to 0°. In the quad rotor biplane vehicle, lift augmentation is provided by the wings. In order to measure the performance of the propeller-wing system, the setup shown in Fig. 4.9 is used. The wing is attached at the base of the motor mount in a manner similar to how it is installed on the vehicle. In order to maintain the same wing-propeller system proportion as on the vehicle, the aspect ratio of the wing was chosen to be 2.75. Aspect ratio of a single wing on the vehicle is about 5.5. The chord was maintained the same. The wing was installed such that the chord was parallel to the propeller rotation axis. The plane of the propeller was about 1.5 inches offset from the leading edge of the wing. The rest of the conditions were maintained the same from the isolated propeller tests. The primary forces of interest in this experiment are those parallel (F_z) and perpendicular (F_y) to the propeller rotation axis as shown in Fig. 4.10. Slight

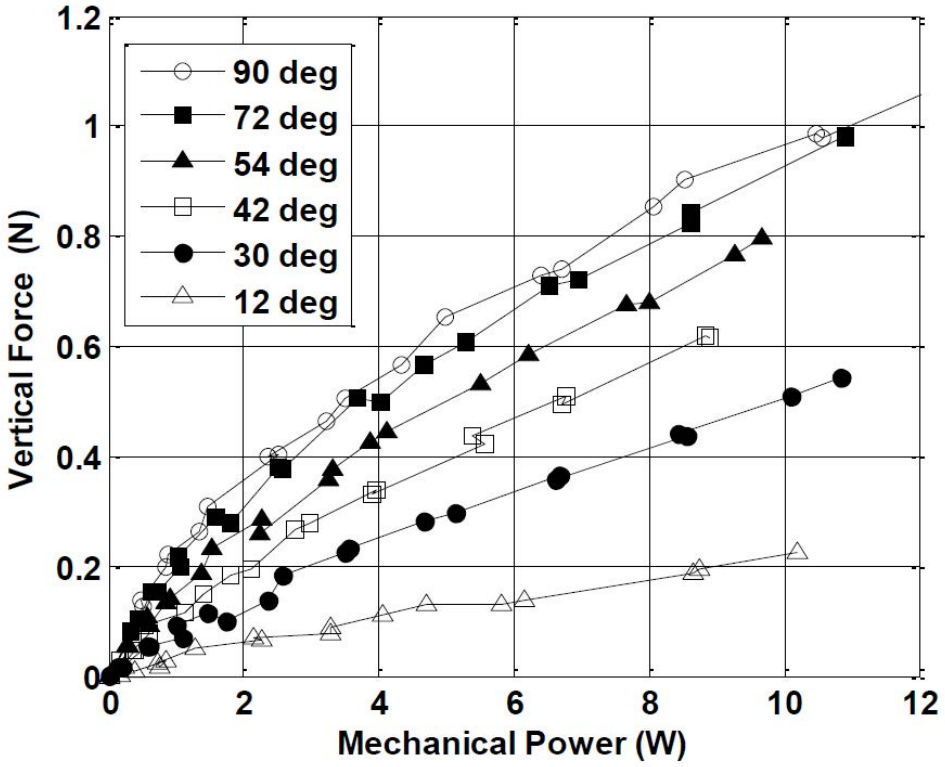

FIGURE 4.8: Vertical force variation with power for isolated propeller in 7.4 m/s wind

imbalances in the forces produced on either side of the wing can affect torque measurements. Static tests showed that the penalty due to wing drag was only about 5% of the total force for a given power input when compared with a propeller without the wing in its downwash. As a result, mechanical power results from the isolated propeller experiments are used for trim analysis. Results of pitching and rolling moments are also not shown since these are affected by the position of the load sensor, which may be different from the actual vehicle setup. The procedure for these tests is similar to that used for the isolated propeller experiments. When an upstream flow is input, the tare values for F_z and F_y are removed prior to operating the propeller. These represent the lift and drag of the wing-body system which are later used for trim analysis. The results presented in this section are the

pure effect of operating the propeller with a wing in its downwash in the presence of external flow at various shaft angles.

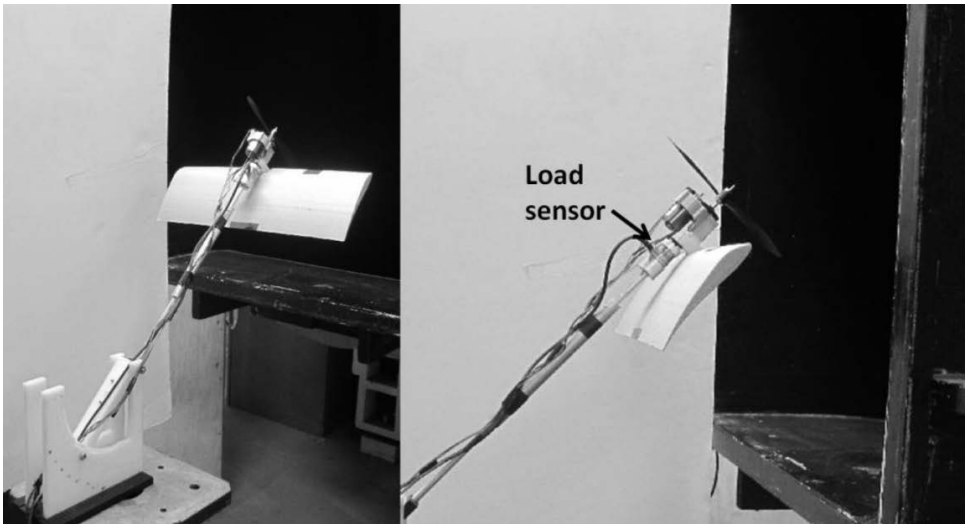

FIGURE 4.9: Setup to measure performance of propeller-wing combination

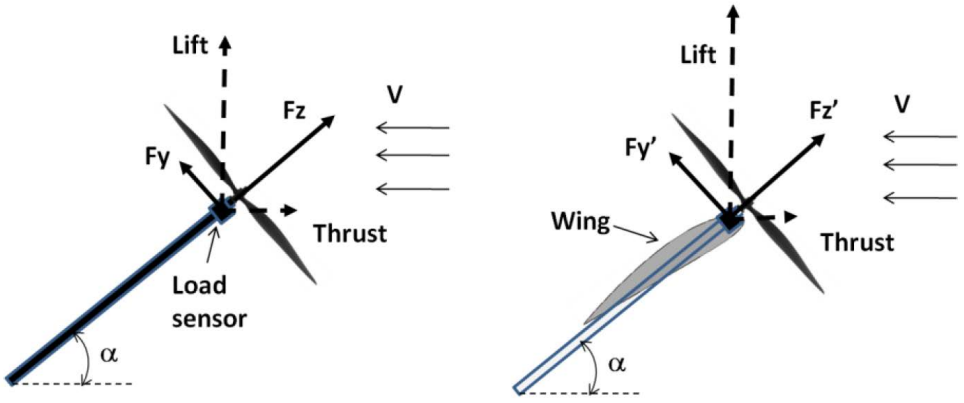

FIGURE 4.10: Differences in forces produced by a propeller in non-axial flow, with and without wing

4.3.1 Results

Variations of vertical and horizontal forces produced by the propeller-wing system at representative shaft angles and wind speeds are shown in Fig. 4.11. It is critical to note that the effect of pure wing lift, drag, and bluff body drag are removed from these analyses. Therefore, any differences in performance between the isolated propeller experiments and the following results are purely due to the effect of the wing on the propeller slipstream and vice versa. At angles close to hover mode, the majority of the force is produced in the vertical direction as can be seen from Fig. 4.11(a). Additionally the magnitude of vertical force increases with wind speed. The horizontal force is mainly in the direction of the upstream. This force reduces as wind speed increases. From Fig. 4.11(b) it can be seen that there is a greater drag produced with the propeller-wing system when compared with an isolated propeller. These effects can be explained by the effect of the wing on the propeller slipstream. At lower shaft angles such as 42°, there is still a major contribution to total thrust in the vertical direction. Variation of the forces with wind speed is reduced. At very low shaft angles (Fig. 4.11(e), 4.11(f)), contribution from the horizontal force is greater. A greater variation with wind speed is also exhibited which is expected since the component of upstream momentum into the propeller disk is increased. It is interesting to note that there is still a substantial amount of lift being produced at these low shaft angles when compared with the isolated propeller.

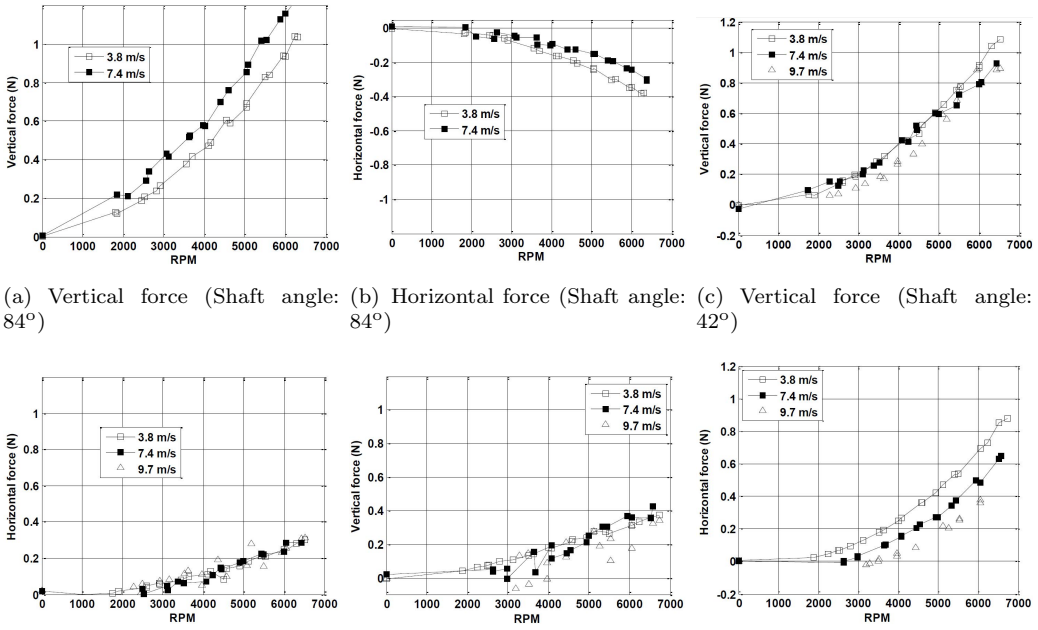

(a) Vertical force (Shaft angle: 84°) (b) Horizontal force (Shaft angle: 84°) (c) Vertical force (Shaft angle: 42°)

(d) Horizontal force (Shaft angle: 42°) (e) Vertical force (Shaft angle: 6°) (f) Horizontal force (Shaft angle: 6°)

FIGURE 4.11: Variation of forces with RPM for propeller-wing system at various shaft angles

4.4 Differences Between Isolated Propeller and Propeller-Wing System

As observed from the previous results and the isolated propeller experiments, there are substantial differences between the forces produced in the two cases. These are better summarized in Fig. 4.12. It shows the variation of vertical and horizontal forces produced by the propeller with and without the wing as a function of shaft angle and at a wind speed of about 6.2 m/s and 6500 RPM. Again, it is noted that the effect of pure wing lift and drag, and the bluff body drag will be included later for trim analysis. From Fig. 4.12, some key differences are:

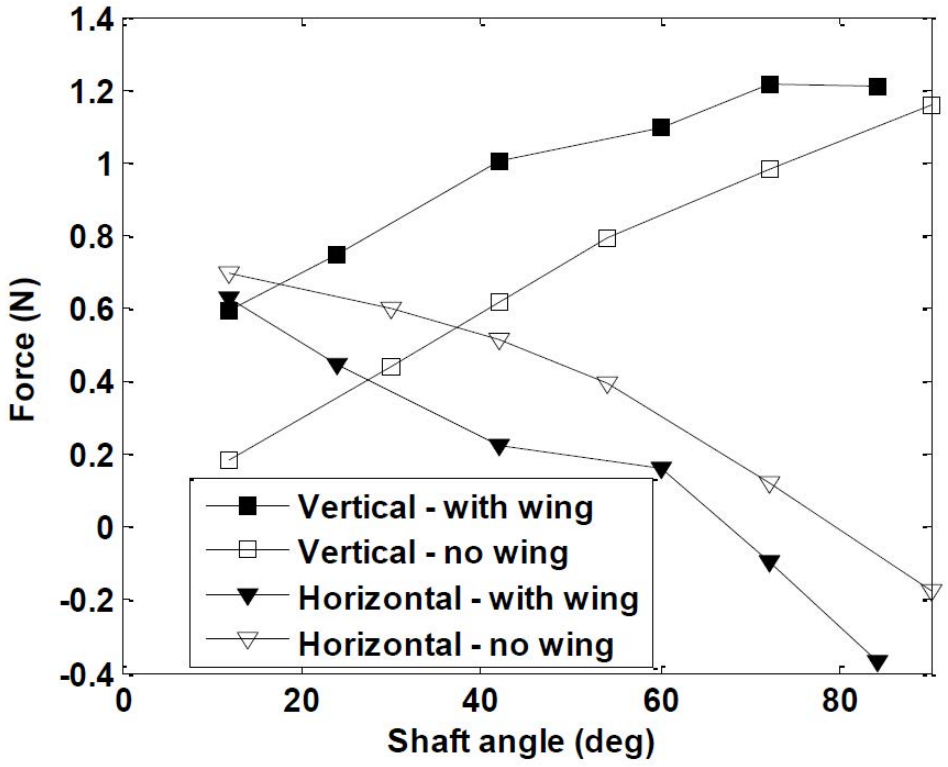

FIGURE 4.12: Differences in forces produced by a propeller as function of shaft angle, with and without wing

1. A uniformly greater contribution in vertical force of the propeller with wing case.

2. The contribution to total thrust from vertical and horizontal forces are equal at much lower shaft angles for the propeller with wing case.

This was about 40° for the isolated propeller whereas about 12° for the propeller-wing system. Additionally, the isolated propeller can produce a given horizontal force at much higher shaft angles as opposed to the propeller-wing system. These differences may be possibly explained by the effect of propeller slipstream on wing force as well and vice versa. Consider the schematic shown in Fig. 4.13. In non-axial flow conditions, the momentum of the upstream flow is changed in both

magnitude and direction by the induced flow generated by the propeller. Due to this change in momentum, forces are generated parallel and perpendicular to the propeller shaft. However, if a wing is placed in the downwash of the propeller, the direction of the upstream momentum is changed to a greater extent due to the presence of the wing surface. As a result, the magnitude of the force perpendicular to the propeller shaft increases. This causes an increase in vertical force and a decrease in horizontal force which is what is observed in Fig. 4.12. There is however one more factor that needs to be considered, which is the effect of propeller slipstream on the forces generated by the wing. When the propeller is operated, it induces an increase in velocity over a portion of the wing surface as shown in Fig. 4.14. This contributes to a reduction in positive horizontal force and an increase in vertical force. A more detailed explanation would require careful analysis of the effective angle of attack before and after the propeller is switched on, wing stall and other factors which can be studied in the future. Based on the above discussion and comparison with isolated propeller experiments, it can be concluded that there are significant interaction effects between the propeller and wing, which has a profound influence on the forces produced by the propeller and should be factored into the trim analysis.

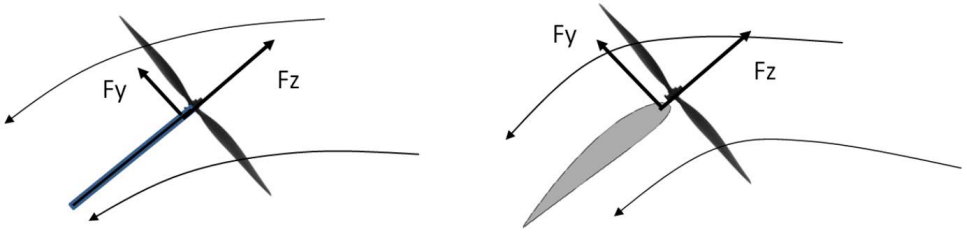

FIGURE 4.13: Effect of wing on propeller slipstream

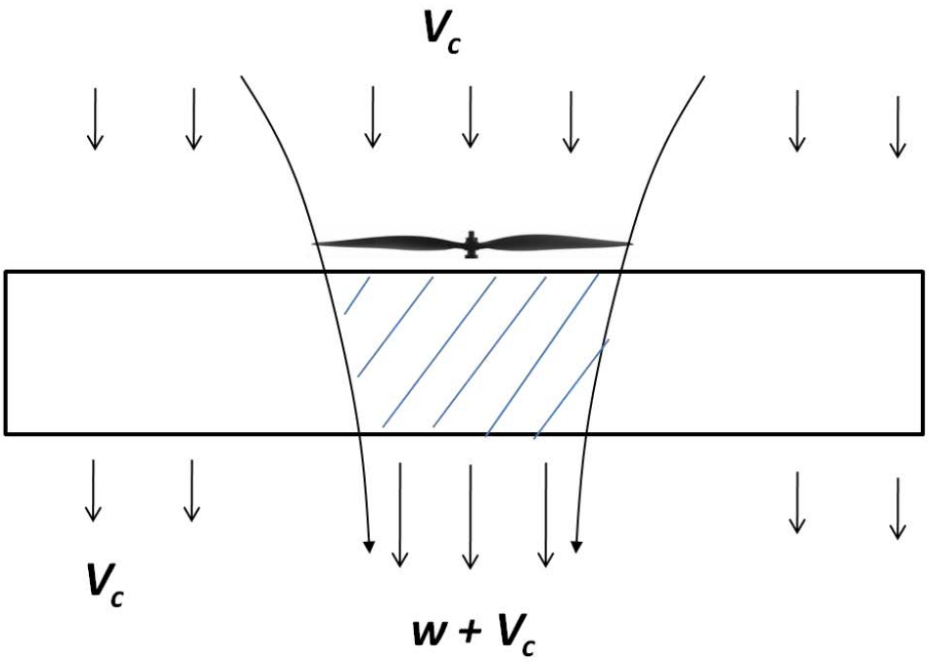

FIGURE 4.14: Effect of propeller slipstream on wing

4.5 Trim Analysis

The previous section described the variation of the vertical and horizontal forces generated by the propeller-wing system at various shaft angles and wind speeds where all the forces generated by the wing and bluff body were removed. It is of interest to use this information to determine the forward flight capabilities of the system. In order to do this, the tare values of lift and drag generated by the system prior to propeller operation (RPM = 0) are first determined (Fig. 4.18). It can be seen that the lift and drag values can be approximated satisfactorily with quadratic and cubic variations with wind speed. These values are then added to the previously determined vertical and horizontal forces as shown below:

$$L_{\text{Total}}(\alpha, \Omega, V) = L_{\text{prop-wing}}(\alpha, \Omega, V) + L_{\text{tare}}(\alpha, V) \tag{4.5}$$

$$T_{\text{Total}}(\alpha, \Omega, V) = T_{\text{prop-wing}}(\alpha, \Omega, V) + T_{\text{tare}}(\alpha, V) \tag{4.6}$$

where, α is the shaft angle, Ω is the propeller RPM, and V is the forward velocity. L_{tare} and T_{tare} are the lift and thrust forces measured on the propeller-wing system in non-axial flow with the propeller in the static condition. It can be seen that α and Ω are the two variables that determine the magnitude of horizontal and vertical forces and forward velocity. These variables have to be determined to establish trimmed flight at various angles of transition from 90° to 0°. Figure 4.16 shows a schematic of the propeller-wing system in a state of trim. This implies a steady level flight where the net horizontal force is zero and the vertical force balances the weight of the aircraft. As mentioned earlier, the wing-propeller system represents one-quarter of the complete vehicle. Since the vehicle weighs about 2.4 N, the required vertical force from the single propeller-wing system is 0.6 N. It is noted that moments are not considered since they can be controlled appropriately in the assembled vehicle.

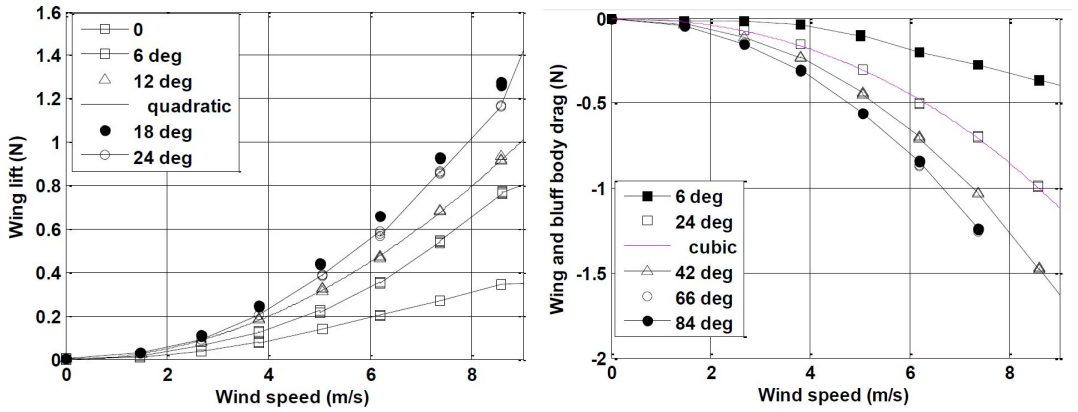

(a) Lift force

(b) Drag force

FIGURE 4.15: Tare lift and drag forces (RPM = 0)

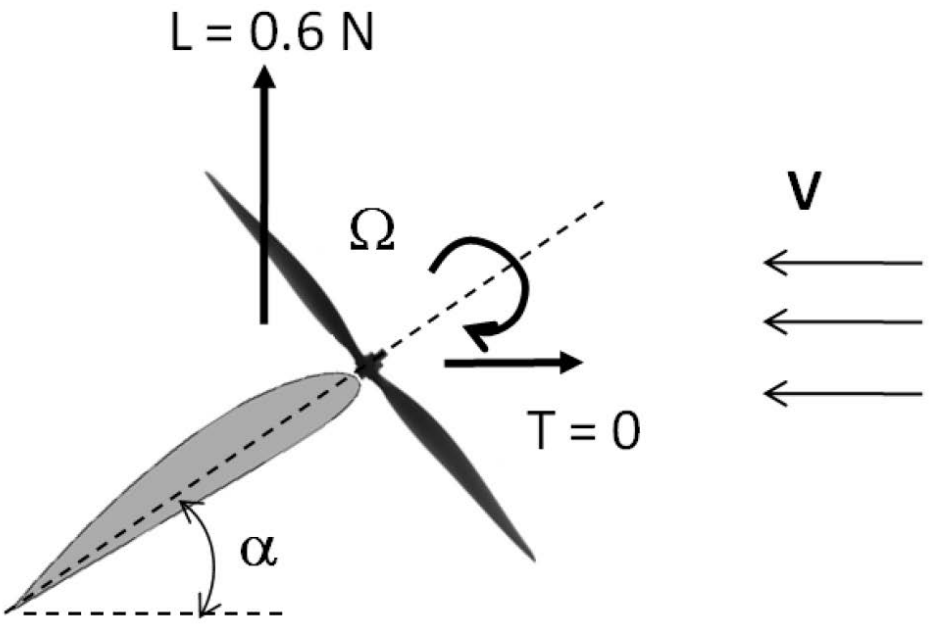

FIGURE 4.16: Propeller-wing system in state of trim

Representative results for the vertical and horizontal forces produced by the system with and without tare values are shown in Fig. 4.17 for a shaft angle of 18° and wind speed of about 6.4 m/s. It can be clearly seen there is a significant contribution to total lift from the wing. The magnitude of this contribution would vary with shaft angle and wind speed. Considering the case shown in Fig. 4.17 when the propeller is operated at an RPM of about 5700, the total horizontal force is zero. However, the total lift is greater than 0.6 N which would not result in level flight. This can imply:

1. Extra payload carrying capacity at these conditions
2. Wing dimension scaled down to match total lift of 0.6 N
3. Vehicle should fly slower than 6.4 m/s at 18° shaft angle

For the present study, it is assumed that the lift requirement and wing dimensions are held constant. Therefore, the only variables are wind speed and shaft angle. Estimates of velocity and required propeller RPM at various shaft angles can be obtained from an analysis of trim conditions based on wind tunnel measurements. Figure 4.18(a) shows the trim velocity at various shaft angles. At a shaft angle of about 6°, in order to achieve trim the vehicle should travel at about 7 m/s. As the angle is reduced even further, there is a sharp increase in velocity requirement. At 0°, a minimum velocity of 11 m/s is required to achieve trim. At high shaft angles such as 60°, the forward velocity is about 2 m/s. Velocities lower than 1.5 m/s cannot be measured accurately in the wind tunnel facility and hence are not included. Extrapolation of the velocity-angle curve indicates that for hover, the shaft angle is between 84-90°, which correlates well with free flight hover tests. It is also clear that the required propeller RPM at these various trim conditions is not constant. Figure 4.18(b) shows the variation of propeller RPM with shaft angle that achieves required forward velocities. In hover the RPM is about 5000, which remains approximately constant up to 50°. Below this angle, there is a steady reduction in required RPM to as low as 3500 at 18° shaft angle. At 0°, there is a sharp increase to about 7500 which correlates with the higher power required to maintain trimmed flight at that shaft angle.

From a performance perspective, the propeller RPM, shaft angle, and wind speed can be used to estimate the required power to achieve trimmed flight at all shaft angles. As mentioned earlier, the power measurements from the isolated propeller experiments are used. Figure 4.19 shows the variation of required power as a function of wind speed. The power is 5 W in hover and this requirement drops to as low as 1.5 W at a speed of about 4-4.5 m/s. This is more than a three-fold decrease in power required when compared to hover condition. If a wing is absent,

the propeller would be required to produce both propulsion and lift which drives up the required power significantly at a given wind speed. This highlights the utility of utilizing lift augmentation such as the propeller-wing system. The speed when hover power and cruise power are equal is 8 m/s. The maximum speed is about 11 m/s which requires about twice the hover power.

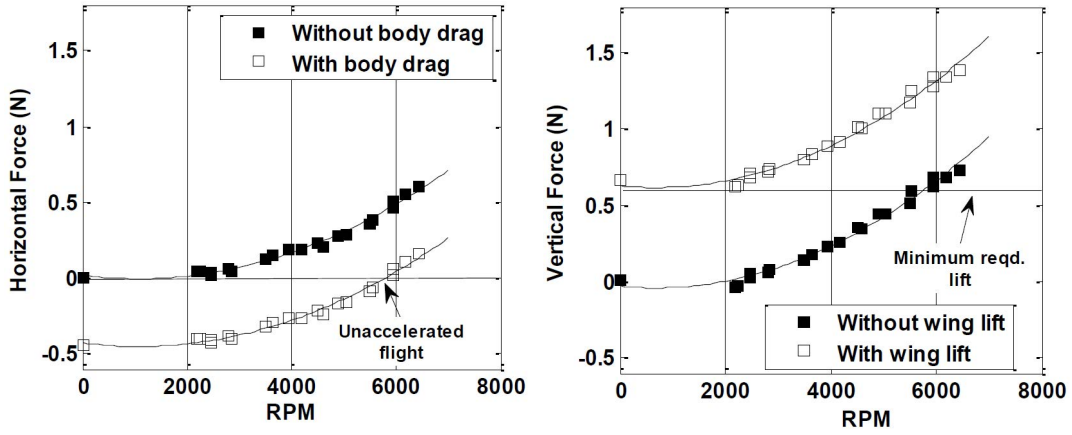

(a) Net horizontal force (b) Net vertical force

FIGURE 4.17: Net forces for 18° shaft angle and 6.4 m/s wind

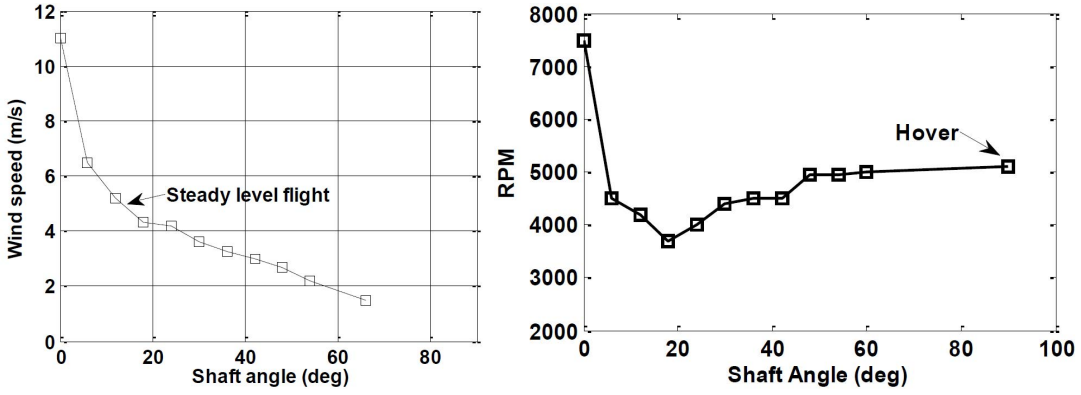

(a) Variation of wind speed with shaft angle for steady, level flight (b) Required RPM versus shaft angle based on wind speed

FIGURE 4.18: Trim analysis plots

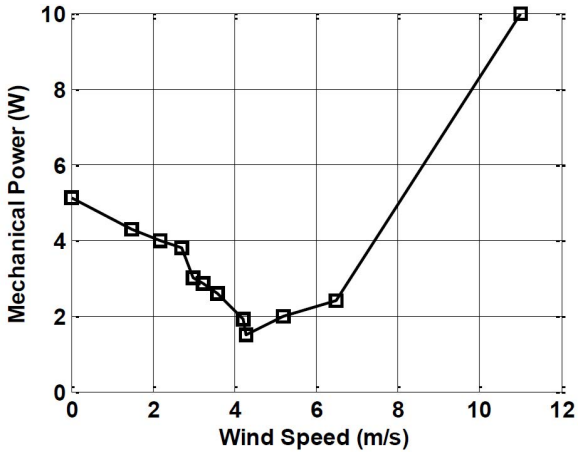

FIGURE 4.19: Power requirements at different forward flight speeds

4.6 Conclusions

In this chapter, investigations of non-axial flow conditions and their effect on vehicle performance were presented through a systematic series of bench-top wind tunnel experiments. The test apparatus included a rotor utilized on the quad-rotor biplane and a proportionally sized wing (one-quarter configuration). Measurements were taken for numerous flight conditions and upon review, revealed significant interaction effects between the propeller and wing at all angles of transition. The vertical force and horizontal force produced by the propeller-wing system were uniformly higher and lower respectively when compared to the isolated propeller system. This difference could be attributed to the combined effect of wing on propeller slipstream and effect of propeller downwash on wing generated forces. Trim analysis showed that the maximum speed and cruise speed achievable by the proof-of-concept system were 11 m/s and 4 m/s respectively. The maximum power required during cruise is approximately one-third of that required for hover.

Chapter 5

Vehicle Control

As mentioned earlier in Chapter 2, one of the main advantages of the quad-rotor biplane is that it is completely controllable without the use of aerodynamic control surfaces. Vehicle roll, pitch, and yaw are adjusted solely via variable proprotor RPM techniques. Control inputs for the quad-rotor biplane are very similar to conventional quad-rotor controls, regardless of the vehicle flight mode. These inputs are used in conjunction with a quaternion-based feedback controller and both topics will be detailed in this section.

5.1 Control Inputs

The vehicle utilizes an inertially fixed reference frame for all controls. This means that the axes do not vary with vehicle movements. Vehicle attitude and positioning is defined through a quaternion system as well. This is done to avoid gimbal lock which would be an issue when using Euler angles to define vehicle location and attitude after transitioning from hover to forward flight.

The various operating flight modes of the vehicle concept are shown in Fig. 5.1. Vertical take-off and landing operations will be performed through quad-rotor mode. Transition will involve a steady pitching moment provided through RPM variation of the propellers. Variations in RPM generate thrust differentials that provide the necessary pitching moment as the vehicle enters into the horizontal flight mode. At sufficiently high speeds, the entire body weight is supported by the wings. Therefore, it can be seen that one of the main utilities of the present

configuration is that quad-rotor control methodology is retained in both hover and forward flight conventions. There are no actuators that are redundant in either of these flight modes.

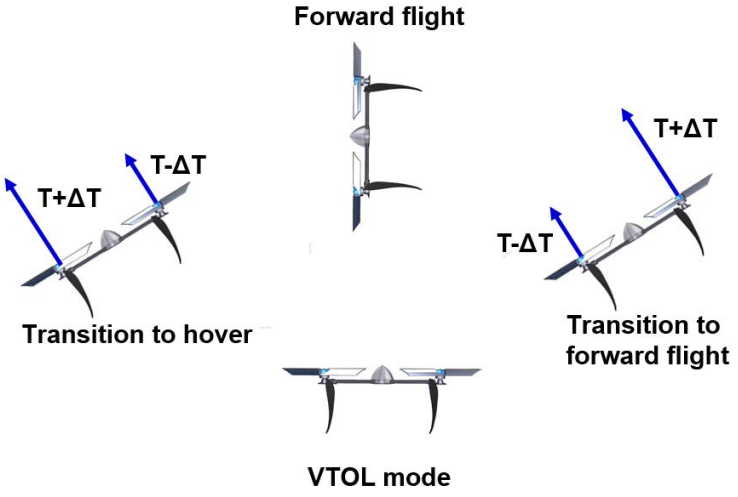

FIGURE 5.1: Vehicle achieving various flight modes via pitching moments

5.1.1 Control Axes in Transition

It is important to consider that the actuator control inputs that control pitch, roll, and yaw are not the same in hover and forward flight mode. The schematic shown in Fig. 5.2 helps to provide a better understanding of this concept. The pitch, roll, and yaw axes are defined based on the inertial frame in hover mode. Therefore, in hover mode, the pitch axis is parallel to the wings and perpendicular to the chord, the roll axis is perpendicular to the wing span and chord, and the yaw axis is parallel to the wing span and chord. It can be seen from Fig. 5.2(b) that as the vehicle transitions from hover to forward flight, the roll and yaw axes change with respect to the body reference frame. However, unlike these two control axes, the pitch axis is invariant with transition angle. Therefore, it is important

to appropriately map the control inputs to the inertial frame of reference. This frame is the same as the pilot reference frame. Let the pitch, roll and yaw controls in hover be $\delta_{\theta 0}$, $\delta_{\phi 0}$, and $\delta_{\psi 0}$ respectively. Then the control inputs for pitch, roll, and yaw at an arbitrary transition angle, α, can be written respectively as,

$$\delta_\theta(\alpha) = \delta_{\theta 0} \tag{5.1}$$

$$\delta_\phi(\alpha) = \delta_{\phi 0} cos\alpha - \delta_{\psi 0} sin\alpha \tag{5.2}$$

$$\delta_\psi(\alpha) = \delta_{\psi 0} cos\alpha + \delta_{\phi 0} sin\alpha \tag{5.3}$$

It can be seen that in forward flight mode, the roll and yaw controls are interchanged with respect to the hover configuration. Therefore, to accurately transfer the control inputs, it is of utmost importance to determine the angle of transition. Traditionally, for hover and low speed applications on rotorcraft, where the fuselage does not encounter large angles of deviation from hover, Euler angles are used to define vehicle attitude and location. However, when the vehicle enters into forward flight mode, it encounters a singularity, also known as gimbal lock. This problem is alleviated by determining a four dimensional vector called the quaternion. The quaternion is defined via real time sensor signals from which the transition angle can be calculated. Additionally, the quaternion formulation can also be used in developing the control strategy, which will be discussed below.

5.1.2 Quaternion Formulation

As mentioned above, it is imperative that the attitude of the quad-rotor biplane vehicle be described in a non-singular manner. Consider the rotation between two

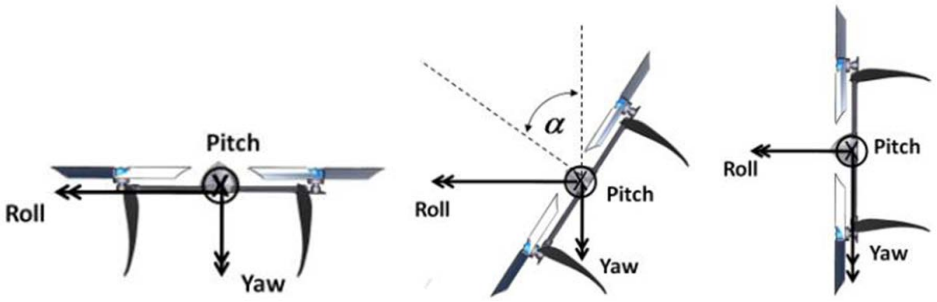

(a) Hover (b) Transition (c) Forward flight

FIGURE 5.2: Frames of reference in different flight mdoes

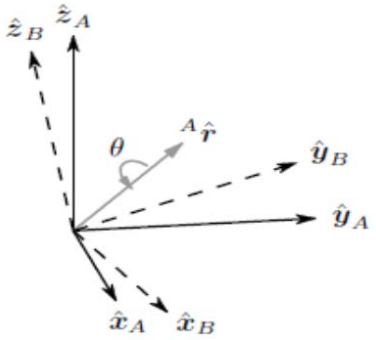

FIGURE 5.3: Rotation between frames A and B described by rotation about r^A

coordinate frames of reference A and B (Fig. 5.3) . This transformation can be described as a rotation about an axis (r^A). This rotation axis can be defined as a vector of four parameters, $\gamma = [\gamma_0, \gamma_1, \gamma_2, \gamma_3]$ [43]. The first parameter is a scalar quantity. The remaining quantities are the scaled components of the unit-length axis of rotation. These quantities satisfy the norm,

$$\gamma_0^2 + \gamma_1^2 + \gamma_2^2 + \gamma_3^2 = 1 \tag{5.4}$$

Euler angles representing yaw, pitch, and roll can also describe the orientation of frame B. This is done by applying sequential rotation angles about axes from the initial frame A. These angles can also be derived from the quaternion. From

Fig. 5.2, it can be seen that the transition angle is related to the pitch angle by,

$$\alpha = -\theta \tag{5.5}$$

This angle can then be calculated via quaternions by,

$$\alpha = -asin(2\gamma_1\gamma_3 + 2\gamma_0\gamma_2) \tag{5.6}$$

Therefore, it is of interest to calculate the quaternions from real-time sensor data, This will allow for vehicle attitude estimates. These quaternions are computed from the on-board gyro and accelerometer measurements. More details about these sensors can be found below in Section 5.2. The data coming from the gyro can be viewed as a measurement of the rate of change between two reference frames as the body is rotating. The accelerometers are used to measure the gravity vector with respect to the body frame of reference. Let the gyro measurements be represented as $\omega = [0, p, q, r]$. In this new representation, p, q, and r are the roll, pitch and yaw rates respectively. Kuipers showed in Ref. [44] that the time derivative of the quaternions are related to the gyro measurements by,

$$\dot{\gamma} = \frac{1}{2}\hat{\gamma} \otimes \omega \tag{5.7}$$

In this instance, $\otimes$ represents the composition of two different quaternions. The quaternion vector can be propagated via time marching,

$$\gamma_t = \hat{\gamma}_{t-1} + \dot{\gamma}\delta t \tag{5.8}$$

It is worth noting that the integration of gyro measurements is susceptible to drift over time. Therefore, the quaternion estimate from Eq. 5.8 is corrected by a measurement update which comes from the accelerometer. The accelerometer vector, denoted as $\hat{a}$, is ideally equal to the gravity vector, $\hat{g}$, that is rotated from the inertial frame to the body frame. However, due to slight measurement errors and vehicle vibrations, there is often a discrepancy between the two vectors. This error can be represented as,

$$e = \hat{\gamma}^* \otimes \hat{a} \otimes \hat{\gamma} - \hat{g} \tag{5.9}$$

If e is defined as an objective function, then $\hat{\gamma}$ can be determined using an algorithm such as the gradient descent method (Ref. [45]). This solution is then updated in Eqs. 5.1, 5.2, and 5.3 [43].

5.2 Feedback Control

After the vehicle quaternion is defined, this data is fed into a feedback loop with the on-board flight controller. The controller utilizes the Embedded Lightweight Kinematic Autopilot (ELKA-R) board [46]. This board can be seen in Fig. 5.4. The ELKA-R is a lightweight autopilot system featuring state-of-art hardware, low power microcontrollers, and improved software methodology. The board features a Cortex-M4 microprocessor which was selected for its high clock speed and memory. For an IMU, the ELKA-R has an MPU-9150. It includes an integrated 3-axis accelerometer, 3-axis gyro, and 3-axis magnetometer. The board also features a 2.4 GHz wireless transceiver and operates on a 1000 Hz loop rate. Altogether,

the board weighs only 1.7 grams and has a thickness of 1 mm. This autopilot is included in the control algorithm depicted in Fig. 5.5.

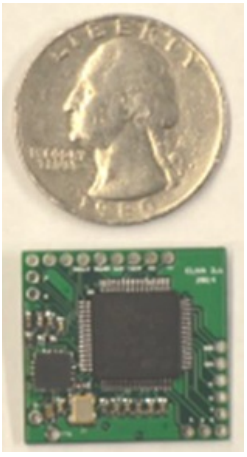

FIGURE 5.4: ELKA-R board

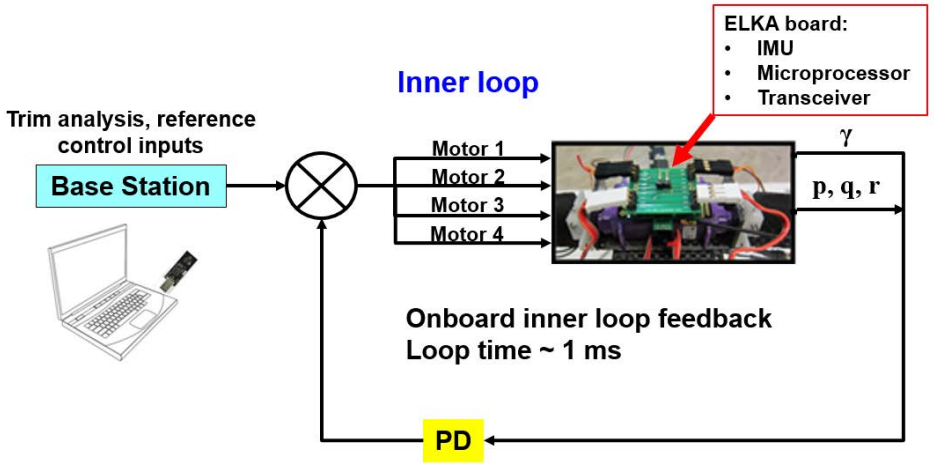

FIGURE 5.5: Feedback control loop

In this feedback control loop, the base station sends inputs to the four vehicle motors. These inputs are based off of trim analysis, discussed in Chapter 4, as well as feedback from the previous control loop. The motors react accordingly, altering their RPMs, generating vehicle movements. These movements are then quantified as position and attitude changes, gauged by the gyro and accelerometers

found on the ELKA-R board. The data from these sensors is used to generate a new vehicle quaternion as well as the pitch, roll, and yaw rates used to calculate error and drift. These values are then fed back into the feedback control loop with the proper gains and the loop is repeated at a rate of 1000 Hz.

In Chapter 4, it was seen that the propeller-wing system could generate adequate forces for level transition flight from helicopter to forward flight mode. In order to verify the quad-rotor biplane's ability to perform the transition maneuver, flight testing of the vehicle was performed, utilizing the flight control methods and the feedback controller detailed above.

5.3 Flight Testing

The quaternion based controller was tested for its ability to maintain stable hover. As can be seen from Fig. 5.6, satisfactory hover flight was obtained.

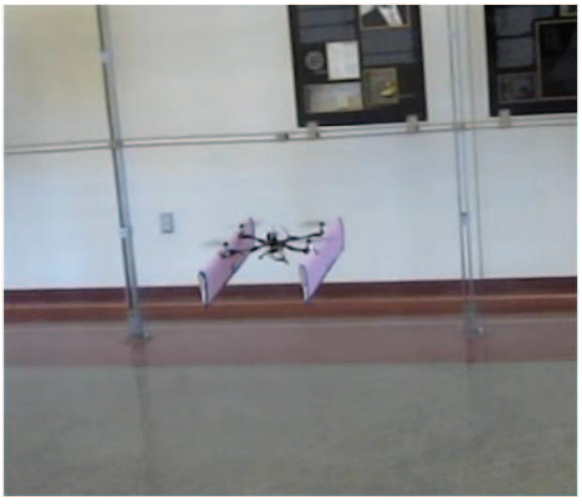

FIGURE 5.6: Quad-rotor biplane in hover

Free flight transition was performed with the vehicle initially in the hovering flight mode. After achieving stable hover, the pilot would issue a pitch-forward command. The throttle was held close to the hover value throughout the transition. The vehicle transitioned smoothly from helicopter to forward flight mode within a time frame of about 2 seconds. The quad-rotor biplane went on to proceed in forward flight mode. An average vehicle speed of about 7 m/s was observed via video analysis. The sequence of events is shown in Fig. 5.7. The sequence of events detailing transition from forward flight back to hover is shown in Fig. 5.8. In this case, a pitch-back command was supplied by the pilot. It is noted that since the throttle value was held the same as during forward flight, an excess lift was generated as the vehicle returned back to the hover attitude. Consequently an increase in altitude was observed. Further tests will be conducted to determine throttle modulation to obtain transition flights in both modes without change in altitude.

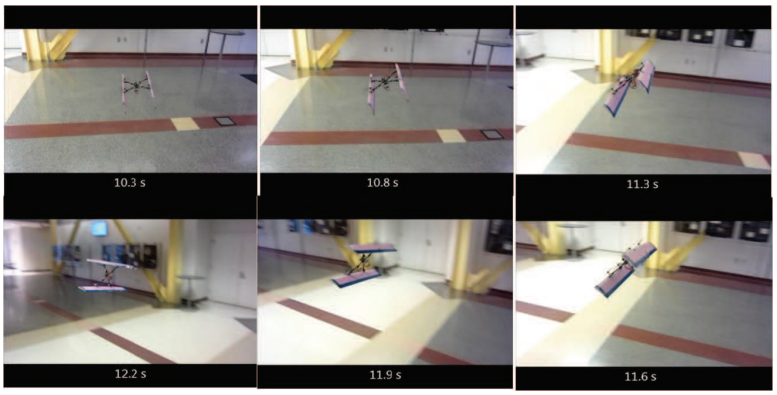

FIGURE 5.7: Transition from hover to forward flight

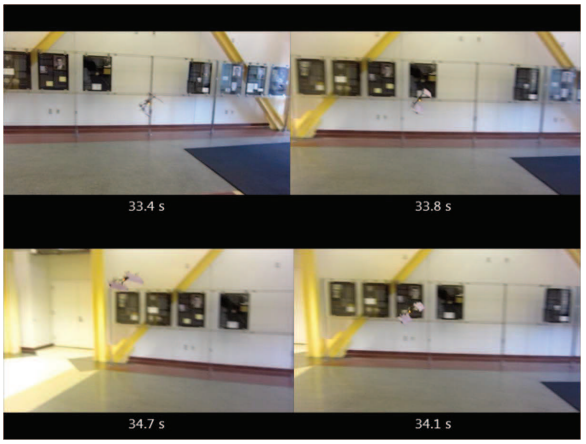

FIGURE 5.8: Transition from forward flight hover

5.3.1 Low Roll Control

While multiple flight tests were successful, some flights resulted in vehicle crashes. Figure 5.9 shows one such test flight. In this figure, it can be seen that the vehicle achieves hover and transition smoothly. However, during forward flight, roll control authority suffers and the vehicle crashes, resulting in damage. This is shown in Fig. 5.10. Multiple control augmentation methods are developed and tested in Chapter 6.

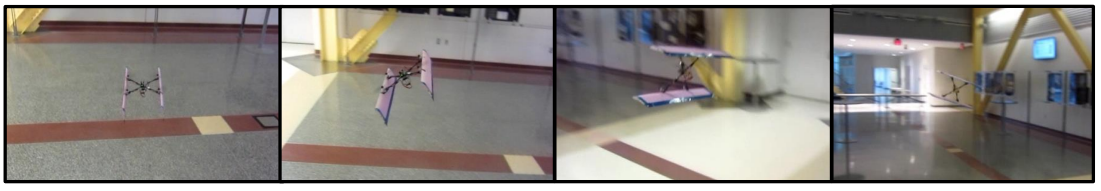

FIGURE 5.9: Vehicle flight leading to crash

FIGURE 5.10: Vehicle damaged during flight tests

5.4 Conclusions

The quaternion based feedback control loop is shown to be an effective control scheme for the quad-rotor biplane. It helps to avoid singularity and gimbal lock when the vehicle transitions into forward flight and has been shown to allow for stable hover and transition. Unfortunately, in forward flight, the original quad-rotor biplane exhibited poor roll control authority, which led to hard crashes and severe vehicle damage. Vehicle improvements, including enhanced roll control in forward flight are explored in depth in the following chapter.

Chapter 6

Design Improvements and Flight Testing

As a result of numerous flight testing trials of the quad-rotor biplane, multiple design improvements were deemed necessary. Due to the vehicle's lightweight design and the inherent load paths of the tail-sitter configuration, damage from landings was found to be a frequent occurrence. This led to large amounts of time spent on vehicle maintenance and repair. In an effort to avoid these setbacks, attempts were made to increase vehicle structural integrity and decrease the chance of vehicle crashes. This was done via the integration of additional structural parts and systems redesigns. As mentioned in Chapter 5, it was observed during forward flight that the original design of the quad-rotor biplane vehicle suffers from a lack of sufficient roll control authority. This led to vehicle crashes and therefore, more repair and maintenance. This section explores the deficiencies of the installed roll control method and investigates several other suitable control systems. These include a pair of pivoting wing tips, thrust vectoring via angled proprotors, and a variable collective pitch proprotor method.

6.1 Wing Spars

An unfortunate side effect of having a lightweight vehicle is that it tends to be fragile as well. This was certainly the case with the original configuration of the quad-rotor biplane. Since the vehicle is a tail-sitter and uses the wing trailing

edges as landing gear, hard landings would lead to crumpling and degradation of the thin, foam wings.

In order to increase wing rigidity, carbon fiber spars were implemented at the wing quarter chord and along the trailing edge. A vehicle with these spars installed can be seen in Fig. 6.1. However, these wings, while increasing wing stiffness, are heavy. Each set of spars adds approximately 25 grams to the vehicle, representing more than a 10% increase in vehicle weight. Although the spars provide a large increase in wing rigidity and structural integrity, the vehicle still suffered from a weak motor-wing connection point. These weak points are highlighted in Fig. 6.1. The epoxied motor mount attachments would detach during landings and crashes, requiring major wing repairs often. This issue is alleviated through adjustments made in the following section.

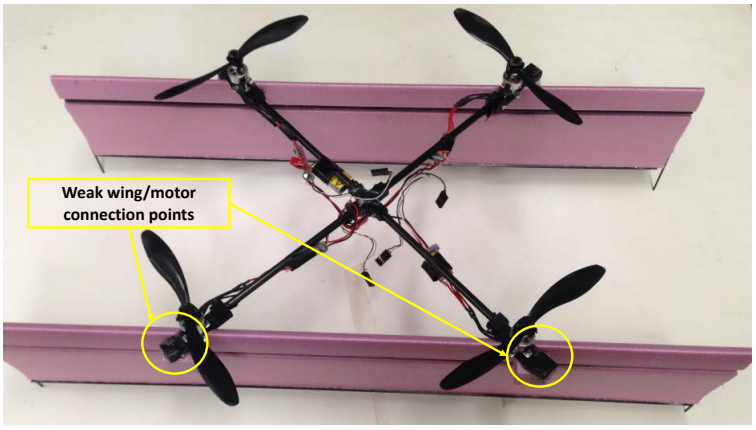

FIGURE 6.1: Vehicle utilizing carbon fiber spars

6.2 Motor Mounts

Weight savings and overall increased vehicle structural integrity were achieved through a redesigning of vehicle frame and landing gear. In order to solve the issue

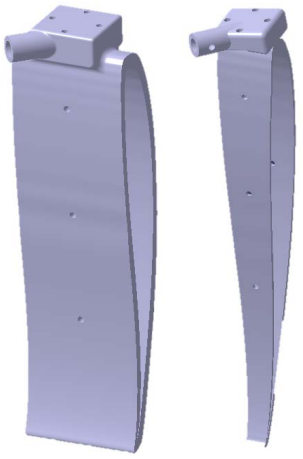

(a) Drawing of 3D printed motor mount

(b) Drawing of lighter motor mount

FIGURE 6.2: Redesigned vehicle motor mounts

of landing on fragile wing tips and increase overall vehicle rigidity, a completely new method of wing attachment was designed. 3D printed wing mounts, which can be seen below in Fig. 6.2(a), were designed to take the brunt of the force during landings and transmit them to the vehicle's "X" frame rather than the delicate wings. The motors are attached directly to these airfoil shaped mounts, further unloading the foam wings. Over time, these mounts were slimmed down further to save weight. Figure 6.2(b) shows a more up-to-date, lighter version of the 3D printed mount and they can be seen attached to the vehicle in Fig. 6.3. Overall, these mounts drastically improve vehicle survivability, as noted through flight tests, and offer a much more lightweight alternative to heavy spars. A vehicle with these mounts included weighs approximately 220 grams, representing a 7% decrease in vehicle weight. As shown in Section 6.5.2, these mounts will aid the vehicle in more ways than structural rigidity.

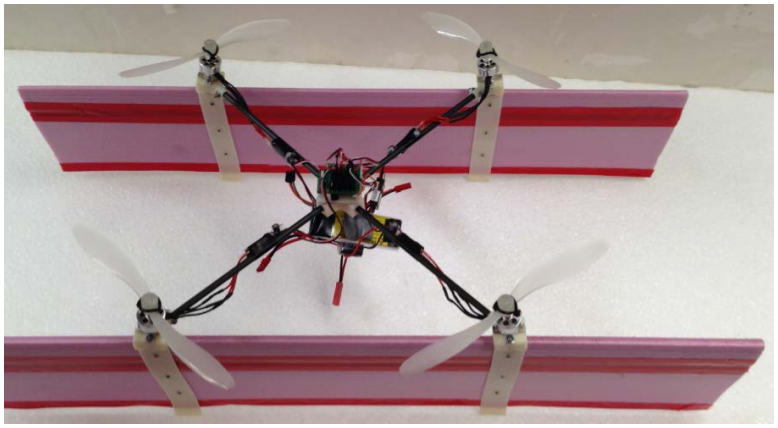

FIGURE 6.3: Vehicle with 3D printed motor mounts

6.3 Vertical Fins

The quad-rotor biplane was originally designed to be tail-less. The lack of aerodynamic surfaces allows for a more lightweight and compact vehicle. Without a tail, however, it can be difficult to counteract undesirable flight actions, such as side-slip and loss of yaw control. In order to account for these issues, while keeping vehicle weight low, an easily constructed and passive method was explored and implemented. Thin foam vertical fins were installed near the wing trailing edges of the quad-rotor biplane in order to enhance forward flight yaw stability and prevent any instances of side-slip. These fins are 2" in width and weigh approximately 2 grams each. The vehicle can be seen successfully flying with these fins installed in Fig. 6.4.

6.4 Current Roll Control System

Currently, the MAV utilizes a standard quad-rotor yaw system to roll during transitional flight. This system can be seen in more detail in Fig. 6.5. In order to

FIGURE 6.4: Vehicle with lightweight fins installed

generate a rolling moment, the RPMs of diagonal proprotors are altered in order to create a torque imbalance amongst the two pairs of motor and proprotor combinations. Total thrust for the entire system remains constant. For example, in order to create a clockwise moment, the two motors which are rotating in that direction would have their RPMs decreased by a certain magnitude. Conversely, the other two motors, which are rotating in the counter-clockwise direction, would then have their RPMs increased by a similar magnitude to balance out the loss in thrust. This would cause a reactionary torque imbalance between the clockwise and counterclockwise directions which would lead to clockwise roll without sacrificing thrust or coupling other moments.

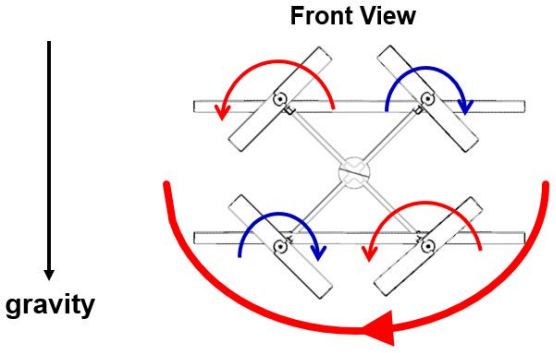

FIGURE 6.5: Clockwise roll in forward flight using current system

In order to evaluate the control authority of the conventional system, it was necessary to investigate the performance of the GWS 6x5 propeller in hover and axial flight in the wind tunnel. It should be noted that in hover, this proprotor is operating at a low Reynolds number of approximately 51,500. The test setup can be seen in Fig. 6.6. Performance data generated by the propeller in hover as well as a flight speed of 6.25 m/s can be seen below in Fig. 6.7(a) and Fig. 6.7(b). It is important to observe that all control techniques will be compared at a flight speed of 6.25 m/s. This will be discussed in more detail throughout the chapter.

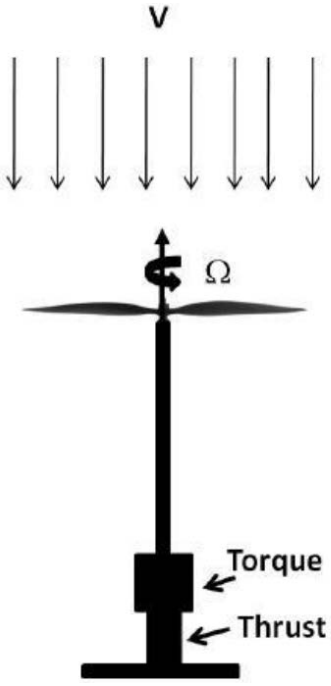

FIGURE 6.6: Axial flow testing diagram

Figure 6.7 shows graphs of measured thrust and torque versus RPM for the GWS 6x5 propeller. The low levels of torque generated, which reach a maximum of approximately 15 N-mm, in hover do not allow for necessary roll moments with high axial flow speeds. As mentioned earlier, it was observed during vehicle flight tests that high roll control in forward flight is not attainable using this technique.

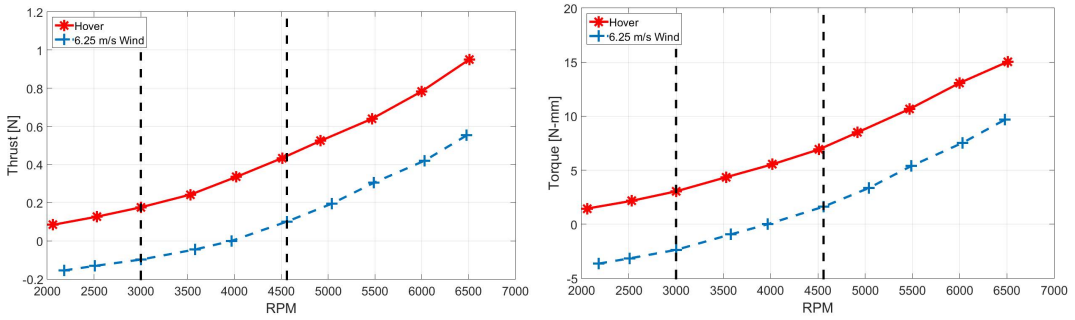

(a) Thrust versus RPM (dashed lines represent RPM operating range)

(b) Torque versus RPM (dashed lines represent RPM operating range)

FIGURE 6.7: Original roll control performance plots with GWS 6x5 proprotor

The remainder of this section will explore a series of alternate roll control solutions with the intent of increasing control authority.

6.4.1 "Baseline" System Analysis

For the sake of comparison between roll control methods in this chapter, a "baseline" case will be defined based on the aforementioned measurements. Test results from experiments completed for a single propeller in axial flight have been extrapolated to simulate a quad rotor biplane flying at 6.25 m/s. As detailed in Chapter 3, a GWS 6x5 propeller was tested through a series of RPMs in axial flow of varying wind speeds. The results for a wind speed of 6.25 m/s are also shown in Figs. 6.7(a) and 6.7(b) and once again, Fig. 6.6 shows a diagram of the test setup. Based on the data presented above, in order to maintain a constant flight speed of 6.25 m/s, all four proprotors of the vehicle must operate at 3970 RPM. At this RPM, the proprotors generate no net thrust and thus, no net acceleration. To conduct a clockwise roll maneuver using the conventional roll technique (Fig. 6.5) within suitable RPM levels for the proprotor, clockwise rotating rotors will decrease their RPM to 3000 and counterclockwise rotors will increase their RPM to

4560. The vertical lines in Fig. 6.7(b) intersect the torque curve at these indicated RPMs, showing maximum achievable torque at this flight condition. This will create a net roll moment equal to 8.0 N-mm while essentially keeping thrust constant. All further roll techniques are measured against this baseline case.

6.5 Alternate Control Methods

6.5.1 Pivoting Wing Tip

One option for improving roll control is a pair of servo-driven flapping wing tips. Operating much like the ailerons on an airplane wing, the pivoting wing tips can generate moments using directional lift vector changes. The completed design and completed vehicle can be seen below in Figs. 6.8(a) and 6.8(b). Each wing tip takes up one quarter of the entire span of the top wing in the biplane configuration.

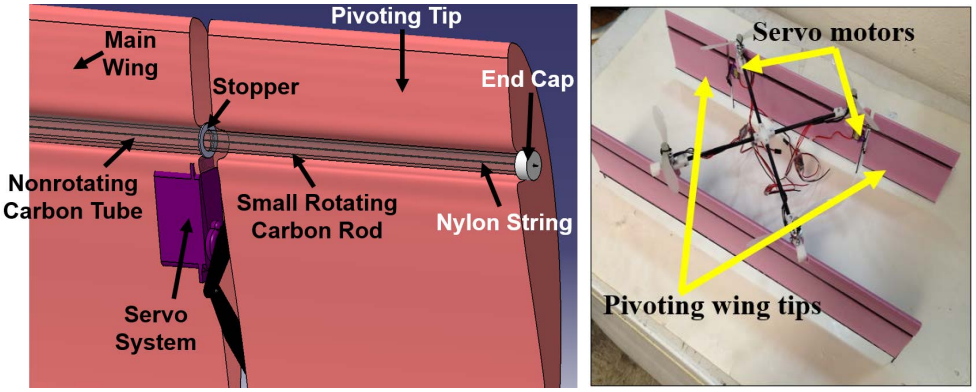

(a) Close up drawing of wing tip system

(b) Vehicle with flapping wing tip system

FIGURE 6.8: Pivoting wing tip system

The wing tip system is actuated by a servo motor which is connected to an arm. This arm rotates and contains a pin joint which allows it to abduct and adduct accordingly. A drawing of this motor-arm system can be seen in Fig. 6.9. When

the servo motors on either side of the wing are driven by a pulse-width modulated signal, they rotate and pivot their respective wing tips in opposite directions. This causes lift vectoring at each end of the wing which in turn supplies a pure roll moment to the vehicle.

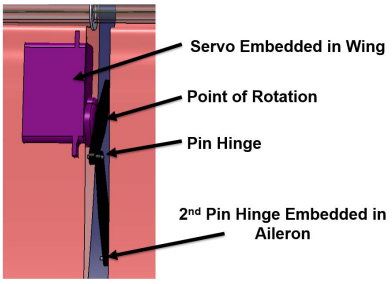

FIGURE 6.9: Close up drawing of servo arm system

Wind tunnel testing was conducted and has shown that this system can indeed generate large roll moments in forward flight. Fig. 6.10 shows the torque generated by a single wing tip traveling into the wind. The test setup can be seen in Fig. 6.11.

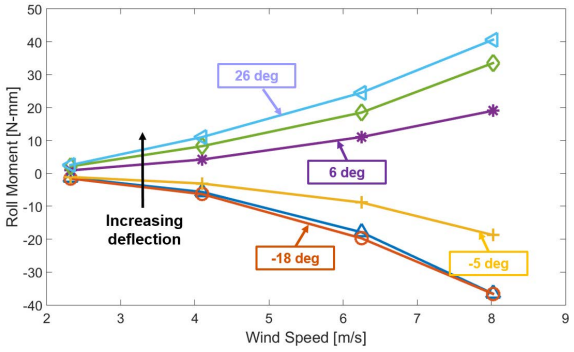

FIGURE 6.10: Torque generated by a single wing tip in forward flight

During the test, one half of the span and one wing tip were exposed to wind while the flap was deflected. The deflected tip generated up to 40 N-mm of torque at maximum wind speeds. With two wing tips each generating approximately 40 N-mm of roll moment, the vehicle will experience much greater roll control authority in forward flight.

FIGURE 6.11: Wing with moving wing tip placed in front of open jet wind tunnel

6.5.1.1 Control Authority for Full Scale Vehicle

Data for a pivoting wing tip in 6.25 m/s wind is shown below in Fig. 6.12. In order to compare this model to the baseline model discussed above, the pulse-width modulated signal input to the wing tip control servo will correspond to the input given to achieve the RPM differential of the baseline control model. It was seen that, in order to conduct a clockwise roll, the left and right wing tips would be rotated to 4.2° respectively and vice versa for counter-clockwise roll. This would generate a roll moment equal to 15.61 N-mm. However, the maneuver would also generate additional drag. In order to make up for the increase in drag, the propellers would each need to spin at higher RPMs, leading to an increase in power consumed.

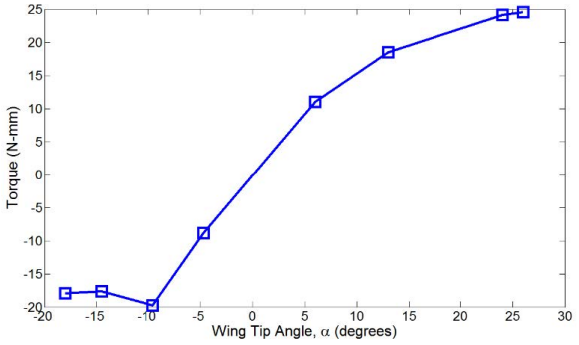

FIGURE 6.12: Torque versus wing tip angle in 6.25 m/s wind

It should be noted that the entire flap system is both heavy and delicate, leading to performance degradation in other regards as well. A wing with an installed pivoting wing tip system weighs 57 grams more than a wing without the system. This represents a 23.75% increase from the 240 gram initial total vehicle weight. A system such as this would drive up the entire weight and sizing of the MAV and also lead to an increase in maintenance required. Also, it is important to note that this system benefits from a high aspect ratio wing design. Using a longer wing allows for an increased moment arm for each pivoting wing tip, increasing the total moment generated. A shorter wing with a longer chord would degrade the performance of such a system. Deflecting the wing tip of a low aspect ratio wing would lead to increased drag and a lower roll moment.

6.5.2 Angled Motor Mounts

A second option which is explored is that of angling the motors in order to employ thrust vectoring, or simply, shaft tilt. Fig. 6.13 shows a conceptual design for a vehicle fitted with the mount which allows for the motor and propeller angling. Figure 6.14 shows how shaft tilt vectors the vehicle's thrust. Since the proprotors on the vehicle are angled slightly, as shown in Fig. 6.14, they will provide a side-force for the vehicle. When the motor shafts are tilted inward at an angle, α_s, toward the mid-span of their respective wings, these side-forces will provide a valuable moment which will aid in roll. A mount angle of 10^o was chosen as it provides a considerable increase in sideways thrust and a minimal decrease in vertical thrust. Tilting the proprotor at an angle of 10^o allows for 17

In order for the sideways thrust of the propeller to assist in roll control, the variable RPM method must also be utilized. In this manner, the inherent differential

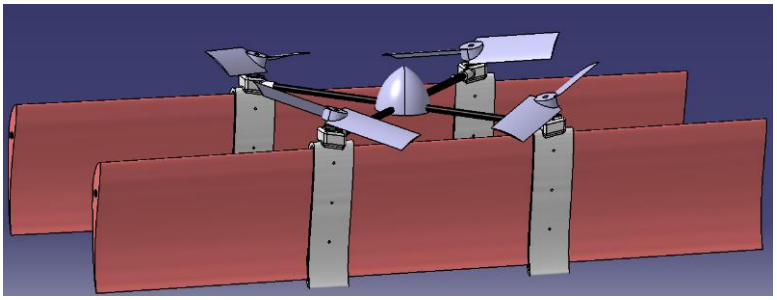

FIGURE 6.13: Conceptual vehicle design with angled motor mounts

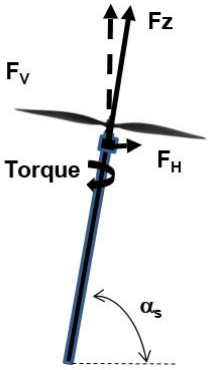

FIGURE 6.14: Force generation for propeller with nonzero shaft tilt, α_s

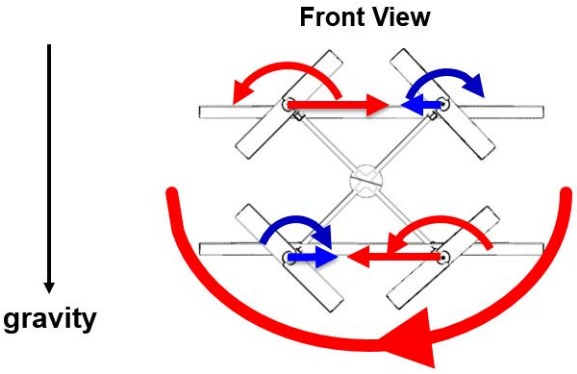

FIGURE 6.15: Diagram of thrust vectoring approach

reactionary torque as well as the moment generated through vectored thrust will complement each other to enhance the roll control authority. Figure 6.15 shows the direction and relative magnitude of the new forces which, when coupled with

a moment arm, will generate a large roll moment in the clockwise direction, which is the desired direction of rotation.

Previous tests and current design characteristics prove that this system will enhance roll control. Figures 6.16(a) and 6.16(b) show torque and thrust measurements respectively during hover for the 6x5 Slow Flyer propeller when flown in the conventional level manner versus the new tilted flying position. The angled system torque measurements are significantly higher because the torque measurements now include the moment generated by the thrust differential coupled with the moment arm to the central axis of the vehicle. The moment arm is 4.5 inches.

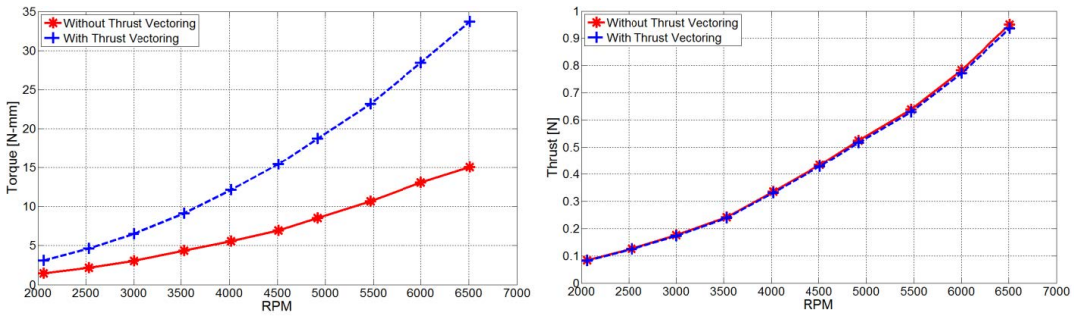

(a) Roll moment measurements for the two flying conventions

(b) Thrust moment measurements for the two flying conventions

FIGURE 6.16: Pivoting wing tip system

The above plots make it clear that thrust vectoring is an effective method of roll control. The vehicle experiences an average increase in roll performance of 117.4% while only sacrificing an average of 1.5% of vertical thrust.

6.5.2.1 Data Extraction for Full Scale Vehicle

Data for the angled proprotor in 6.25 m/s wind is shown in Figs. 6.17(a) and 6.17(b).

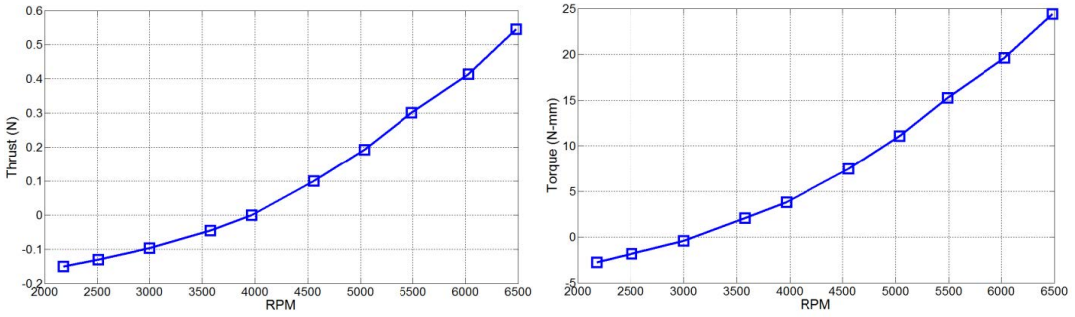

(a) Angled proprotor thrust versus RPM in 6.25 m/s wind

(b) Angled proprotor torque versus RPM in 6.25 m/s wind

FIGURE 6.17: Angled proprotor performance comparison

According to the figures and using the same methodology as the baseline calculation mentioned earlier, to roll in a clockwise manner, clockwise rotating proprotors will decrease their RPMs to 3000 and counterclockwise rotating proprotors will increase their RPMs to 4560. This will yield a net roll moment of 15.79 N-mm while keeping thrust virtually the same.

6.5.3 Variable Collective Pitch Approach

The final option that has been explored is a variable propeller pitch technique. This method is very similar to the aforementioned variable RPM method in which torque imbalance is generated. However, instead of varying the RPM for each pair of propellers, the collective pitches of the diagonal rotors will be similarly varied. For example, in order to rotate in a counter-clockwise direction, the collective pitches of the propellers rotating in that direction will be decreased. As a result, the reactionary torque in the clockwise direction is decreased. The propellers rotating clockwise would then have their pitches increased equally to increase the reactionary torque in the counter-clockwise direction, thus inducing roll in this direction. Tests have been conducted using a variable pitch propeller with blades

shaped identically to the GWS 6x5 Slow Flyer propeller to gauge the effectiveness of such a roll system. Figure 6.18 shows a picture of the servo-actuated variable pitch hub system and Fig. 6.19 shows a picture of the test setup. The system contains a hollow shaft motor with a vertically translating rod which is driven by a servo motor. The rod is connected to a non-rotating swashplate which provides variable collective for the proprotor when actuated in the vertical direction.

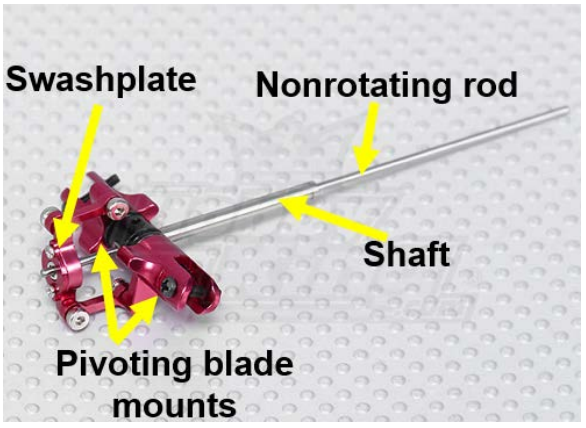

FIGURE 6.18: Servo-driven variable pitch hub (without motor and proprotor blades

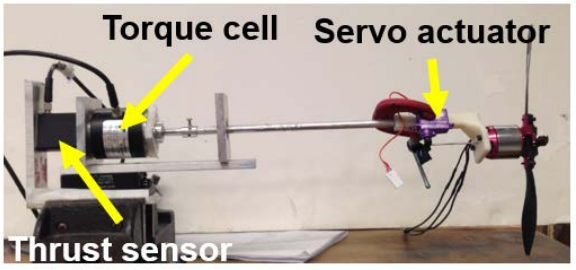

FIGURE 6.19: Variable pitch propeller test setup

Figures 6.20(a) and 6.20(b) show how the different collectives affect hover performance. As expected, increasing blade collective, prior to blade stall, generates greater magnitudes of thrust and torque. The propeller was also subjected to axial flow wind, ranging from 0 to 8 m/s, and swept through its maximum range of

propeller collective angles, which ranged from 6° to 14°. The propeller was also swept through a series of RPMs between 2000 and 4000 to measure thrust and torque under each flight condition. Figure 6.20(c) shows efficiency versus advance ratio for the 3000 RPM test case in forward flight for the variable pitch propeller system.

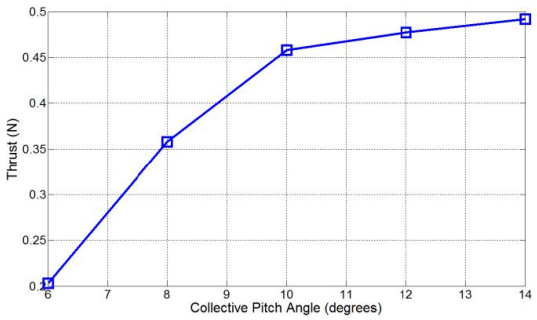

(a) Thrust versus pitch angle in hover

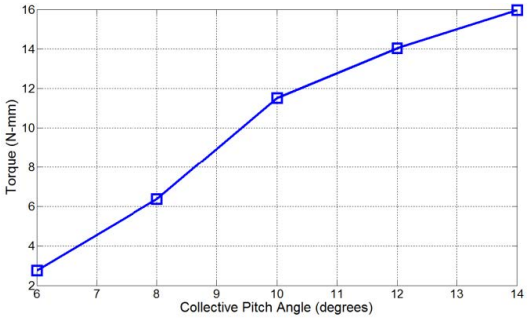

(b) Torque versus pitch angle in hover

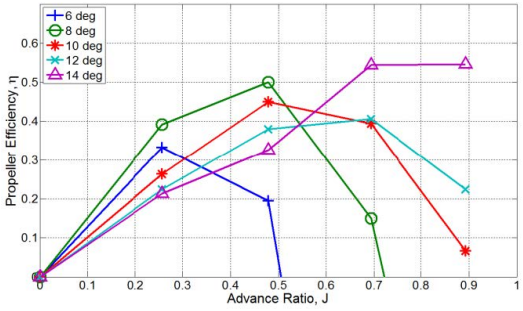

(c) Efficiency versus advance ratio comparison at 3000 RPM

FIGURE 6.20: Variable pitch system performance plots

Figure 6.20(c) shows that the use of higher collective pitches increases the envelope of optimum efficiencies to higher advance ratios. The curves of efficiency versus advance ratio move to the right with increasing collective, allowing for better performance at higher forward flight speeds. This trend is common for all operating RPMs. Also, from this figure, it can be seen that if the collective is fixed, the range of advance ratios for efficient flight is limited.

6.5.3.1 Data Extraction for Full Scale Vehicle

Figures 6.21(a) and 6.21(b) contain flight performance data for the variable pitch hub flying at 6.25 m/s.

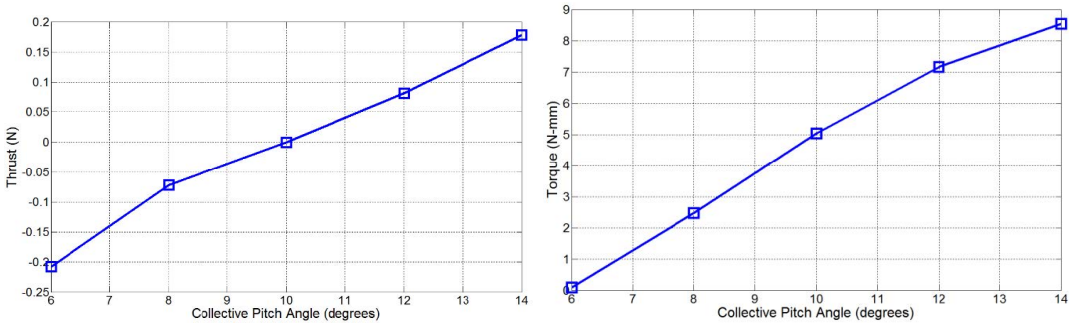

(a) Thrust versus pitch angle in 6.25 m/s wind (b) Torque versus pitch angle in 6.25 m/s wind

FIGURE 6.21: Variable pitch system forward flight performance plots

According to the above plots, in order to complete a clockwise roll, the collective of the clockwise spinning proprotors could be decreased to 6° while increasing the collective of the counterclockwise rotating proprotors to 14°. This would lead to a total rolling moment equal to 15.16 N-mm while altering thrust by a minuscule amount. This shows that altering collective pitch of proprotors is an effective way to control vehicle roll in rapid forward flights.

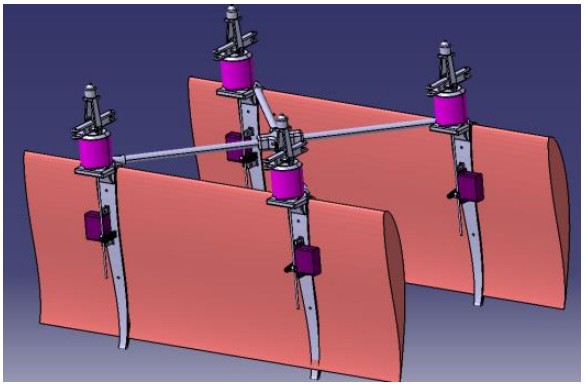

FIGURE 6.22: Vehicle equipped with servo-driven variable collective pitch hubs

Another goal of this chapter is to investigate the possibility of a full scale vehicle equipped with four variable pitch hubs. Figure 6.22 shows a model containing a suite of variable pitch propeller systems to allow for total improved roll control. This vehicle will be constructed and explored in depth in the near future.

6.6 Comparison Between Various Control Concepts

6.6.1 Roll Control

Table 6.1 shows a brief summary of the aforementioned roll control techniques. While all explored systems appear to dramatically improve upon the baseline, variable RPM technique, all methods come with their own benefits and weaknesses.

TABLE 6.1: Roll moment analysis in 6.25 m/s wind

Method	Torque (N-mm)	Percentage Increase
Baseline	7.998	-
Pivoting Wing Tip	15.613	95.21%
Angled Motor Mount	15.793	97.47%
Variable Pitch Hub	15.613	89.48%

The above table shows that the pivoting wing tip control method provides a large increase in roll moment magnitude, generating almost twice the roll magnitude of the baseline model. Based on these results, this method would clearly be a viable option for increasing vehicle roll control authority. Upon further inspection, this may not necessarily be the case. As mentioned earlier, a wing with the pivoting wing tip system weighs 57 grams more than a wing without the system. This

would severely drive up vehicle weight and size. Also, the deflected wing tips generate considerable drag forces. To overcome this increased drag and maintain flight speed, all proprotors would need to spin at an increased rate, driving up power required. It is also worth noting that this system would generate even less roll moment if installed on a wing with a lower aspect ratio or shorter span, which is desirable for most compact MAVs. Due to all of these qualities, this method may not be the most effective for full scale vehicle implementation.

The angled motor mount method creates a significant increase in achievable roll moment in forward flight. This method also has the benefit of implementing no additional moving parts to the system and essentially no increase in vehicle weight. However, the angled motor mount method utilizes the same constant collective proprotor as the baseline method and therefore, cannot by itself alter efficiency of the vehicle in forward flight.

According to Table 6.1, the variable pitch method increases the roll moment achievable by a considerable amount. However, the increase in roll moment magnitude achieved is still slightly less than the other explored options. Ideally, this method would be implementable with another explored option. When combined with a system such as the vectored thrust method, the variable pitch system could further increase roll control authority to a new regime. For example, installing a variable pitch hub system on an angled mount would lead to a 185.6% increase in roll moment generated.

6.6.2 Efficiency

The only method which allows for a simultaneous increase in efficiency as well as roll control is the variable pitch hub approach. Figure 6.23 shows how altering

collective pitch can increase vehicle efficiency depending on vehicle flight regime. At higher advance ratios, or rapid forward flights, higher collective proprotor pitch allows for greater efficiency. At lower advance ratios, which can occur during vehicle transitions or slow, high angle of attack flights, a lower collective will provide highest aerodynamic efficiency. This means that a variable collective hub effectively expands the flight envelope for the vehicle.

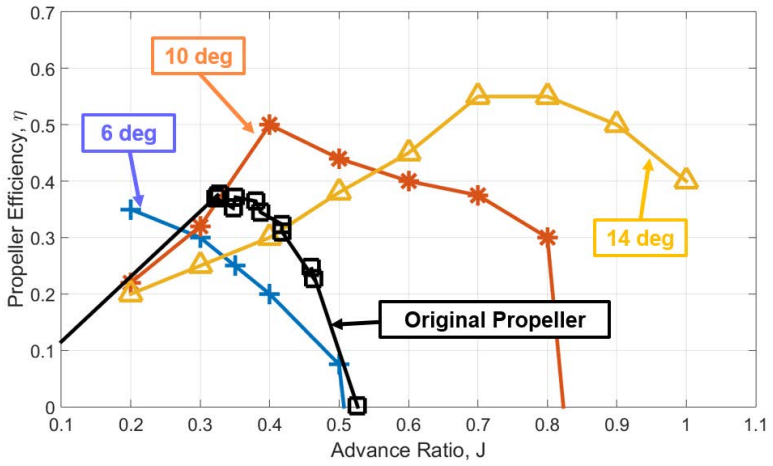

FIGURE 6.23: Efficiency versus advance ratio: variable pitch propeller and original propeller

While the variable pitch method clearly allows for increases in aerodynamic efficiency, much like the pivoting wing tip system, this is inherently heavy. The current servo-actuated swashplate hub and hollow shaft motor pair involves many moving parts and weighs about 5 times as much as the motors and non-moving hub utilized in the baseline control method. In order for the variable pitch system to be effective on the quad-rotor biplane MAV, a much lighter system must be explored and implemented.

6.7 New Vehicle Design and Flight Testing

A new, more compact vehicle design has been designed and built utilizing the angled motor mounts. This vehicle can be seen below in Fig. 6.24. The vehicle is comprised of two wings each with a chord of 6.25 inches and a span of 15 inches, leading to an aspect ratio of 2.4. The compact design allows for most of the span to stay within the downwash of the proprotors which has been proven to improve aerodynamic performance and can ideally improve gust tolerance. This test vehicle has been used to conduct numerous successful flight tests, one of which can be seen below. The new quad-rotor biplane can be seen completing a round circuit in Fig. 6.25, thus demonstrating the utility of the design (see https://www.youtube.com/watch?v=p4jwYW_LV6M).

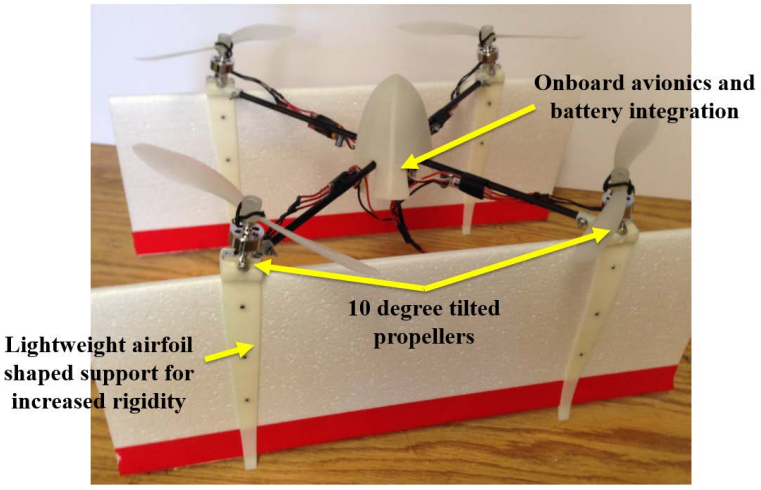

FIGURE 6.24: Vehicle constructed with angled motor/wing mounts

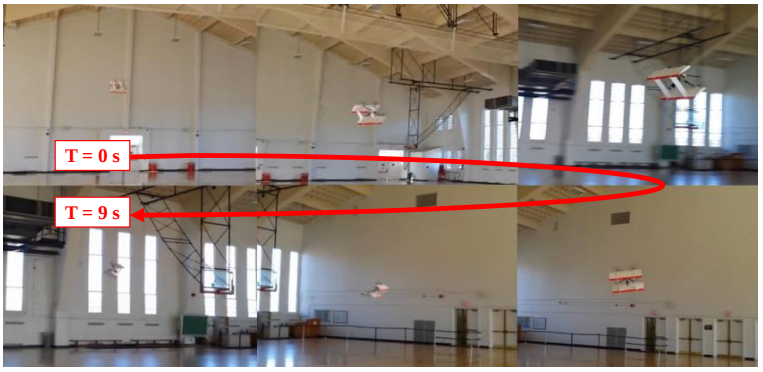

FIGURE 6.25: New vehicle completing circuit flight

6.8 Conclusions

This chapter discussed multiple vehicle improvements ranging from structural to performance alterations. New motor mounts led to a redesigned vehicle configuration utilizing a simpler and more modularized construction process. Vehicle structural soundness and survivability both improved drastically without severe changes to vehicle weight.

During forward flight, roll control was found to be insufficient for the quad-rotor biplane. This led to hard vehicle crashes and severe vehicle damage. In order to alleviate this issue, new roll control concepts were designed and tested. These included: wing-tip pivoting, shaft tilting, and variable collective pitch. In this chapter, three roll moment control techniques were systematically explored and tested for a range of flight conditions, covering hover and airplane modes. The objective of this research was to help the MAV system achieve a maximum roll moment rapidly enough to control the vehicle in a gusty environment. This chapter encompasses all phases of design, development, and flight testing of the control system.

According to the analyses, all control methods improved roll control in forward flight, some more than others. The pivoting wing tip system provided the greatest increase in roll moment as compared to the original, baseline control method. However, this system is not the most effective due to its inherent heft and increased power requirements during implementation and performs well only in high aspect ratio wing systems. Since compactness is of major importance in MAV systems, low aspect ratio wings are preferred and such a system would render the pivoting wing tips less practical. The shaft tilting method is inherently simple and provides more than sufficient control authority in roll. The variable pitch proprotor was proven to increase roll control as well as propeller efficiency during forward flight. This makes it an attractive roll control method, assuming a lightweight option can be developed. This system has the added benefit of improving the vehicle flight envelope from an advance ratio of 0.4 to an advance ratio of 1. Combining the thrust vectoring method via angled motor mounts with the variable pitch proprotor system would yield a vehicle with enhanced roll control as well as the ability to increase efficiency in all flight regimes. Combining the improvements in roll control from the variable pitch method with a thrust vectoring, moment arm system would allow for nearly a three-fold increase in roll moment and control authority. A system comprised of both of these roll control methods would certainly lead to a compact aerial vehicle capable of high performance flight.

Future studies will explore the development and flight testing of a full scale vehicle with an integrated lightweight variable collective pitch system. Data from these experiments will allow for further assessment of the systems usefulness at small scales. The chapter successfully supplied information to be utilized in the construction of a high-speed, high-endurance quad-rotor biplane micro air vehicle.

Chapter 7

Case Study and Scalability Analysis

7.1 *Distributed Logistics in an Urban Setting Using Small Unmanned Aerial Vehicles*

Based on the work presented thus far, a case study was conducted to validate the usefulness of the quad-rotor biplane vehicle. In accordance with the 32nd Annual AHS International Student Design Competition 2015 Request for Proposal (RFP), a large-scale quad-rotor biplane, the *AirEZ* vehicle, was designed and simulated for a parcel delivery system [47]. The project outlined in the RFP was titled *Distributed Logistics in an Urban Setting Using Small Unmanned Aerial Vehicles* and students were tasked with designing a UAV system to deliver up to 5,000 packages a day. The *AirEZ* vehicle, which weighs 38.42 lbs and was sized using an in-house sizing algorithm, can be seen with dimensions below in Fig. 7.1.

The large quad-rotor biplane was designed in order to deliver packages up to a size of 12"x12"x16", weighing as much as 5 lbs, to customers within a 50 mile by 50 mile square region of urban environment (see Fig. 7.2. 5,000 packages were requested in a typical 8 hour day and the vehicle had a maximum of 2 hours to complete a delivery to any location in the 2,500 square mile region. A fleet of 400 vehicles working together in a mesh networking system ensures delivery to the customer's door within 90 minutes of order placement at a low delivery price of $9.03 dollars per package. As part of the logistics network, the vehicles function as a completely self aware node capable of grid communications, mesh networking, HUMS, and precise navigation in an urban canyon. Performance plots can be

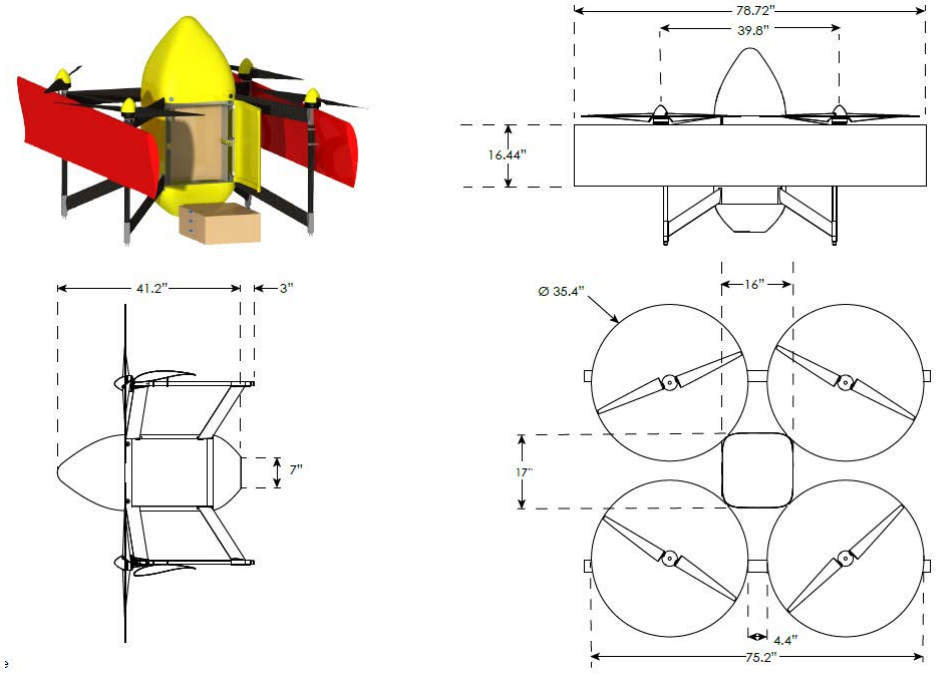

FIGURE 7.1: The *AirEZ* vehicle design

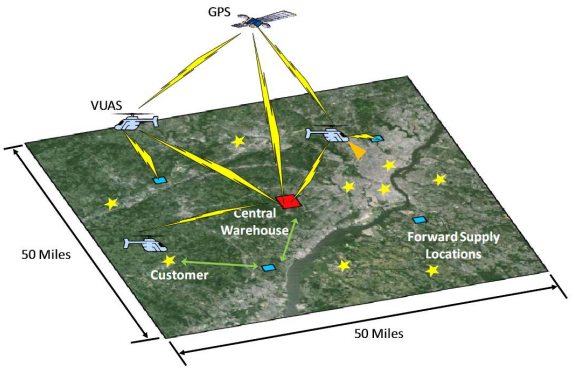

FIGURE 7.2: Map of delivery range

seen below in Figs. 7.4 and 7.5. The design features a variable pitch hub, which has been proven in Chapter 6 to increase efficiency in different flight regimes. A drawing of the hub can be seen in Fig. 7.3.

The hub allows for substantial power savings in both hover and forward flight. The ariable pitch allowed for a figure of merit of 0.74 and a propulsive efficiency of

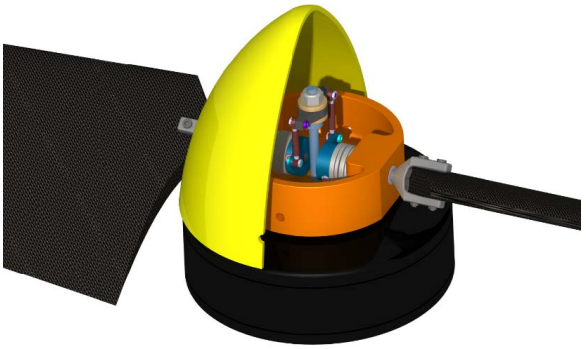

FIGURE 7.3: The *AirEZ* variable pitch rotor hub

0.85, and as a result, *AirEZ* is able to operate in cruise at 55 kts, attain maximum dash speeds of 87 kts, hover at altitudes of over 8,000 ft, and fly for up to 7 hours. It can be seen by 7.4 that the large-scale quad-rotor biplane experiences similar power savings to the small-scale vehicle, making it an attractive option for long-distance and high-speed travel. This vehicle is capable of much higher speeds than a conventional multi-rotor aerial vehicle as seen in Fig. 7.5.

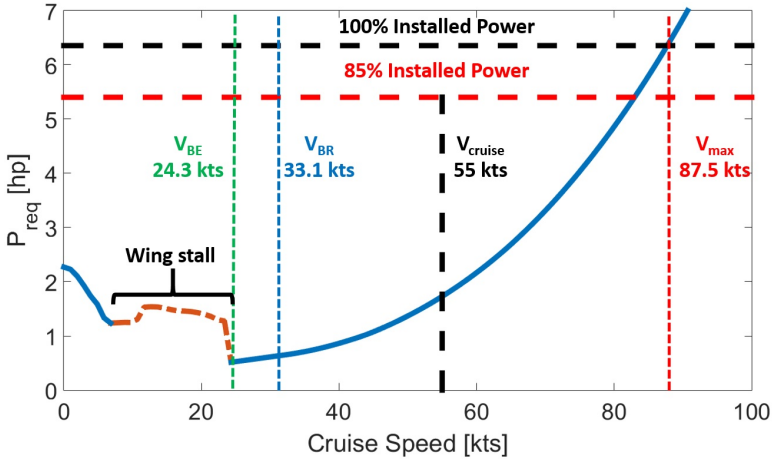

FIGURE 7.4: Power versus forward flight speed for the *AirEZ*

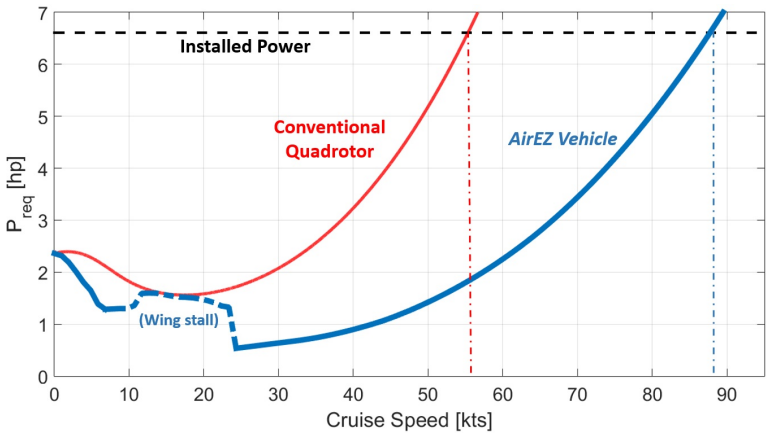

FIGURE 7.5: Power comparison between conventional quad-rotor and *AirEZ*

The *AirEZ* system is a multi-redundant system with safety measures built into every logistics node. The avionics suite onboard the *AirEZ* vehicle features multiple power loss and sensors capability loss failure mode mitigation strategies built in to safely guide the vehicle away from high-risk scenarios. Furthermore, the vehicle design is such that in the case of battery/motor failure, the rotors can either autorotate to the ground or safely operate in an one-motor inoperative condition. If however, a system level failure occurs, an inbuilt parachute system can guide the vehicle safely to the ground.

Some relevant system specifications are shown in Table 7.1 in a comparison between the larger *AirEZ* vehicle and the quad-rotor biplane MAV.

TABLE 7.1: Design specifications for *AirEZ* vehicle and quad-rotor biplane MAV

	AirEZ vehicle	Quad-rotor biplane
Rotor diameter	35.4”	6.0”
Wing span	78.7”	15.0”
Wing chord	16.4”	6.3”
Max speed	87.5 kts	21.4 kts
Gross weight	38.4 lbs	0.5 lbs

7.2 Scaling Objective

The following sections make use of the data presented in Chapter 4 which has already proven the feasibility of the small quad-rotor biplane vehicle. The data is used to corroborate the claims made in the AHS Graduate Student Design Report, mentioned in Section 7.1 and to validate the proposed design, the *AirEZ* vehicle [47]. The report states that the *AirEZ* vehicle, a large-scale quad-rotor biplane, can take off and land vertically, transition between vertical and horizontal flight, and fly at rapid forward speeds. In order for the small scale vehicle data to be used in this study, a relationship between the two quad-rotors is defined via scaling. The data for the 0.5 lb vehicle is non-dimensionalized and then subsequently scaled to provide operating variables for the proposed full-scale vehicle in different flight modes. This scaled data proves that the large-scale quad-rotor can maintain steady level flight along its entire delivery mission profile, while staying within installed power constraints.

7.3 Pre-Test Predictions

Utilizing the aforementioned studies, this scaling validation substantiates claims made in the AHS Student Design Report that state a quad-rotor biplane is capable of delivering packages through a defined mission profile. As previously mentioned, the validation is conducted through data scaling which is outlined below.

7.3.1 Scaling Analysis and Predictions

In order to complete the scaling desired, the non-dimensionalized data is applied to the *AirEZ* vehicle dimensions. Once completed, the data yields trim flight conditions for all flight angles which prove that the *AirEZ* vehicle is capable of completing its specified mission profile. Dynamic scaling is used to apply the non-dimensionalized data to the final vehicle dimensions, [48]. This scaling technique has been used to explore the effects of rotor size on vehicle performance characteristics and has been applied to vehicles which are comparably sized with the proposed delivery vehicle. This technique provides a realistic baseline with which to compare the scaled data. It is predicted that these two scaling techniques proves that the full scale vehicle is capable of flight in any required regime.

7.3.2 Data Scaling

The studies conducted in Chapter 4 provided over 3,000 unique, raw test cases for the wing and wing-propeller systems which required calibration beforehand as well as tare value calculations, scaling, and analysis. As mentioned earlier in Chapter 4, these processes were repeated for a range of wind speeds, shaft angles, and RPMs. Upon completion of all test cases, data was reduced and scaled. All raw thrust, lift, and torque measurements were reduced to non-dimensionalized coefficients, scaled, and fit to polynomial best-fit curves. The scaling conducted was done in accordance with Refs. [48] and [49]. According to Mettler and Consdale, non-dimensional force coefficients do not change based on vehicle scaling. For example, while Reynolds number effects ignored, a C_T calculated from a case during small-scale MAV wind tunnel tests would be the same C_T for a corresponding case of the full-scale /AirEZ vehicle. This allows for simple scaling to new cases through

size and speed ratios. Wolowicz, et al. [50] state that proper aircraft speed scaling is dependent on the ratio between the wing span length of the original and scaled models, n, for incompressible flow. The wing span ratio is defined and utilized to determine scaled vehicle flight speed below in Eqs. 7.1 and 7.2:

$$n = \frac{\text{Span}_{\text{scaled}}}{\text{Span}_{\text{model}}} = \frac{78.7”}{22”} = 3.57 \tag{7.1}$$

$$V_{\text{scaled}} = V_{\text{model}} n \tag{7.2}$$

Since the quad-rotor biplane testing was conducted at wind speeds up to 32 ft/s, Eq. 7.2 shows that the upscaled quad-rotor biplane vehicle data would run up to 114 ft/s. The rotor scaling factor is defined as [49]:

$$\lambda = \frac{R_{model}}{R_{scaled}} \tag{7.3}$$

This scaling factor, $\lambda = .168$, is used to define new forces, such as axial rotor thrust, which can be broken down to lift and thrust based on α as shown earlier. Vehicle rotor forces are dependent upon a factor of λ^3 and therefore scale accordingly [49]. Utilizing non-dimensionalized force coefficients with scaling factors for the rotor provide new force values for a full-scale *AirEZ* vehicle like so:

$$F_{scaled} = \frac{\frac{1}{2}\rho C_F \pi R_{model}^2 (\Omega R_{model})^2}{\lambda^3} = \frac{F_{measured}}{\lambda^3} \tag{7.4}$$

Combining raw data with these scaling factors results in test and trim data for a quad-rotor biplane on the scale of the *AirEZ* vehicle and the following section details how this data is utilized.

7.3.3 Test Case Example

Upon scaling, all data cases were fit to best-fit polynomial curves and analyzed to extract steady, level flight trim cases. For example, Figs. 7.6(a) and 7.6(b) show this process for the cases of $\alpha = 6^{o}$. In these plots, each blue line represents a best-fit curve for a different wind speed. The roots of the plot in Fig. 7.6(a) (highlighted in black) show the RPM values where the forward thrust is equal to 0. These roots are then plotted in Fig. 7.7(a) against their respective wind speeds. Each case plotted in Fig. 7.7(a) is then used to plot Fig. 7.7(b). This figure shows the lift generated at these cases with 25% of the vehicle weight subtracted. When the line in Fig. 7.7(b) crosses 0, this represents a case of steady, level flight, to be used in trim analysis. For instance, at 6^{o} shaft tilt, to generate zero net thrust and enough lift to carry its own weight, the upscaled quad-rotor biplane would need to fly at 27.2 kts and have a proprotor RPM equal to 2350. Figure 7.8 shows an example trim analysis as applied to the vehicle system; with and without body drag as well as with and without wing lift.

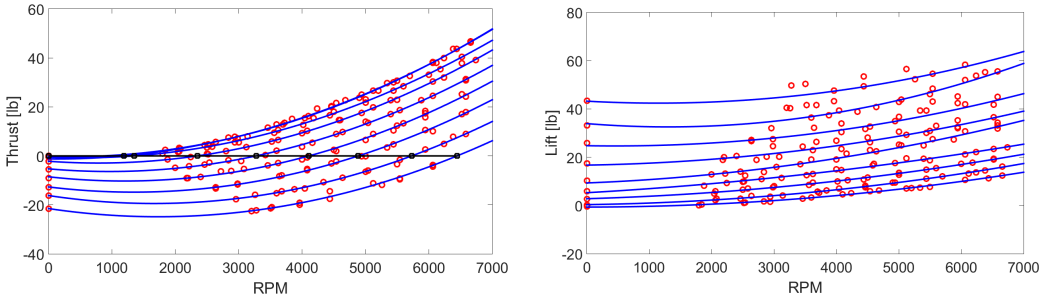

(a) Thrust curves for different airspeeds

(b) Lift curves for different airspeeds

FIGURE 7.6: Polynomial curve fits of test data

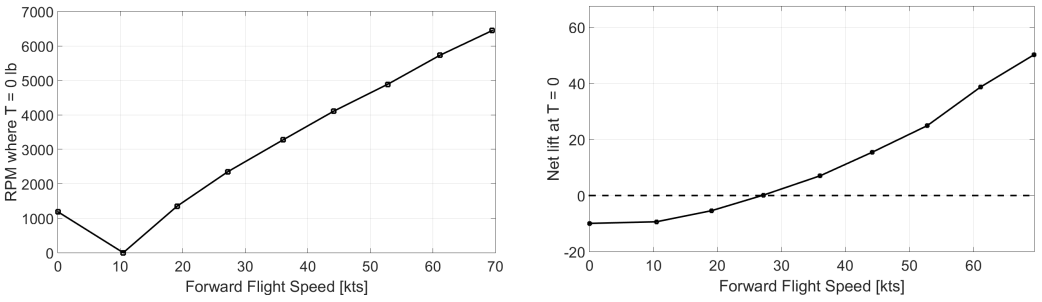

(a) RPMs where the net thrust is 0

(b) Net lift values where the net thrust is 0

FIGURE 7.7: Data extraction for trim condition

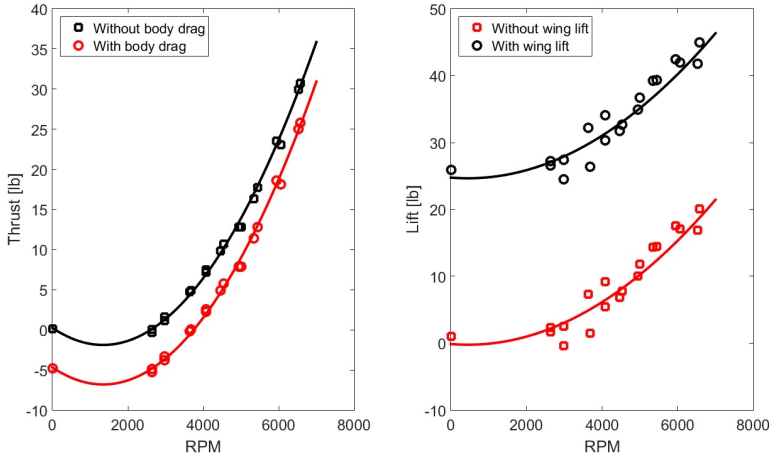

FIGURE 7.8: Trim analysis

7.3.4 Results

The process detailed in the previous subsection is completed for all pitch angles, ranging from 0^o to 90^o. This provides a trim case for every shaft angle from which, such variables as wind speed, rotor RPM, and even rotor power required can be extracted. Figures 7.9(a) and 7.9(b) show curves for speed and RPM versus shaft angle, α. It can be noted that these curves very closely match the trends presented in Chapter 4. Figure 7.9(a) shows that, as expected, the vehicle slows as it pitches up from $\alpha = 0^o$ to $\alpha = 90^o$ and Fig. 7.9(b) shows a trend very similar to that

shown in the corresponding plots in Figs. 4.18 and 4.19.

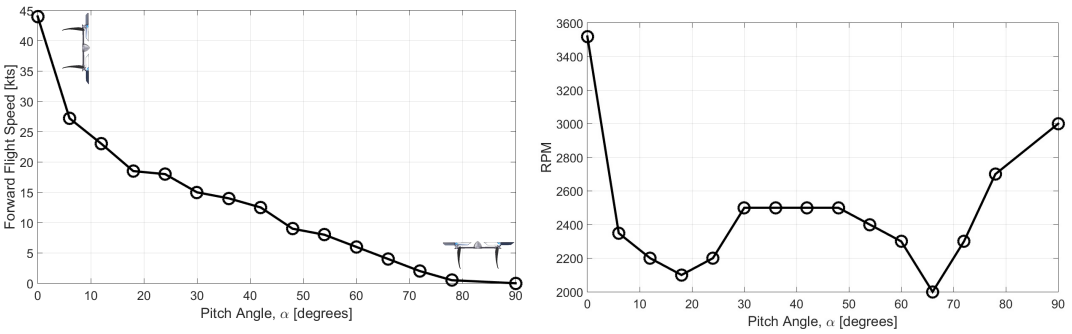

(a) Forward flight speed versus shaft angle

(b) Required rotor RPM versus shaft angle

FIGURE 7.9: Trim analyses for scaled quad-rotor biplane MAV

Figure 7.10 shows a comparison of power curves between the scaled model data and the actual *AirEZ* vehicle. It can be seen that although the magnitudes are slightly different, the curves' trends are very similar. The magnitude differences can be attributed to the differences in vehicle systems. The *AirEZ* vehicle, as detailed in the design report, has a very large representative flat plate area, especially in the hover and edgewise flight configurations. This contributes drastically to overall vehicle drag and low speed, high α forward flight power requirements. The scaled quad-rotor biplane has the same body shape as shown in Fig. 2.1 and does not include the large fuselage for storing packages, which would allow for the scaled MAV to utilize less power in these flight regimes. It is also important to note that the rotors utilized in both cases are very different in design. The *AirEZ* vehicle's proprotor and motor systems were designed with greater emphasis on propeller and cruise efficiency, leading to a slightly degraded performance in low speed flight regimes. The vehicle represented by the curve named "Test Data" utilizes an upscaled rotor with the same geometry as the GWS 6x5 SlowFlyer propeller. The *AirEZ* vehicle utilizes a specially designed variable pitch rotor. This allows the *AirEZ* vehicle to travel rapid forward flight speeds efficiently, which explains

the more steep increase in power required for the scaled test data. The *AirEZ* rotor design is fully explained in the report [47] and is not detailed in this thesis. However, it is important to note that via the simple scaling done, the magnitudes of the power required curves are still similar and of the same order of magnitude. Both curves have a minimum power required per rotor of approximately 90 W and a maximum of about 500 W. The power curves both show a peak during wing stall as well. This helps to validate the claims made about power required for the *AirEZ* vehicle in the design report.

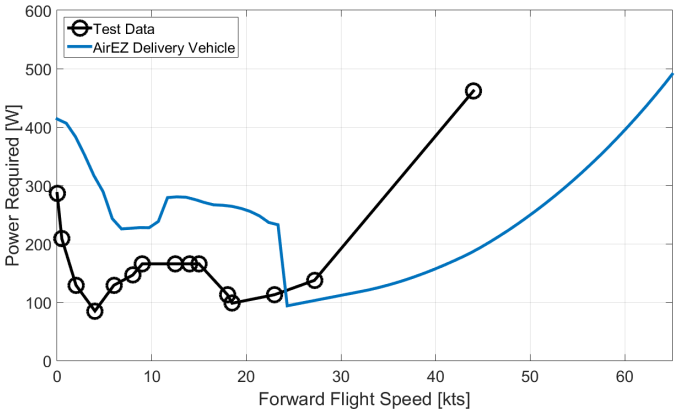

FIGURE 7.10: Power curve comparison for scaled MAV and the AirEZ vehicle

7.3.5 Scaled *AirEZ* Vehicle

Recently, at the University of Maryland, a scaled-down version of the *AirEZ* vehicle was designed and constructed. Figure 7.11(a) shows the the *AirEZ-Micro* vehicle which weighs 0.67 lbs. The *AirEZ-Micro* is a $1/5^{\text{th}}$ scaled vehicle. The vehicle has a wing span of 1.36 ft and a length of 1.31 ft. As was noted in the previous section, a major reason for the discrepancies in power curves between the test data and the *AirEZ* vehicle is lack of similar fuselage. However, this problem has been mitigated by the scale model. The *AirEZ-Micro* vehicle has a relative

flat plate area which is far more commensurate with the full-scale *AirEZ* vehicle. This allows for more direct scaling of power values at different flight speeds. A more detailed breakdown of the vehicle can be seen in Fig. 7.11(b).

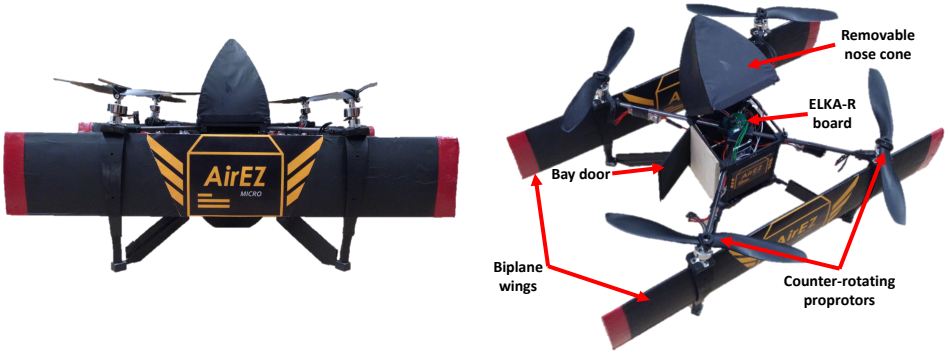

(a) The *AirEZ-Micro* vehicle (b) Vehicle component breakdown

FIGURE 7.11: *AirEZ-Micro*

7.3.6 FlightTesting

Upon completion of vehicle construction and ELKA-R integration (Chapter 5), flight testing was conducted. Figure 7.12 shows the *AirEZ-Micro* demonstrating stable hover. Further flight testing was conducted outdoors to demonstrate transition and high pitch attitude flight in gusty environments. These tests can be seen in Fig. 7.13. Additional flight tests will be conducted in the future. However, the initial tests clearly demonstrate the scalability of the *AirEZ* design, thus enhancing its versatility.

7.4 Conclusions

Overall, the scaled data showed close matching to the vehicle trends presented in Chapter 4 and the design report for the *AirEZ* vehicle [47]. This helps to validate

FIGURE 7.12: *AirEZ-Micro* hover flight testing

FIGURE 7.13: *AirEZ-Micro* outdoor flight testing (https://www.youtube.com/watch?v=p4jwYW_LV6M)

the quad-rotor biplane's scalability and the claims made in the report which state that the *AirEZ* vehicle is capable of achieving steady, level flight in all of its flight modes; hover, transition, and forward flight. This study also corroborates the power values calculated for the *AirEZ* vehicle. In the report, it was stated that the *AirEZ* vehicle would require 110 W to cruise at 30 kts while the hardware validation analysis claims a value of 190 W at this speed for a similarly scaled quad-rotor biplane. This discrepancy can be explained by the improved variable pitch proprotor design implemented on the *AirEZ* vehicle. The design changes implemented on the *AirEZ* vehicle allow it to travel much more rapidly than a scaled version of the quad-rotor biplane built and tested at the University of Maryland, proving the advantages of such a design. The scalability of the quad-rotor biplane was demonstrated by both the design of the *AirEZ* vehicle as well as the construction and testing of the *AirEZ-Micro*.

Chapter 8

Summary and Conclusions

The quad-rotor biplane MAV has redefined rotary wing aviation for small scale vehicles. It is a fast, efficient, and simple configuration capable of both edgewise and forward flight that requires no redundant or complicated aerodynamic control surfaces. It combines the most desirable characteristics of fixed and rotary-wing concepts to operate efficiently in all flight regimes. Simple RPM variation allows for vehicle control regardless of vehicle orientation. The components and subsystems are designed in a time-saving and modular fashion utilizing manufacturing techniques that allow for ease of maintenance and repair.

8.1 Vehicle

The original proof-of-concept vehicle weighs approximately 240 grams and has two wings, each with a span of 22" and a chord of 4". The wings are spaced by 10". Since the initial vehicle design, multiple iterations have been designed and built. A more current vehicle, weighing 220 grams, has a span of 15" with a chord length of 6.25", allowing for a more compact ground footprint. The vehicle also utilizes enhanced construction that allows for increased rigidity, as well as enhanced and more robust performance in forward flight. New motor and wing mounts as well as vertical fins have helped lead to an improved quad-rotor biplane vehicle design.

8.2 Parametric Studies

Multiple vehicle subsystems and parameters have been carried out to examine their effects on performance. A study conducted to compare three high performance, low Reynolds number airfoils revealed that the FX 63 airfoil had superior flight characteristics and was subsequently installed on the vehicle. Differences in performance between 3.8 and 2.4 aspect ratio wings were found to be small. Wing spacings below 1.5c could be avoided so as not to degrade flight performance. It was seen that placement of the propeller axis along the wing chord provided the best performance. A boxed-wing configuration, where the wing tips are enclosed by an aerodynamic surface, was explored, as well. The boxed-wing design configuration was found to supply no aerodynamic benefits and has since been avoided.

8.3 Vehicle Aerodynamics

An in-depth study of the propeller-wing system helped to validate vehicle flight-worthiness in hover, transition, and forward flight. A single propeller attached to a proportionally scaled wing with a vertical force requirement of 0.6 N was tested at various shaft angles and forward flight speeds. The performance of the isolated propeller was initially studied at various angles of flight. The wing was subsequently added to the system to investigate interaction effects between the wing and propeller. Finally, operating variables such as propeller RPM and transition angle were extracted for a given forward flight speed that resulted in steady, level flight. Additionally the power requirements were extracted that can

be used to improve flight speed and maximize efficiency in future designs. The following are some specific conclusions from the study:

1. Contributions from horizontal and vertical forces produced by isolated propeller are equal at 40° shaft angle and at wind speeds greater than 3 m/s.

2. Power required to produce a given total force increases significantly at low shaft angles due to effects of increased inflow.

3. For the propeller-wing system, a higher vertical force and a lower horizontal force is produced at a given shaft angle and wind speed when compared with the isolated propeller.

4. Contributions from horizontal and vertical forces produced propeller-wing system are equal at much lower shaft angles of about 12°.

5. Forward flight velocity that satisfies steady level flight increases steadily as shaft angle decreases with a sharp increase at 0° shaft angle.

6. Required propeller RPM is close to 5000 in hover mode and up to shaft angles of 50°. At 0°, the required RPM rises sharply to 7500.

7. The minimum power requirement during cruise is 3 times lower than the hover power requirement. Maximum achievable velocity is about 11 m/s for the present configuration.

8.4 Design Improvements and Flight Tests

Flight testing showed that the quaternion-based PID feedback controller effectively stabilized the vehicle in hover, forward flight and transition states. Numerous successful level transition flights were obtained. A flight velocity of about 7 m/s was attained with a shaft angle of close to 5° from horizontal. This correlated well with predictions from the trim analysis.

Horizontal flight is a critically important flight mode for the quad-rotor biplane, and during this flight regime, roll control was found to be insufficient. Multiple alternative roll control techniques were designed and tested. These included a pivoting wing tip system, angled motor mounts and rotor shaft tilting, and a variable collective pitch system. This study included a range of flight conditions between hover and airplane modes. As a result of the testing, it was found that each of the roll methods improved control authority from that of the baseline vehicle in forward flight. However, most systems had inherent weaknesses, rendering them undesirable for vehicle inclusion. The pivoting wing tip system provided large magnitude roll moments as compared to the baseline control system. This system was not chosen due to its high weight and increased power requirements during implementation, among other reasons. The angled motor mount is the most simple and lightweight option, which provides suitable roll moments and control authority, making it an obvious choice for vehicle implementation. The variable pitch method is the only method which simultaneously increased roll control and forward flight efficiency. Further research will need to explore a lightweight variable pitch system as the benefits of the system have been made clear.

It was also found that utilizing a system of variable pitch proprotors with the proven shaft tilt method would yield a vehicle with drastically enhanced roll control, as well as the ability to increase efficiency in all flight regimes. 185.6% increase in roll moment and control authority can be achieved by combining these two designs. A system which combines both of these roll control methods would be preferable for a compact MAV.

8.5 Scalability and Functionality

A case study proved the utility of the quad-rotor biplane system and provided a look into possible system of systems implementation. All in all, this vehicle configuration has been shown to be viable through multiple designs and flight testing processes. The *AirEZ* vehicle showed large scale implementation of the quad-rotor biplane in a system of systems package delivery service. The *AirEZ-Micro*, which was designed and built in-house to be a scaled model of the *AirEZ* vehicle, showed the scalability of that design. Multiple variants of the quad-rotor biplane have been designed and constructed. Every vehicle that has been subjected to flight testing has achieved steady flight in at least one of the desired flight modes, if not all three. This has truly helped to demonstrate the viability and functionality of the design. Through these multiple vehicle iterations, the quad-rotor biplane is shown to be a novel design which allows for multiple mission profiles ranging from parcel delivery to surveillance and beyond.

8.6 Recommendations for Future Work

The work presented in this thesis examined the design, as well as aerodynamic and flight testing, of the quad-rotor biplane. Parametric studies examined the performance effects of varying many design qualities, including but not limited to wing design and spacing. Systematic aerodynamic experimentation led to a better understanding of the aerodynamics of a low Reynolds number propeller-wing system. Flight control algorithms and software were explained and subsequently demonstrated through flight tests. Throughout the work, multiple variants of the quad-rotor biplane were constructed and flown, highlighting the vehicle's versatility and dependability. However, based on the studies shown, there are several areas in which further research needs to be performed. These improvements will complete or at least enhance the knowledge gained by the present study.

As mentioned earlier, this thesis examined interaction forces between wings and propellers. Multiple wing-propeller system factors and their effects on vehicle performance were studied, including axis offset as well as type of airfoil and propeller. It was found that interaction effects lead to an increase in vertical force generation and a decrease in horizontal force. However, wing-propeller interaction at low Reynolds number is a complicated and poorly understood phenomena. Further investigation can be conducted regarding careful analysis of the effective angle of attack before and after the propeller interaction, wing stall, and other propeller-wing system factors.

It was seen in Chapter 5 that the quad-rotor biplane experiences a slight altitude gain when transitioning from forward flight to hover. This is a result of the

pitch-up command, which leads to an increase in vehicle lift. Furthermore, improvements must be investigated regarding vehicle transition out of hover. The inherent altitude gains associated with the transition can lead to vehicle crashes when in enclosed and crowded locations which must be avoided. An in-depth study should be conducted regarding vehicle dynamics between hover and forward flight with the goal of more efficient gain scheduling. Also, implementing sensors to detect the state of wing lift would be valuable when used for real-time feedback control. All of this will allow for smoother transition flight control, as well as ideally providing enhanced gust tolerance.

The wings utilized on the quad-rotor biplane are untwisted, non-tapered, non-staggered, and unswept. The vehicle exhibited preferable flight performance with this basic wing setup, achieving both high maximum speeds and highly efficient flight at lower speeds. However, multiple fixed-wing aircraft are flown featuring wings which incorporate non-zero twist, taper, and sweep. Biplanes also typically utilize wing staggering, placing the upper wing ahead of the lower. Future investigations can study the effects of varying these parameters on quad-rotor biplane performance and control. These studies may prove that greater lift-to-drag ratios can be achieved on the quad-rotor biplane, allowing for higher flight speeds and more efficient cruise.

Much of the testing done to prove vehicle functionality and utility was conducted through a systematic series of wind tunnel and flight tests. These tests proved that the quad-rotor biplane can reach any desired mode of flight smoothly and efficiently. However, more studies should be conducted on future models through aerodynamic stability analysis before flight tests are conducted to help further validate the designs. These validations may help to avoid crashes during flight testing if a certain vehicle variant is not deemed flight-worthy beforehand.

As shown in Chapter 6, a quad-rotor biplane with variable collective pitch capability can experience improved roll control, as well as heightened efficiency in all flight regimes. Unfortunately, it was shown that the variable pitch system explored in this thesis is too heavy to consider for vehicle implementation. Therefore, it is imperative that a lightweight variable pitch system be developed and implemented on the quad-rotor biplane vehicle. A vehicle with added variable pitch actuators will have added control capabilities. Currently, the quad-rotor biplane is controlled simply via the variable RPM approach. A vehicle with both variable collective and RPM control inputs will ideally be more maneuverable, as well as more efficient.

This study examined multiple quad-rotor biplane configurations of varying weights and sizes, mostly of a small scale. Currently, a vehicle capable of carrying a 1 lb payload is under construction at the Alfred Gessow Rotorcraft Center. The vehicle has a wing span of 36", a rotor diameter of 15.2", and a gross takeoff weight of 8 lbs. Upon completion, this will help, once again, to demonstrate the scalability of the vehicle concept. In the future, a larger scale quad-rotor biplane, comparable to the *AirEZ* vehicle and its 5 lb payload outlined in Chapter 7, should be designed, built, and tested.

A likely use of the quad-rotor biplane is rapid payload delivery. However, up to this point, no investigations have been made into the payload carrying capabilities of the constructed vehicle. Payload integration should be explored and implemented to improve vehicle usability and utility. A hub allowing for payload attachment must be designed and integrated into the vehicle. Studies must then be conducted to gauge payload fraction capabilities and examine ways to increase it, if necessary.

Bibliography

[1] Wilson, S. B., "Micro Air Vehicles (MAV)," August 1999, Presentation at the AIAA Student Chapter meeting at the University of Maryland, College Park, Oct 19, 2000 Presentation prepared Dec 14, 1999.

[2] Maxey, K., "DARPA's Multi-Role UAV," March 2014, http://www.engineering.com/DesignerEdge/DesignerEdgeArticles /ArticleID/7277/DARPAs-Multi-Role-UAV.aspx, [Online; accessed June-2015].

[3] McMichael, J. M. and Francis, C. M. S., "Micro Air Vehicles Toward a New Dimension in Flight," *U.S. Department of Defense Weapons Systems Technology Information Analysis Center (WSTIAC) Newsletter*, Vol. 1, No. 1-3, January-July 2000.

[4] Laitone, E. V., "Wind tunnel tests of wings at Reynolds numbers below 70,000," *Experiments in Fluids*, Vol. 23, 1997, pp. 405–409.

[5] Grasmeyer, J. and Keennon, M., "Development of the Black Widow Micro Air Vehicle," Aerovironment, inc., American Institute of Aeronautics and Astronautics, 2001.

[6] Hein, B. and Chopra, I., "Hover performance of a Micro Air vehicle: Rotors at Low Reynolds Number," *Journal of American Helicopter Society*, Vol. 52, No. 3, July 2007.

[7] Bohorquez, F., *Rotor Hover Performance and System Design of an Efficient Coaxial Rotary Wing Micro Air Vehicle*, Ph.D. thesis, University of Maryland, College Park, MD, 2007.

[8] Hanford, S., Long, L., and Horn, J., "A Small Semi-Autonomous Rotary-Wing Unmanned Air Vehicle (UAV)," *American Institute of Aeronautics and Astronautics, Infotech Aerospace Conference, Paper No. 2005-7077*.

[9] Bohorquez, F., Samuel, P., Sihori, J., Pines, D., and Rudd, L., "Design, Analysis and Performance of a Rotary Wing MAV," *Journal of the American Helicopter Society*, Vol. 48, No. 2, April 2003, pp. 80–90.

[10] Hrishikeshavan, V., *Experimental Investigation of a Shrouded Rotor Micro Air Vehicle in Hover and in Edgewise Gusts*, Ph.D. thesis, University of Maryland, College Park, MD, 2011.

[11] Krashanitsa, R., Silin, D., and Shkarayev, S., "Flight Dynamics of Flapping-Wing Air Vehicle," *AIAA Atmospheric Flight Mechanics Conference and Exhibit, Honolulu, Hawaii*, August 2008.

[12] Mayo, D. B., Lankford, J. L., Benedict, M., , and Chopra, I., "Experimental and Computational Analysis of Rigid Flapping Wings for Micro Air Vehicles," *Journal of Aircraft*, Vol. Ahead of Print, pp. 1–18.

[13] Coleman, D., Benedict, M., Hrishikeshavan, V., and Chopra, I., "Design, Development and Flight-Testing of a Robotic Hummingbird," *AHS 71st Annual Forum, Virginia Beach, Virginia*, edited by A. H. Society, May 2015.

[14] Ackerman, E., "Video Friday: Robotic Hummingbird, Baxter Treats Ebola, and Dexterous Bomb-Squad Robot," May 2015, [Online; accessed June-2015].

[15] Stone, R., Anderson, P., Hutchison, C., Tsai, A., Gibbens, P., and Wong., K., "Flight Testing of the T-Wing Tail-Sitter Unmanned Air Vehicle," *Journal of Aircraft*, Vol. 45, No. 2, July 2008, pp. 673–685.

[16] Frank, A., McGrew, J. S., Valenti, M., Levine, D., and How, J., "Hover, Transition, and Level Flight Control Design for a Single-Propeller Indoor Airplane,," *AIAA Guidance, Navigation and Control Conference and Exhibit, Hilton Head, South Carolina, AIAA Paper 2007-6318*, 2007.

[17] Kubo, D. and Suzuki, S., "Tail-Sitter Vertical Takeoff and Landing Unmanned Aerial Vehicle: Transitional Flight Analysis," *Journal of Aircraft*, Vol. 45, No. 2, July 2008, pp. 292–297.

[18] Satoshi, S., Ren, Z., Yoshikazu, H., Kenzo, N., Gaku, K., Toshio, B., Daisuke, H., Mituhiro, F., and Kenta, Y., "Attitude Control of Quad Rotors QTW-UAV with Tilt Wing Mechanism," *Journal of Aircraft*, Vol. 45, No. 2, July 2008, pp. 673–685.

[19] Hrishikeshavan, V. and Chopra, I., "Design and Control of a Tilt-Wing Micro Air Vehicle in Hover," *American Helicopter Society 68th Annual Forum, Fort Worth, Texas*, May 2012.

[20] Mahadik, R., Karpatne, A., and Sirohi, J., "Design and Testing of a Morphing Micro Aerial Vehicle," *American Helicopter Societys International Specialists Meeting on Unmanned Rotorcraft and Network Centric Operations, Phoenix, AZ*, January 2011.

[21] Carr, R., Moschetta, J., Thypiopas, C., and Mehta, G., "A Tilt-Body Fixed-wing Micro Air Vehicle for Autonomous Transition Flight," *IMAV Conference, 2010, Braunschweig, Germany*, July 2010.

[22] Stewart, J., "Google Tests Drone Deliveries in Project Wing Trials," August 2014, http://www.bbc.com/news/technology-28964260, [Online; accessed June-2015].

[23] Hrishikeshavan, V., Sirohi, J., Tishchenko, M., and Chopra, I., "Design and Development of a Shrouded Rotor Micro Air Vehicle with Anti Torque Vanes," *Journal of American Helicopter Society*, Vol. 56, No. 1, January 2011.

[24] Green, W. and Oh, P., "Autonomous Hovering of a Fixed-Wing Micro Air Vehicle," *IEEE International Conference on Robotics and Automation, Orlando, Florida*, May 2006.

[25] Bataille, B., Poinsot, D., Thipyopas, C., and Moschetta, J., "Fixed-Wing Micro Air Vehicles with Hovering Capabilities," *Platform Innovations and System Integration for Unmanned Air, Land and Sea Vehicles (AVT-SCI Joint Symposium) Meeting Proceedings RTO-MP-AVT-146, Paper 38. Neuilly-sur-Seine, France*.

[26] Thipyopas, C., Mehta, G., and Moschetta, J., "Experimental and Computational Analysis of a Fixed-Wing VTOL MAV in Ground Effect," 07-4010, Department of Aerodynamics, Energetics and Propulsion, Institut Suprieur de lAronautique et de lEspace, University of Toulouse 31400 Toulouse, France EOARD SPC.

[27] Benedict, M., *Fundamental Understanding of the Cycloidal-Rotor Concept for Micro Air Vehicle Applications*, Ph.D. thesis, University of Maryland, College Park, MD, 2010.

[28] Benedict, M., Shrestha, E., Hrishikeshavan, V., and Chopra, I., "Development of a Micro Twin-Rotor Cyclocopter Capable of Autonomous Hover," *Journal of Aircraft*, Vol. 51, No. 2, March-Arpil 2014.

[29] Benedict, M., Gupta, R., and Chopra, I., "Design, Development and Flight Testing of a Twin-Rotor Cyclocopter Micro Air Vehicle," *Proceedings of the*

67th Annual National Forum of the American Helicopter Society, Curran Associates, Inc., Virginia Beach, VA, 2011, pp. 135–148.

[30] Benedict, M., Mullins, J., Hrishikeshavan, V., and Chopra, I., "Development of an Optimized Quad Cycloidal-Rotor UAV Capable of Autonomous Stable Hover," *Proceedings of the American Helicopter Society International Specialists Meeting on Unmanned Rotorcraft, Scottsdale, AZ*, January 2013.

[31] Gress, G., "Lift Fans as Gyroscopes for Controlling Compact VTOL Air Vehicles: Overview and Development Status of Oblique Active Tilting," *American Helicopter Society 63rd Annual Forum, Virginia Beach VA*, May 2007.

[32] Nonami, K., Kendoul, F., Suzuki, S., Wang, W., and Nakazawa, D., *Autonomous Flying Robots: Unmanned Aerial Vehicles and Micro Aerial Vehicles*, Springer, 2010.

[33] Moschetta, J., Bataille, B., and Thipyopas, C., "On Fixed-Wing Micro-Air Vehicles with Hovering Capabilities," *Platform Innovations and System Integration for Unmanned Air, Land and Sea Vehicles (AVT-SCI Joint Symposium*, pp. 38.

[34] Nietz, T. and Baber, S., "An Innovative UAV Design," *AIAA 3rd Unmanned Unlimited Technical Conference, Workshop and Exhibit, Chicago, IL*, September 2004.

[35] Stone, H. and Clarke, G., "The T-Wing: A VTOL UAV for Defense and Civilian Applications," *UAV Australia Conference, Melbourne*, February 2001.

[36] Itasse, M., Moschetta, J., Ameho, Y., and Carr, R., "Equilibrium Transition Study for a Hybrid MAV," *International Journal of Micro Air Vehicles*, Vol. 3, No. 4, 2011, pp. 229–245.

[37] Kuhn, R. E. and Draper, J. W., "An Investigation of a WingPropeller Configuration Employing Large-Chord Plain Flaps and Large- Diameter Propellers for Low-Speed Flight and Vertical Take-Off," No. 3307, National Advisory Committee for Aeronautics Technical Note, 1954.

[38] Stone, R., Anderson, P., Hutchison, C., Tsai, A., Gibbens, P., and Wong, K., "Aerodynamic Modeling of the Wing-Propeller Interaction for a Tail Sitter Unmanned Air Vehicle," *Journal of Aircraft*, Vol. 45, No. 1, July 2008, pp. 198–210.

[39] Marretta, M. A., Davi, G., Milazzo, A., and Lombardi, G., "Wing Propeller Coupling Simulation from Tractor to Hover Flight Conditions," *Computer Modeling and Simulation in Engineering*, Vol. 2, No. 3, 1997, pp. 304–321.

[40] Hunsaker, D. and Snyder, D., "A Lifting-Line Approach to Estimating Propeller/Wing Interactions," *24th Applied Aerodynamics Conference, San Francisco, CA, AIAA Paper 2006-3466*, 2006.

[41] Selig, M., Guglilmo, J., Broeren, A., and Giguere, P., *Summary of Low-Speed Airfoil Data*, SoarTech Publications, 1st ed., 1995.

[42] Prandtl, L., "Induced Drag of Multiplanes," No. 182, National Advisory Committee for Aeronautics Technical Note, March 1924.

[43] Hrishikeshavan, V., Bawek, D., Rand, O., and Chopra, I., "Control of a Quad Rotor Biplane Micro Air Vehicle in Transition from Hover to Forward Flight," *American Helicopter Society Specialists Meeting on Unmanned Rotorcraft and Network Centric Operations*, January 2013.

[44] Kuipers, J. B., *Quaternions and Rotation Sequences: A Primer with Applications to Orbits, Aerospace and Virtual Reality*, Princeton University Press, Princeton, NJ, 1999.

[45] Madgwick, S. O., "An Efficient Orientation Filter for Inertial and Inertial/-Magnetic Sensor Arrays," Report x-io, University of Bristol (UK), 2010.

[46] Hrishikeshavan, V. and Chopra, I., "Refined Lightweight Inertial Navigation System for Micro Air Vehicle Applications," *AHS Specialists Meeting on Unmanned Rotorcraft and Network-centric Operations, Chandler, AZ,*, January 2015.

[47] Sidle, S., Bogdanowicz, C., Shishika, D., Winslow, J., Gudenius, B., Wang, X., Nagaraj, V., and Chopra, I., "2015 University of Maryland AHS Student Design Report," Tech. rep., University of Maryland 32nd Annual AHS International Student Design Competition, May 2015.

[48] Mettler, B., Dever, C., and Feron, E., "Scaling Effects and Dynamic Characteristics of Miniature Rotorcraft," *Journal of Guidance, Control, and Dynamics*, Vol. 27, No. 3, pp. 466–478.

[49] Consdale, R., *An Aeroelastic Model Helicopter Rotor*, H.M. Stationery Office, 1973.

[50] Wolowicz, C., Bowman, J., and Gilbert, W., "Similitude Requirements and Scaling Relationships as Applied to Model Testing," 1435, NASA Technical Paper, August 1979.